AD/A-006 259

CENTER FOR HIGH ENERGY FORMING

Steve H. Carpenter

Denver Research Institute

Prepared for:

Advanced Research Projects Agency
Army Materials and Mechanics Research
Center

November 1974

SECURITY CLASSIFICATION OF THIS PAGE (When Data Entered)

REPORT DOCUMENTATION PAGE		READ INSTRUCTIONS BEFORE COMPLETING FORM
1. REPORT NUMBER AMMRC CTR 74-69	2. GOVT ACCESSION NO.	3. RECIPIENT'S CATALOG NUMBER AD/A-006259
4. TITLE (and Subtitle) Center for High Energy Forming		5. TYPE OF REPORT & PERIOD COVERED Final Report
		6. PERFORMING ORG. REPORT NUMBER
7. AUTHOR(s) Steve H. Carpenter		8. CONTRACT OR GRANT NUMBER(s) DAAG46-72-C-0130
9. PERFORMING ORGANIZATION NAME AND ADDRESS Denver Research Institute University of Denver Denver, Colorado 80210		10. PROGRAM ELEMENT, PROJECT, TASK AREA & WORK UNIT NUMBERS ARPA Order No. 720 Program Code: 61101D AMCMS Code: 5910.21.25191
11. CONTROLLING OFFICE NAME AND ADDRESS Army Materials and Mechanics Research Center Watertown, Massachusetts 02172		12. REPORT DATE November 1974
		13. NUMBER OF PAGES 90
14. MONITORING AGENCY NAME & ADDRESS(If different from Controlling Office)		15. SECURITY CLASS. (of this report) Unclassified
		15a. DECLASSIFICATION/DOWNGRADING SCHEDULE

16. DISTRIBUTION STATEMENT (of this Report)

Approved for public release; distribution unlimited.

17. DISTRIBUTION STATEMENT (of the abstract entered in Block 20, if different from Report)

19. KEY WORDS (Continue on reverse side if necessary and identify by block number)

Energy requirements
Energy transfer
Explosive welding

Strain rate effects
Explosive powder compaction
Explosive forming

20. ABSTRACT (Continue on reverse side if necessary and identify by block number)

This report is the Final Technical Report and contains the results of studies conducted in the following areas:

Determination of Optimum Explosion Welding Parameters
Diffusion Studies in Explosion Welded Metals
Explosive Forming of Spherical Gore Segments
Explosive Thermomechanical Processing of Beta III Titanium Alloy
Free Forming of Infinite Plates under Arbitrary Charge Distributions

DD FORM 1 JAN 73 1473

1a

AMMRC CTR 74-69

Center for High Energy Forming

November 1974

Steve H. Carpenter
Denver Research Institute
University of Denver
Denver, Colorado 80210

Final Technical Report   Contract Number DAAG 46-72-C-0130

Prepared for

ARMY MATERIALS AND MECHANICS RESEARCH CENTER
Watertown, Massachusetts 02172

1b

ABSTRACT

This report is the Final Technical Report and contains the results of studies conducted in the following areas:

Determination of Optimum Explosion Welding Parameters

Diffusion Studies in Explosion Welded Metals

Explosive Forming of Spherical Gore Segments

Explosive Thermomechanical Processing of Beta III Titanium Alloy

Free Forming of Infinite Plates under Arbitrary Charge Distributions

IC

FOREWARD

This publication constitutes the final report under the general title: *Center for High Energy Forming*. The work was sponsored by the Advanced Research Projects Agency–ARPA Order No. 720, Program Code No. 61101D. The work was sponsored by the Army Materials and Mechanics Research Center, Watertown, Massachusetts 02172, and was monitored by Mɪ. Arthur F. Jones, with Mr. Philip A.C Carbonaro serving as Contracting Officer's Representative for the termination of Contract No. DAAG46-72-C-0130.

1b

TABLE OF CONTENTS

II

LIST OF FIGURES

LIST OF FIGURES (continued)

II. Diffusion Studies in Explosion Welded Metals

LIST OF FIGURES (continued)

INTRODUCTION

The Center for High Energy Forming was originally established in 1965 under the direction of the Army Materials and Mechanics Research Center through sponsorship of the Advanced Research Projects Agency. Initially the Center was a joint effort by the Martin Marietta Corporation and the Denver Research Institute of the University of Denver. However, since 1972 the Center has been maintained solely at the University of Denver. In the nine years of its existence the Center for High Energy Forming has truly developed into a Center of Excellence in the field of High Energy Metalworking. From its inception the Center has been active in promoting high energy technology, developing and carrying out spin-off research efforts, serving as an information bank or supply house for those seeking information concerning high energy technology and producing trained personnel in the high energy field. The Center has held International Conferences on High Energy Forming on alternate years. These have been very successful with attendees from all over the world. These international conferences will be continued under the sponsorship of the University of Denver with the fifth one scheduled for July 1975. Spin-off research efforts conducted by the Center have included:

Design of Explosive Forming Facility
Explosive Autofrettage
Explosive Welding of Pipelines
Explosive Forming of Thick-Walled Domes
Explosive Welding of Titanium Skins to Stiffeners
Explosive Cladding of Lead to Steel
Explosive Welding and Repair of Aluminum Landing Mats for Airfields
Explosive Compaction of Ti-6A1-4V Powder
Shock Processing of High Strength Steels

The sponsors of the spin-off research efforts have included:

U.S. Army
U.S. Air Force
U.S. Navy
N.A.S.A.
Boeing Company
International Lead Zinc Research Organization
Humble Pipe Line

The Center has also been active in providing education and training in the field of high energy metalworking. Two one-week courses were held in association with ASM which were open to the public. Special training sessions have been arranged for personnel from NASA and foreign engineers from Brazil.

The report contains final results of the investigations carried out by graduate students within the Center.

1

I. DETERMINATION OF OPTIMUM EXPLOSION WELDING PARAMETERS

Faculty Advisor: S. H. Carpenter
Technical Advisor: R. H. Wittman
Graduate Student: S. W. Stivers

The following is a summary of the studies conducted by Mr. Stivers in partial fulfillment of the requirements for A Master of Science degree from the Chemical Engineering and Metallurgy Department, University of Denver. Mr. Stivers received his degree in March, 1974.

Introduction

As was reported in the 1972 Final Report (1), a thorough investigation of nickel, ferritic steel, and nickel-steel combinations was initiated in an effort to develop a more general understanding of the explosive cladding behavior of corrosion resistant alloys to ferric steel.

The research was divided into two major areas: first, the investigation of optimizing the welding parameters of A515 Grade 70 steel. This research lead to a generalized and systematic procedure for determining explosive welding parameters which can be applied to most explosive cladding operations. The cladding of nickel-to-steel is an extension of the procedures developed for steel-to-steel. Consequently, extensive investigations of nickel-steel welds were not conducted and only a few tests were conducted to show the validity of this procedure.

A second area of research was conducted to more extensively investigate the validity of the procedure developed for welding steel-to-steel. This was done by choosing two dissimilar metals, 6061 aluminum and A515 steel. By choosing metals that vary widely in their physical properties, the extreme limits of the welding parameters would need to be used and thereby help confirm or improve the procedure. In addition, the welding conditions for 6061 aluminum have been thoroughly investigated by Wittman (2,3) and a comparison between aluminum-to-aluminum, steel-to-steel, and aluminum-to-steel welds can be made.

FINAL RESULTS OF A515 GRADE 70 STEEL-TO-STEEL AND NICKEL 200-TO-STEEL EXPLOSIVE WELDS

Steel-To-Steel

Previous work (1) had shown improvement in welds with increases in explosive loading from 4 grams/in^2 to 12 grams/in^2. The initial experiments consisted of further increases in loading while maintaining a 1/4 inch standoff. Further breakup of the melt layer was obtained with explosive loading having increased to 15.2 grams/in^2. However, these welds still showed an unsatisfactory interface. From the photomicrograph in Figure 1 the melt layer is obvious. The excessive melt layer has a high tensile strength which greatly exceeds the parent metal strength and lack of ductility both of which characterize martinsitic structure. Microhardness tests were performed on and near the melt area and lend support to this hypothesis. Results of the DPH tests are shown with Figure 2.

At the highest loading of 19.6 grams/in^2 the wave pattern was still poorly defined and the melt layer, while improved was far from ideal. Figure 3 shows this partial breakup in the melt layer. The yield strengths of the weld interface reflect the decrease in the continuous layer of melt. At the lowest explosive loadings, ultimate yield strength was 109,600 psi which is much greater than the parent yield strength of 77,300 psi. At the highest loading, the ultimate yield strength was 95,700 psi characterizing the partial breakup of the melt layer. These tests were performed at 1/4, 1/2, 3/4 the plate length. The specimen configuration and special test apparatus is shown in Figure 7 and Figure 8. It should be mentioned in view of later experiments that high quality welds with tensile strengths in excess of parent metal strength are possible. However, when this occurs the wave pattern is very well defined and in addition what melt that may be present is well broken up into small pockets.

In an effort to overcome both the excessive melt layer and the poorly defined wave pattern the standoff was increased from 1/4 inch to 3/8 inch. Results did partially support this approach which can be seen in Figure 4. The wave pattern is considerably improved and the ultimate yield strength decreased to 83,000 psi. A further increase in the standoff resulted in cracks along the interface (see Figure 5). The problem was not explored in depth but it is thought that the cracks are a result of excessive shear stress caused by the combination of large standoff distances and high explosive loading.

At this time it was felt that the practical limitations of varying explosive loading and standoff distances while using DBA-10HV had been investigated. Results had progressed from a no-weld condition to welds with a continuous melt layer as the loading increased. Further breakup of the melt by increasing the standoff was limited by cracking at the interface. The next area to be investigated was the possibility that the detonation velocity of DBA-10HV was excessively high. Tests performed later showed that for the explosive loading being used, the detonation and hence the collision point velocity was approximately 3800-4000 m/sec which makes the collision point velocity close to the bulk sound velocity of mild steel. Another possible cause of poor welds is that some characteristic velocity which is less than the sonic velocity may govern successful welding. It is difficult to determine which of the characteristic velocities is the pertinent one. Velocities in mild steel range from 2984 m/sec for surface waves to approximately 5900 m/sec for dilatational waves (4). At this time in the investigation, the approach was to use an explosive with a lower detonation velocity. The explosive originally

3
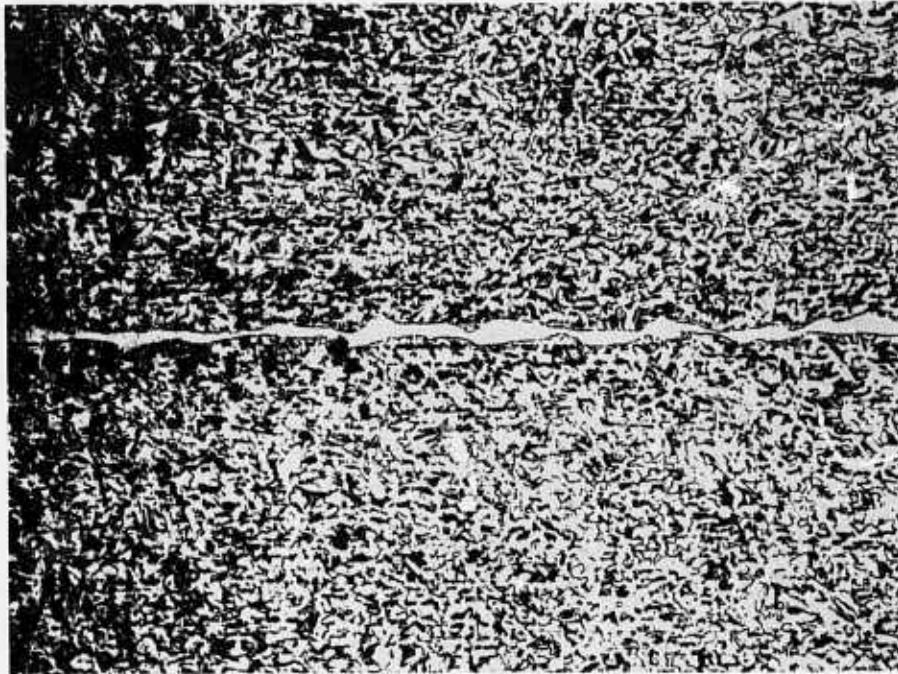
Figure 1. An example of a continuous melt layer
which was common in early welds (X80).

DPH NUMBER
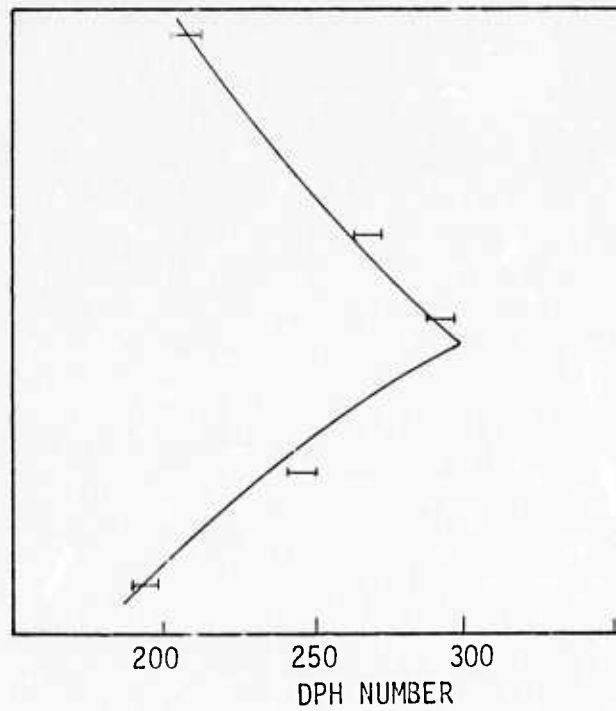
Figure 2. Results of a hardness test (20Kg load) across the melt zone at the
weld interface showing the undesired hardness of this region.

4
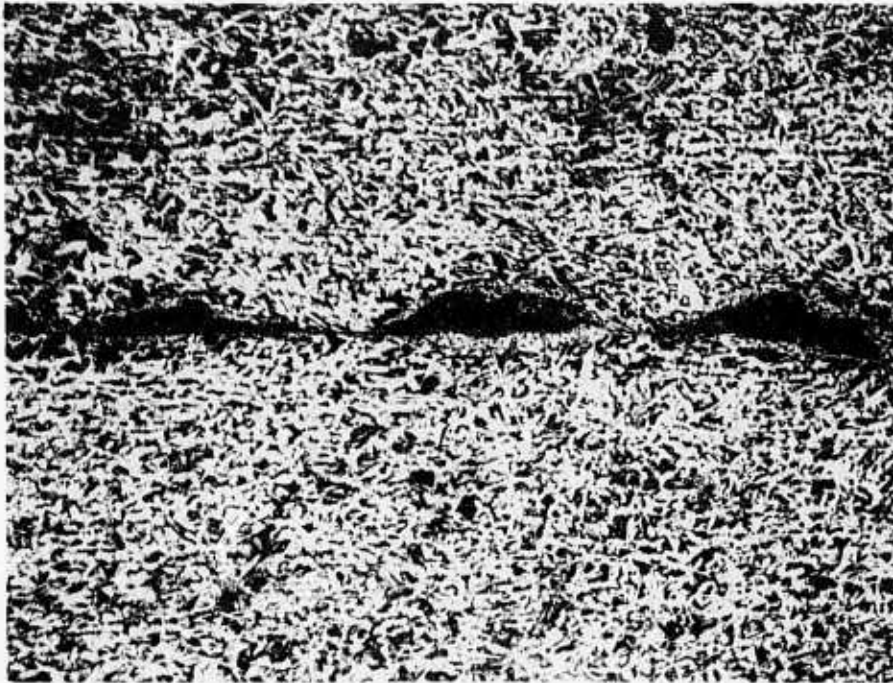
Figure 3. The partial breakup of the melt layer as a result of increasing
the explosive loading (X80).
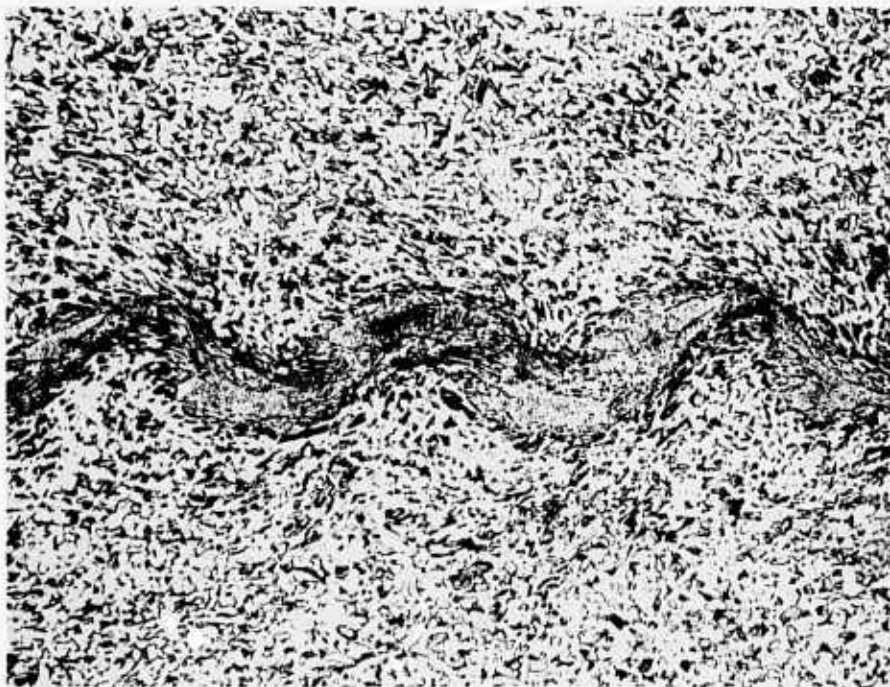
Figure 4. Further breakup of melt as a result of increasing the standoff
distance from 1/4 to 3/8 inch (X80).
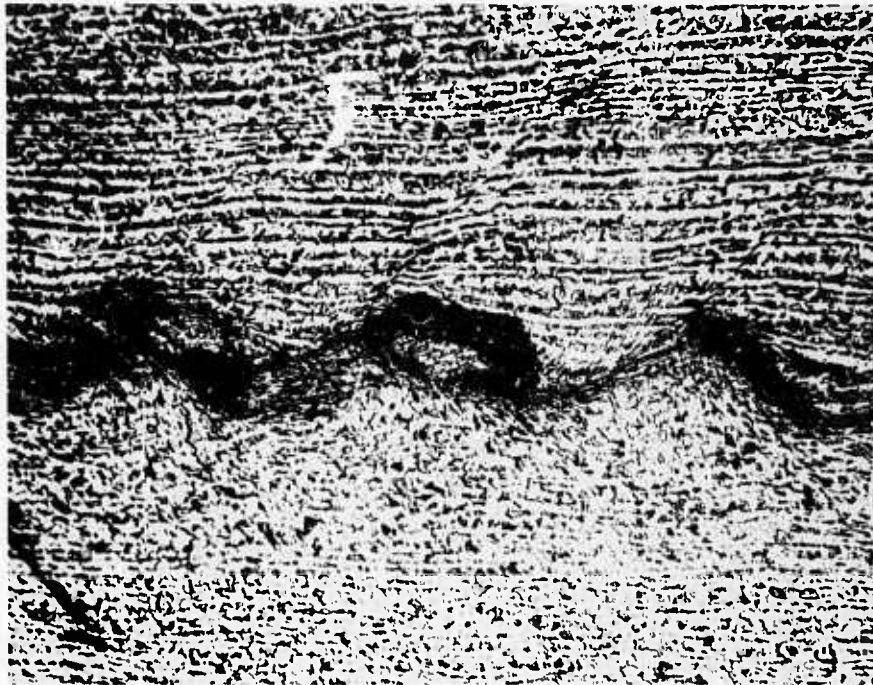
Figure 5. Cracks produced along the interface as a result of increasing
both the explosive loading and the standoff distance (X80).
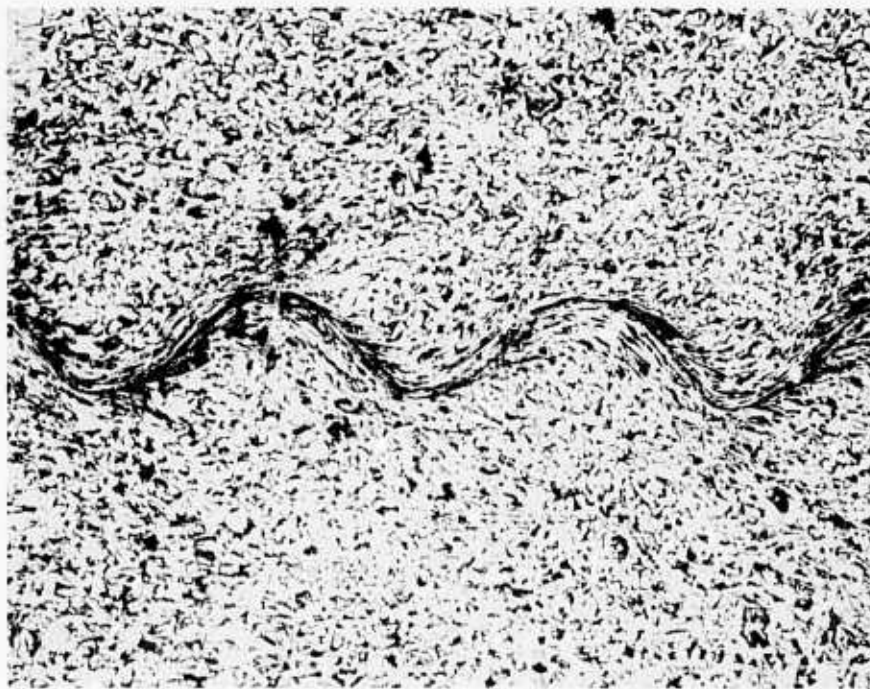
Figure 6. The regular wave pattern and absence of melt seen here is a
result of a substantial decrease in the collision point velocity (X80).

WELD
INTERFACE

.900
+.000
−.005

.700
+.005
−.000

1.50"
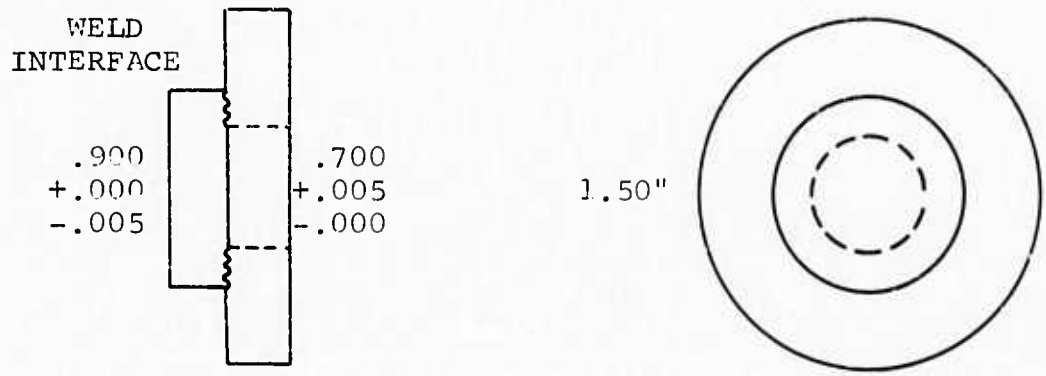
Figure 7. Details of the zero gage length tensile specimen.

LOADING RAM

WELDED INTERFACE

SUPPORT RING
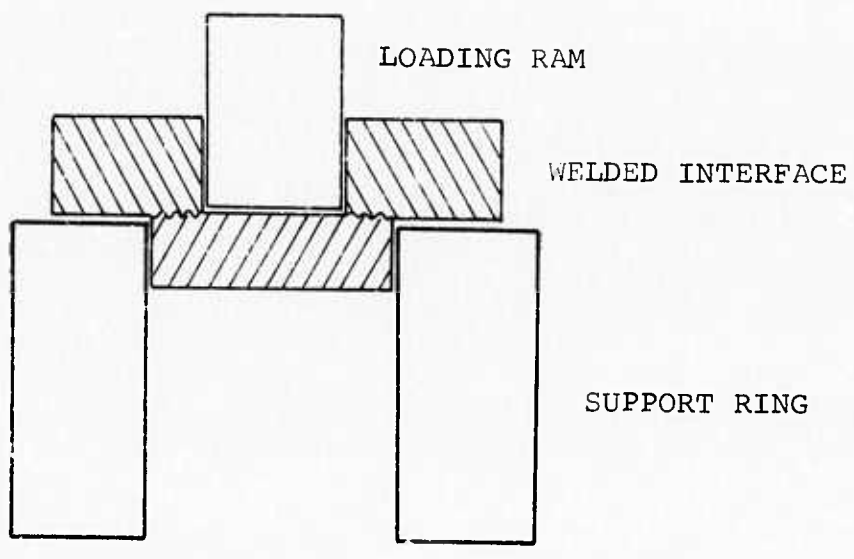
Figure 8. Details of the tensile test apparatus.

chosen was Red Cross 40% Dynamite manufactured by Dupont. It has a detonation velocity (2500-2800 m/sec) substantially less than DBA-10HV (3800-4000 m/sec) and would therefore produce a detectable difference in the wave pattern at the interface. However, due to the unavailability of Red Cross 40% Dynamite, 70% Red Cross was substituted. While the velocity of 70% (3300-3700 m/sec) is higher than 40%, it is still significantly lower than DBA-10HV.

Tests using 70% Dynamite did show some improvement but still lacked in overall quality. Tensile strengths ranged from 1,000,000 psi to 85,000 for these welds reflecting the excessive melt at the interface and hence poor weld quality. The amount of improvement was not substantial enough for definite conclusions concerning the relative importance of the collision point velocity. Consequently further tests were made using free–running dynamite also manufactured by Dupont. The detonation velocity of Red Cross free-running dynamite is much slower than most other explosives being of the order of 2000 m/sec or less, typically 1600-1800 m/sec for the explosive loading being used in these tests. Initial tests using free-running dynamite proved highly successful. The wave pattern was well defined and the tensile strength of the interface was of the same magnitude as the parent metal strength. Figure 6 shows the interface using free-running dynamite.

The objective now became over what range of explosive parameters could quality welds be produced and what material properties limited the range of welding parameters. This was accomplished in a series of fifteen tests in which the dynamic variables associated with explosive welding were measured. Measurements were obtained using a dual velocity probe technique developed by Ribovich, Watson and Gibon (5) and modified for use in explosion welding by Wittman (3). Details of the velocity probes are shown in Figure 9 and the constant current power supply used in conjunction with the probes is shown in Figure 10. The way in which the probes work is straightforward. A skip wound wire whose resistance is 87.76Ω/ft. is placed inside the aluminum cylinder and crimped at one end to provide an electrical connection. The skip wound wire is sufficiently insulated to prevent a direct short along its length, yet capable of being shorted to the aluminum cylinder if the cylinder is slightly compressed. A constant current source supplies a DC signal which is fed through the skip wound wire back through the cylinder to the oscilloscope. As either the explosive front or collision point propagates down the plate, the probe collapses changing the resistance. This signal is displayed as the vertical input on an oscilloscope with an appropriate time base on the horizontal scale. A Tectronics A555 dual beam, single sweep oscilloscope was used throughout the instrumented tests. For the majority of tests, a time scale of 10μsec/cm and 25Ω/cm were used on the horizontal and vertical scales respectively. In order to synchronize the detonation of the explosion with the oscilloscope, a switch was placed beneath the electric detonating cap. Details of the switch are shown in Figure 11. The firing cap simultaneously initiates the explosive and triggers the oscilloscope.

The result is a display like that shown in Figure 13 giving a continuous value of the distance from the initiation point versus time. A graphical differentiation of the two curves gives the values of the detonation and collision velocities. In order to improve the accuracy, the oscilloscope picture was projected and enlarged and all measurements were made from the enlargements. The time between the two slopes for a given resistance represents the time it takes for the flyer plate to travel across the standoff distance and collapse the lower probe (see Figure 14). Knowing the standoff distance from the initial conditions and the time, the plate velocity is easily calculated. The point where the top horizontal line begins to slope downward represents

8

SKIP WOUND WIRE
87.3 Ω/ft

ALUMINUM TUBING

TO CONSTANT CURRENT
POWER SUPPLY
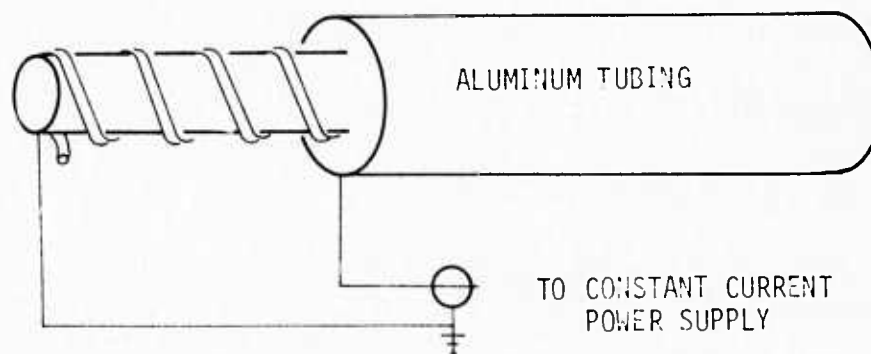
Figure 9. Details of the velocity probe.

30 Ω
2 W

2N174

e   c

mA

TO SCOPE

500 Ω
2 W

b

1N156A

TO PROBE

1800 Ω
2 W

100 Ω
1 W
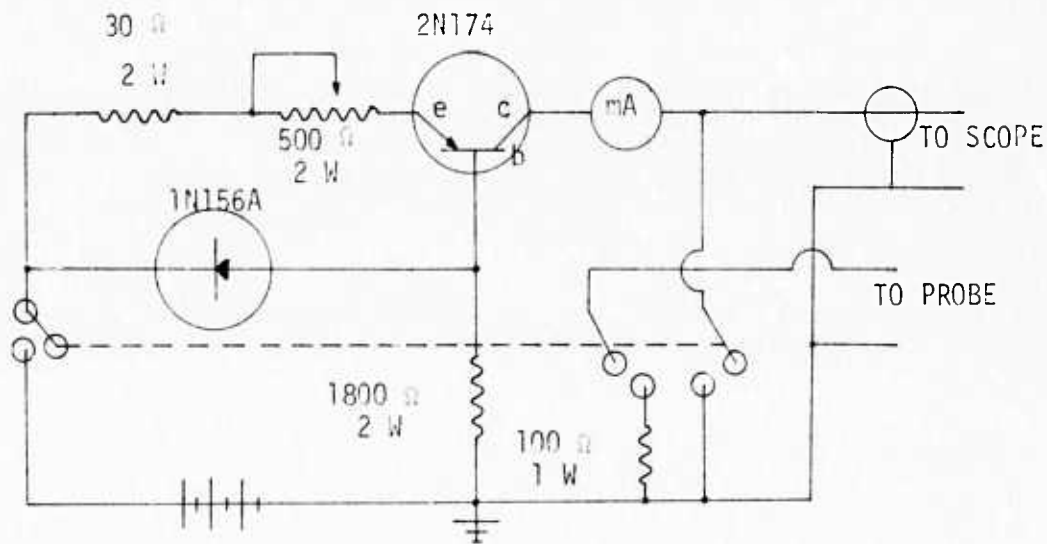
Figure 10. Details of the circuit used to supply a constant current to the velocity probe.

VELOCITY PROBE

VELOCITY PROBE

ELECTRIC
BLASTING
CAP

POWER
SUPPLY

POWER
SUPPLY

EVENT
SWITCH
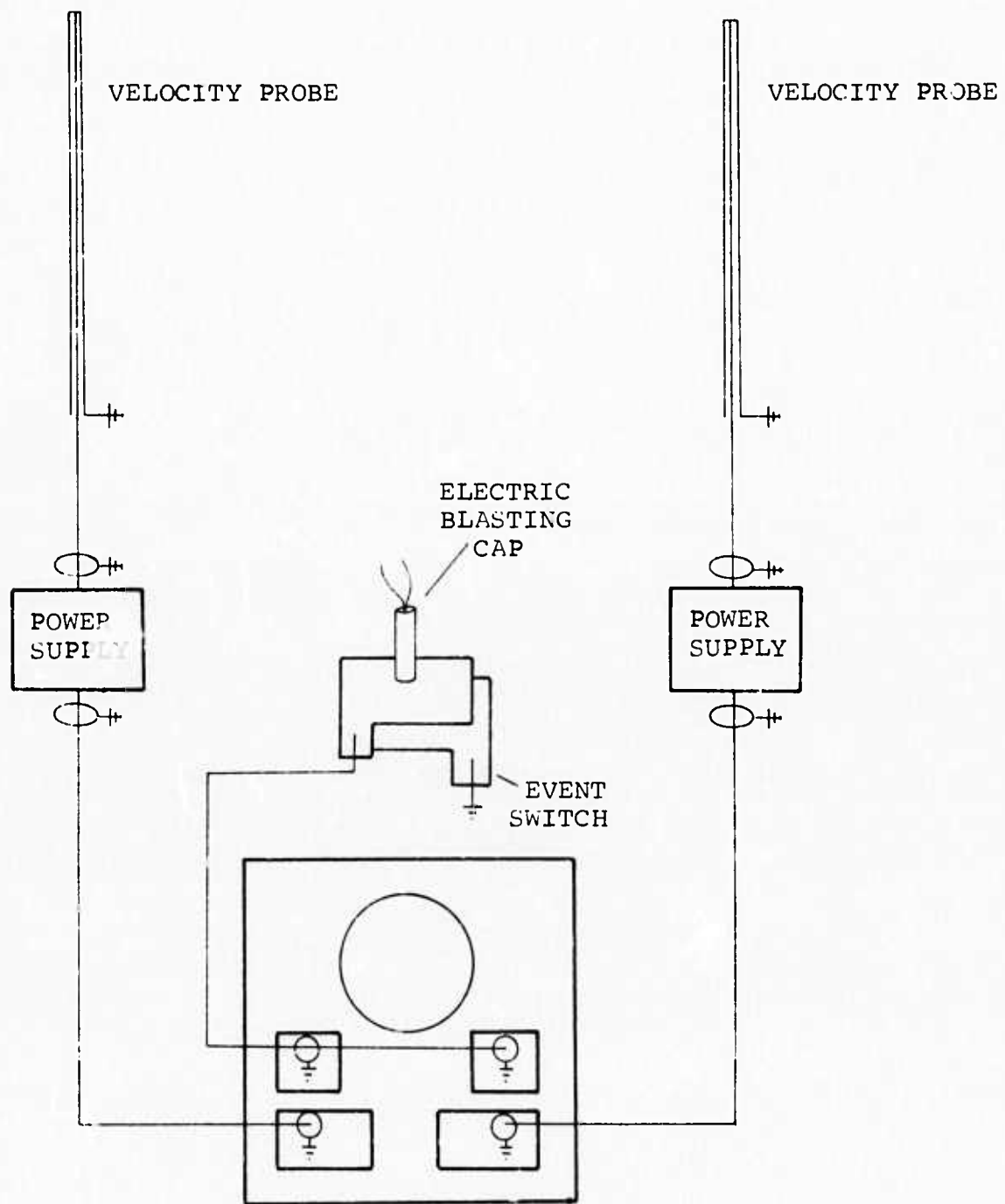
Figure 11. Circuit diagram of the velocity probes and triggering mechanism. Detonation of the electric blasting cap initiates the explosive and triggers the sweep of a dual beam, dual time base oscilloscope.

10

ELECTRIC BLASTING CAP

LINEWAVE GENERATOR

CONTAINER FOR EXPLOSIVE

VELOCITY
PROBE

FLYER PLATE

STANDOFF

BASE PLATE
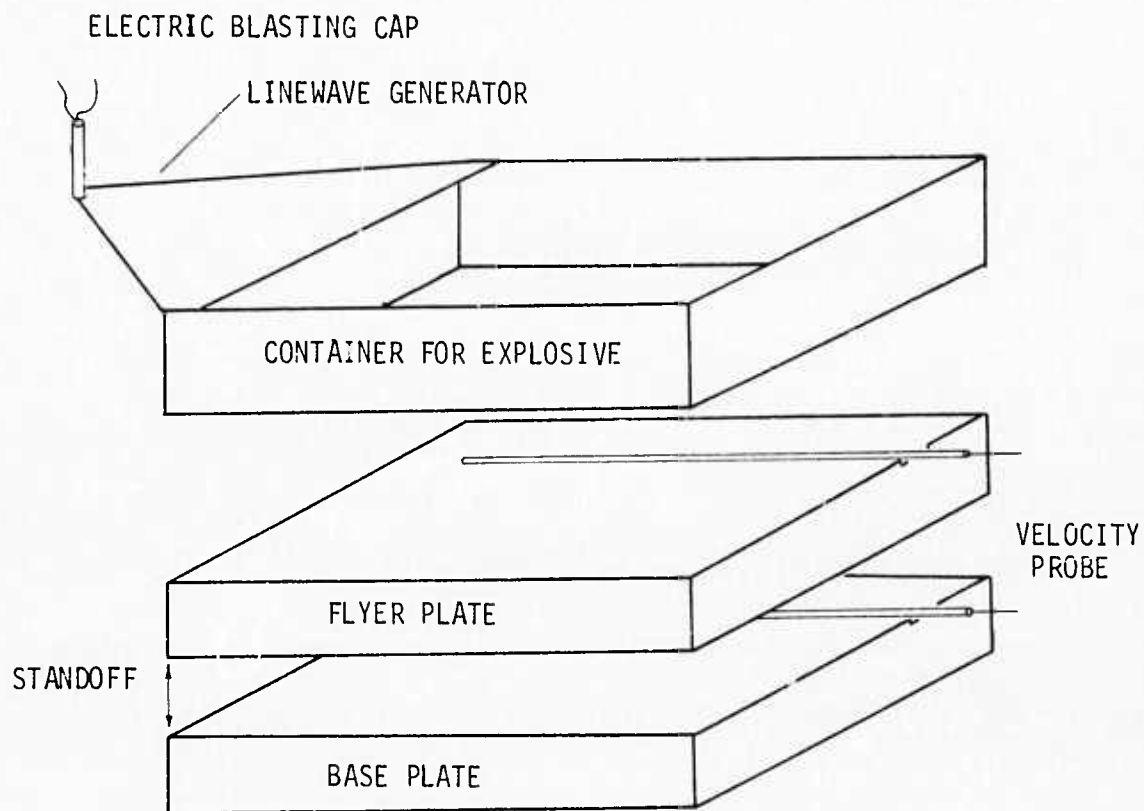
Figure 12. Arrangement of the velocity probes. The probes are of equal length and are placed one directly above the other. Each probe was placed 1-1/2 inches from the detonation end to help insure stable conditions existed before the detonation and collision points encountered the probes.
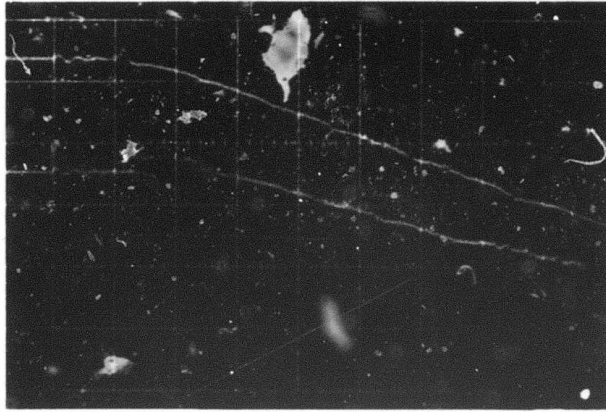
Figure 13. A typical photograph of an oscilloscope display of an instrumented shot.
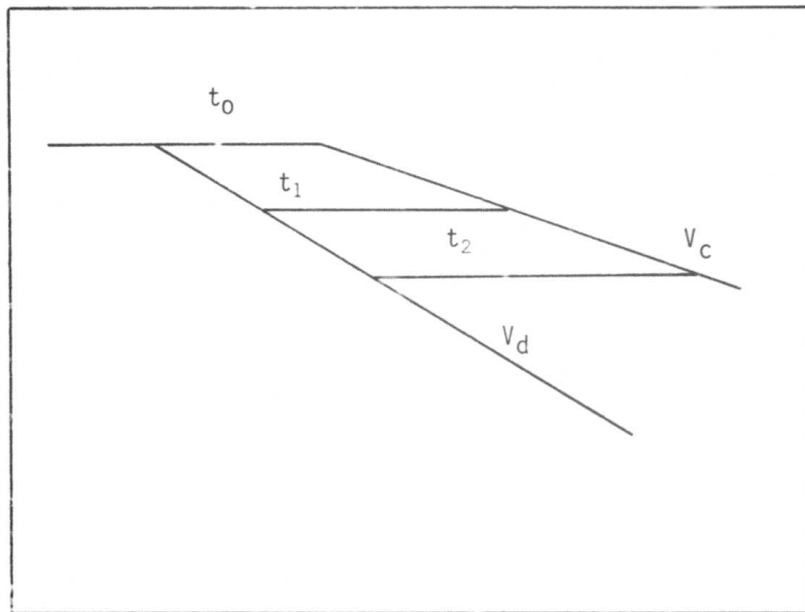
Figure 14. An enlargement of a photograph showing a method of obtaining V_p. The trace for V_c is moved vertically above V_d. The time difference, t_i, is then the time necessary for the flyer plate to travel across the standoff distance and collapse the velocity probe in the interface.

12

the detonation front arriving at the velocity probe. Since the velocity probe is located 1-1/2 inches from the detonation end of the plate, each 5Ω represents 0.6915 inches further down the plate since the skip wound wire has $87.3\Omega/\text{ft.}$, T_0 then represents the time necessary for the flyer plate to travel across the standoff distance and collapse the velocity probe at the interface. For example, at a point, say 2.0 inches down the plate the time might typically be $10.5\mu\text{sec}$. If a preset angle $\alpha = 5.0^\circ$ were used, the distance the flyer plate would have to travel would be $4.42 \times 10^3 \text{M}$. The plate velocity would then be 421 M/sec. Using the relationship that $V_d \sin\beta = V_p$, or $\beta = \sin^{-1}\dfrac{V_p}{V_d} = 4.5^\circ$. Since $\gamma = \beta + \alpha$, then $\gamma = 9.5^\circ$. Using $V_p = V_c \sin\gamma$, $V_p = 2500$ m/sec. This procedure is repeated for points down the plate and the result is a graph shown in Figure 15. The collision and dynamic bend angles are calculated using the relationships shown in Figures 16, 17, and 18. It is then possible to recalculate a more accurate instantaneous collision point velocity using the calculated data rather than using the slope which gave an average velocity.

The mechanical properties as well as the dynamic conditions that produced the properties of the welds can be succinctly displayed. From the geometry of the explosive weld configuration (see Figures 16, 17, 18)

$$V_c = V_p \, \text{Csc}\gamma$$

Plotting $V_c = V_p \text{Csc}\gamma$ with the collision velocity on the abcissa and the collision angle on the ordinate results in the graph shown in Figure 19. The criteria for successful welds are as general as possible: the tensile strengths are equal to or greater than parent metal strength and the interface showed little or no melt accompanied by a well-defined wave pattern.

Figure 19 has been redrawn in Figure 20 in such a way that the area inclosed by the solid lines represents the successful welds in Figure 19. The broken line will be discussed below. The three boundaries of the welding window (inclosed by solid lines) are explained in the following way. The minimum collision velocity is the transition velocity predicted by Cowan et. al. (6). The model was shown to be accurate in predicting the transition point velocity and is further verified by corresponding closely with the experimental determined boundary for quality welds. The plate velocity has been used as a criterion for welding by Keller (7) and Carpenter et. al. (1). In both studies. the plate velocity is associated with providing enough pressure to deform the surface plastically. In a paper by Wittman (3), the minimum plate velocity is found by multiplying the Hugoniot elastic limit pressure by five and converting the pressure value into impact velocity. This result can be closely approximated, according to Wittman, by the emperical relationship

$$V_p = \left(\frac{\text{UTS}}{P}\right)^{\frac{1}{2}}$$

Where UTS is the Ultimate Tensile Strength given as dynes/cm^2 and p is the density in grams/cm^3. For example, the UTS for A515 steel is approximately 77,000 psi (5.48×10^9 dynes/cm^2) and the density of mild steel is 7.86 grams/cm^3. The minimum plate velocity for welding mild steel would then be approximately 260 m/sec, which closely parallels the experimently found plate velocity in Figure 19. The maximum plate velocity is also shown to be a material based limit by Wittman (3).

13
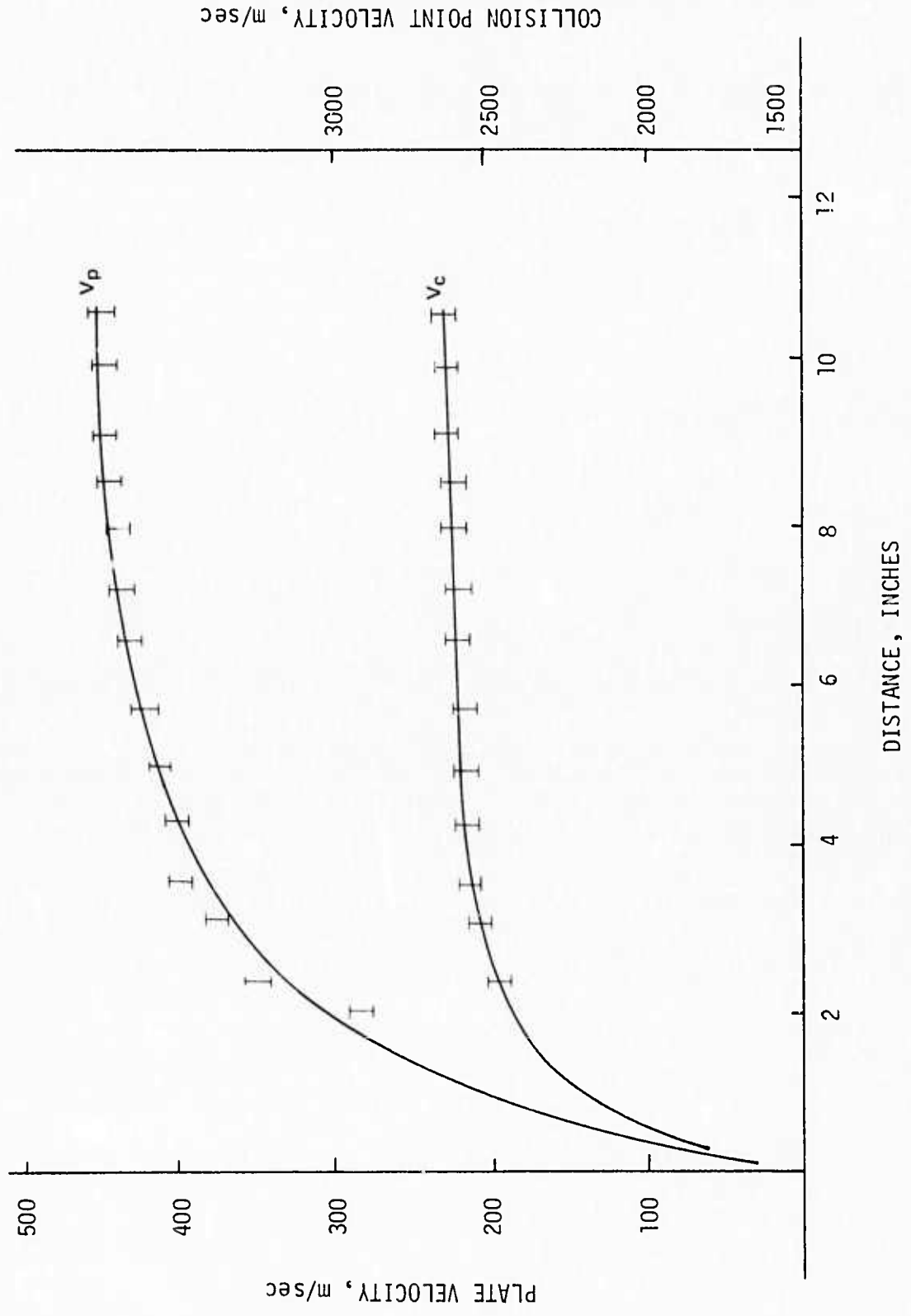
Figure 15. Velocity profile for a typical test. The distance is the distance from the initiation end of the plate. The probes are placed 1-1/2 inches from the end to avoid the unstable conditions at the beginning of welding.
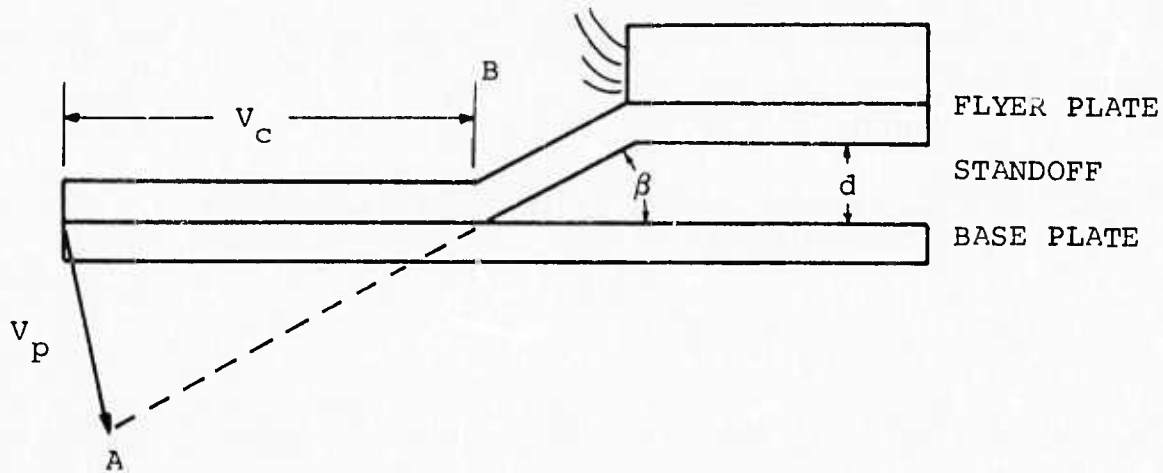
The flyer plate would have traveled a distance A
if it hadn't collided with the base plate. During
the same time period, the collision point has gone
a distance B. Redrawing the triangle below

$$\sin \beta/2 = \frac{V_p/2}{V_c}$$

$$2V_c \sin \beta/2 = V_p \qquad \text{FOR SMALL ANGLES}$$

$$V_c \sin \beta = V_p$$
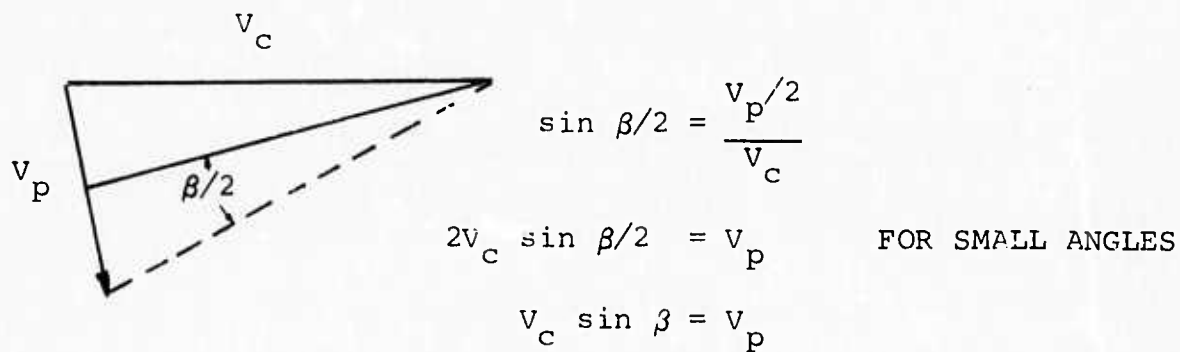
where V_c = collision point velocity

        V_p = flyer plate velocity

        β = collision angle

Figure 16. Diagram showing explosive welding for parallel plate geometry.
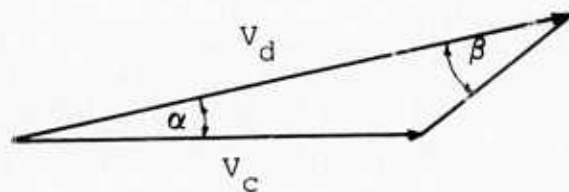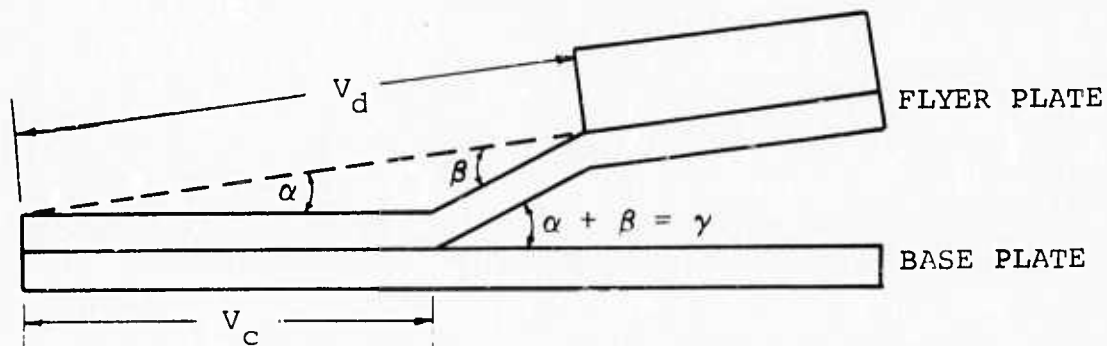
$$\frac{V_c}{\sin \beta} = \frac{V_d}{\sin [\tau - (\alpha + \beta)]}$$

$$\frac{V_c}{\sin \beta} = \frac{V_d}{\sin (\alpha + \beta)}$$

$$V_c = \frac{V_d \sin \beta}{\sin (\alpha + \beta)}$$

Where V_d = detonation velocity

V_c = collision point velocity

β = dynamic bend angle

γ = collision angle

α = preset angle

Figure 17. Diagram showing determination of collision point velocity for non-parallel welding configuration.

16

EXPLOSIVE
FLYER PLATE

BASE PLATE

V_d

α

β

γ

V_p

V_d

V_d

$\beta/2$

$V_p/2$
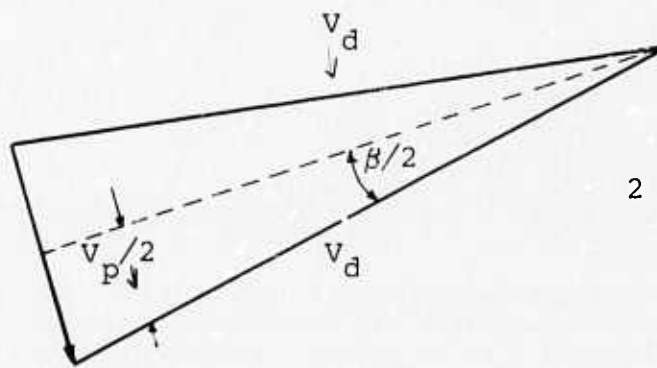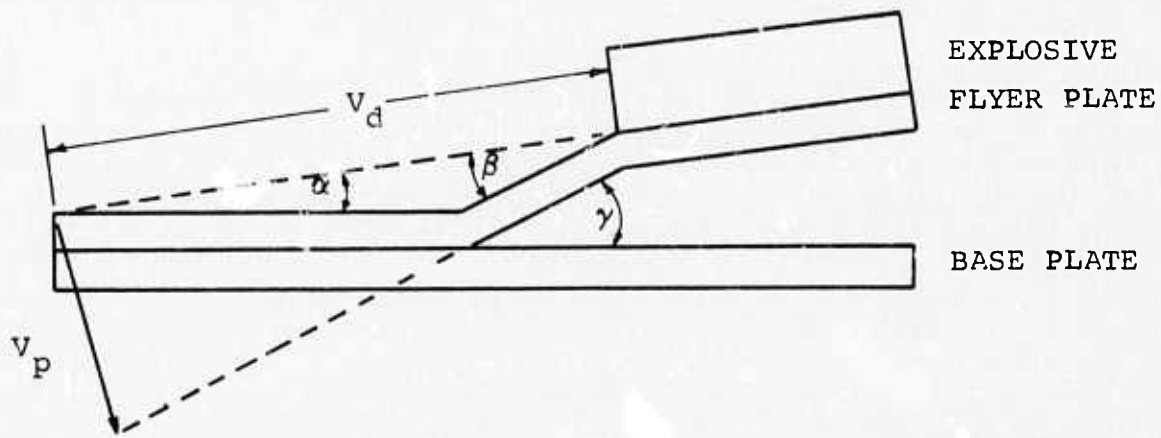
$$\sin (\beta/2) = \frac{V_p/2}{V_d}$$

$$2 V_d \sin \beta/2 = V_p$$

$$V_p = V_d \sin \beta$$

Where α = preset angle

γ = collision angle

β = dynamic bend angle

V_d = detonation velocity

V_p = plate velocity

Figure 18. Determination of flyer plate velocity for preset angle configuration.

17
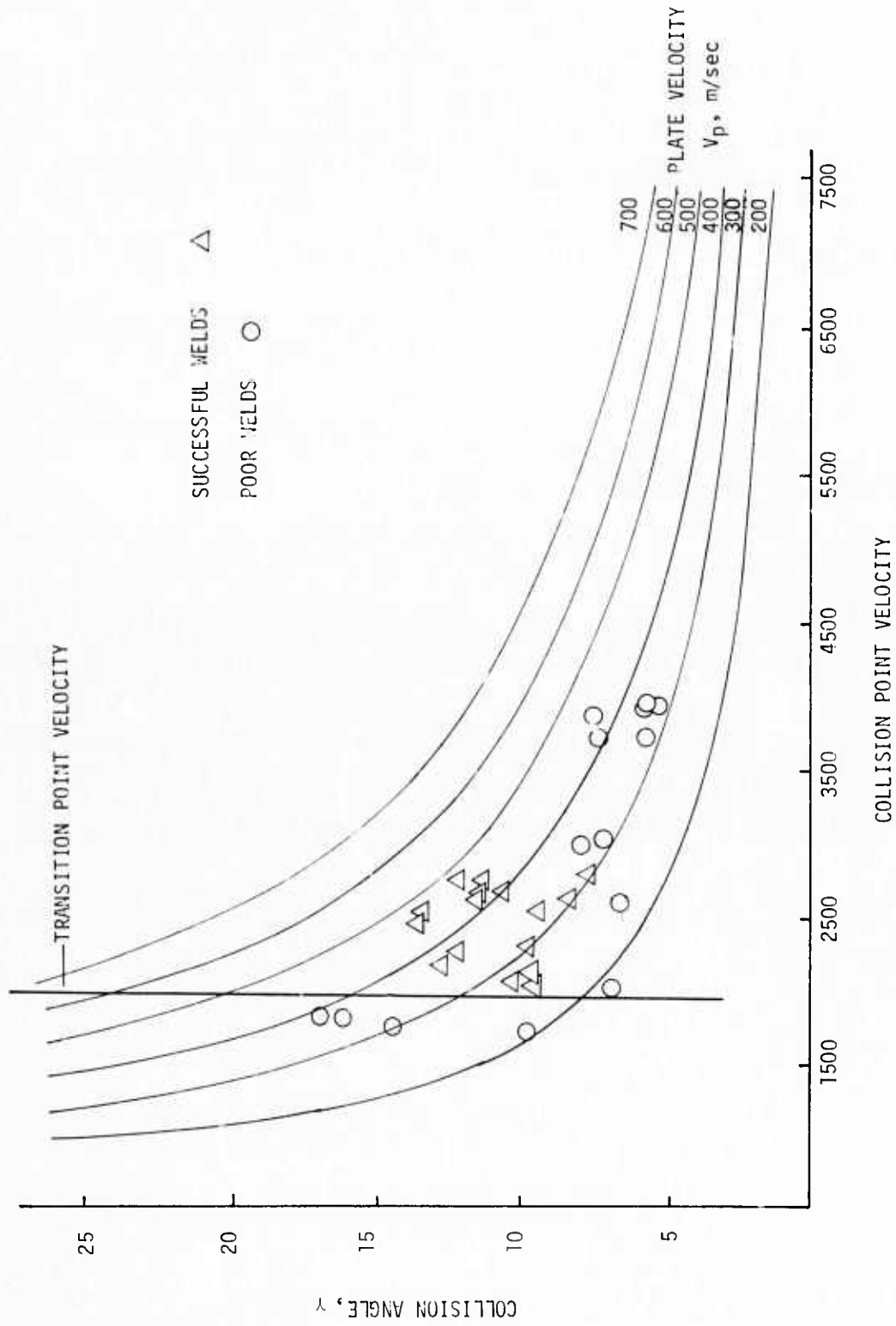
Figure 19. From this display, the grouping of the successful welds indicates a limited range over which quality welds can be obtained.

18
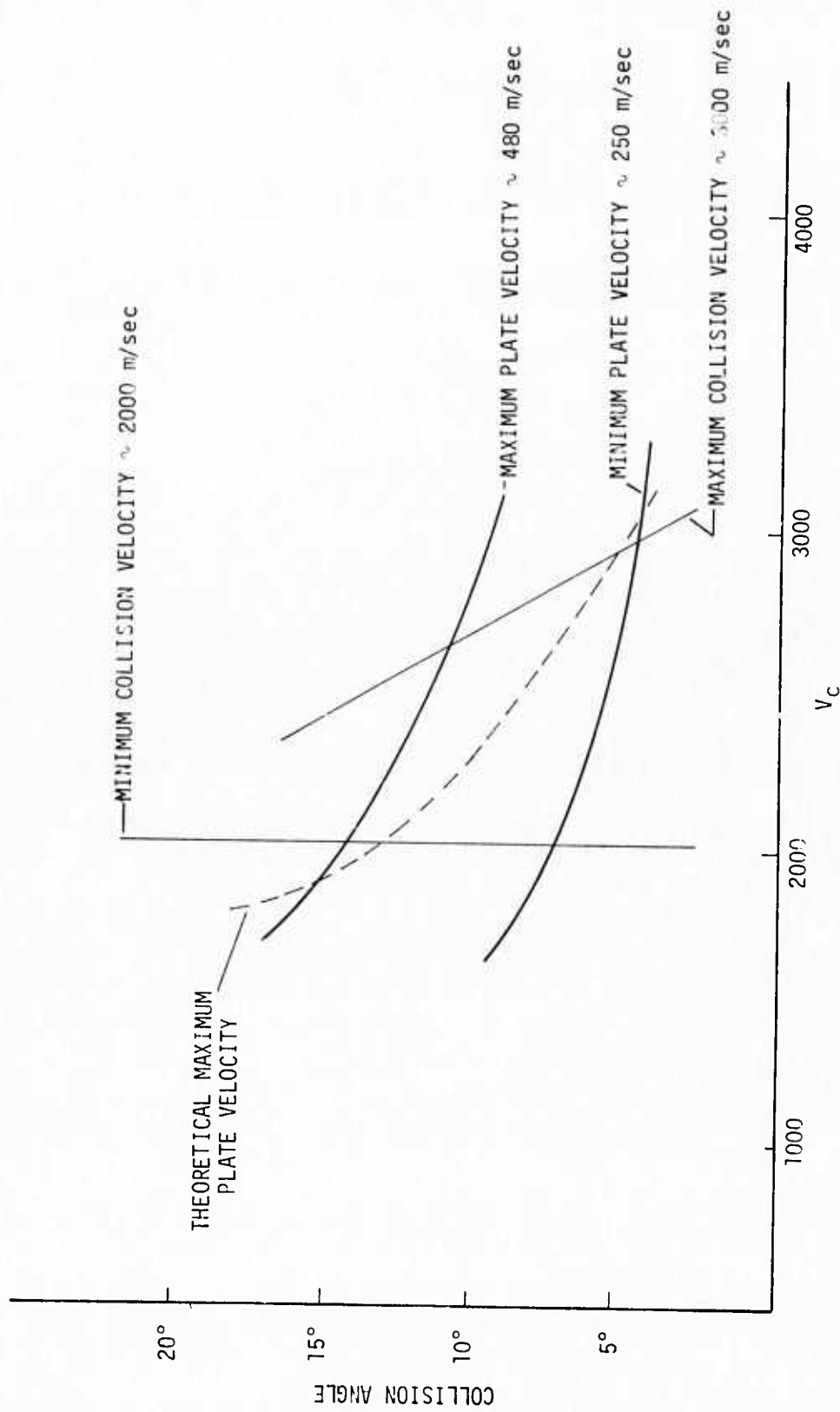
Figure 20. The experimental limitations in Figure 19.

19

As a minimum plate velocity is necessary to cause sufficient deformation, too high a plate velocity causes excessive deformation and consequently melting. A compression wave is generated at the collision point and reflects from the plate surface as a tension wave. If melt is present at the interface when the reflected wave passes through the melt zone, the weld is apt to rupture. The expression derived by Wittman relating the limiting plate velocity to the melting temperature of mild steel is

$$V_p = (Tmp)^{1/2} (3.88 \times 10^8) \, \overline{h}^{-1/4} \, V_c^{-1}$$

Where Tmp is the melting temperature given in degrees centigrade, h is the flyer plate thickness in centimeters, and V_c is the collision point velocity in cm/sec. This boundary has been plotted as a dashed line in Figure 20. A partial explanation as to why the theoretically derived value for maximum plate velocity fails to inclose all successful welds is in the assumption that the melt layer is continuous. In reality the melt layer is broken up and may comprise only a small fraction of the total interfacial surface area. This consideration would have the effect of raising the value of the maximum plate velocity which would then include the experimentally obtained quality welds.

It can be concluded then that the range of optimum welding parameters for A515 Grade 70 steel have now been determined and that they are located within the welding window shown in Figure 20. In addition, the technique developed for determining the optimum welding parameters for A515 steel can be extended and used to determine the welding parameters for other metals in both similar and dissimilar welding situations. The final objective of being able to weld nickel-to-steel is now a straightforward extension of the technique developed for steel-to-steel welds. Figure 21 shows a weld between nickel 200 and mild steel using the technique developed for steel welds.

Aluminum-To-Steel

The aluminum-to-steel welds were done using 6061 aluminum flyer plates in the 0-condition which were 1/4 in thick and mild steel base plates. The results clearly demonstrate the limitations of the methods used to calculate the welding parameters and at the same time raise several questions concerning the fundamental processes involved in explosion bonding.

Figure 22 shows the welding parameters of the tests that will be discussed below. The vertical lines represent the welding conditions that produced the results shown in the photomicrographs 23 through 27. Figure 23 shows the interfacial conditions that one would normally expect with a collision point velocity near that of the transition point and a plate velocity near that of the minimum value. In Figure 24, however, the results are not what one would expect based on results of steel-to-steel with aluminum-to-aluminum welds. In tests in which like metals are being welded, the parameters from a similar area of the welding window produce excellent welds characterized by regular wave formation and an absence of excessive melt. It is expected that some melt would be produced at the interface as a result of the large differences in melting temperatures and mechanical strengths of 6061-0 aluminum with mild steel. However, the interfacial conditions produced by the optimum parameters in Figure 24 do not differ substantially from those seen in Figures 25 and 26. The plate velocity for Figure 25 is
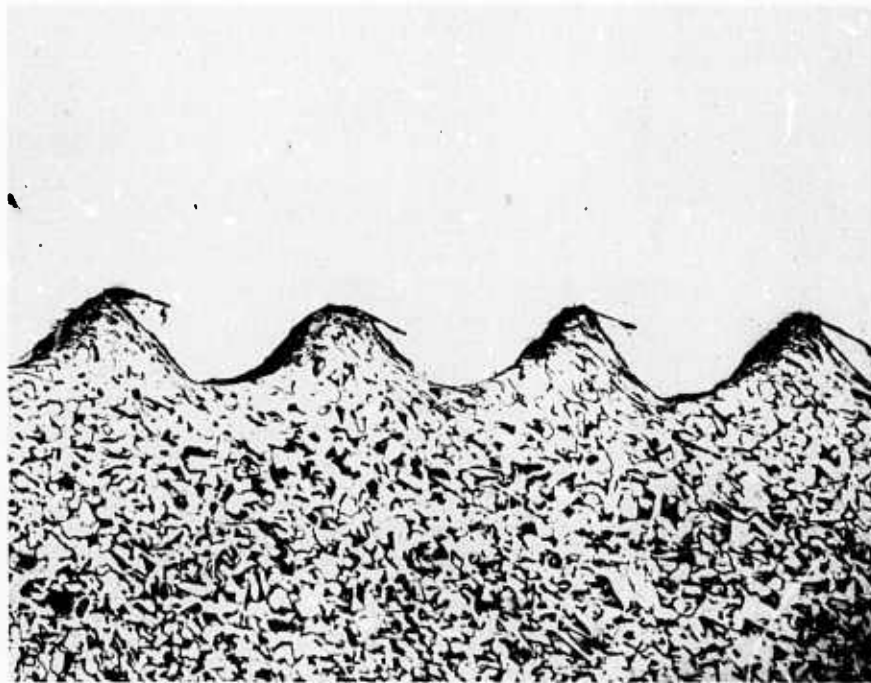
Figure 21. Interfacial conditions between nickel 200 and mildsteel.

21
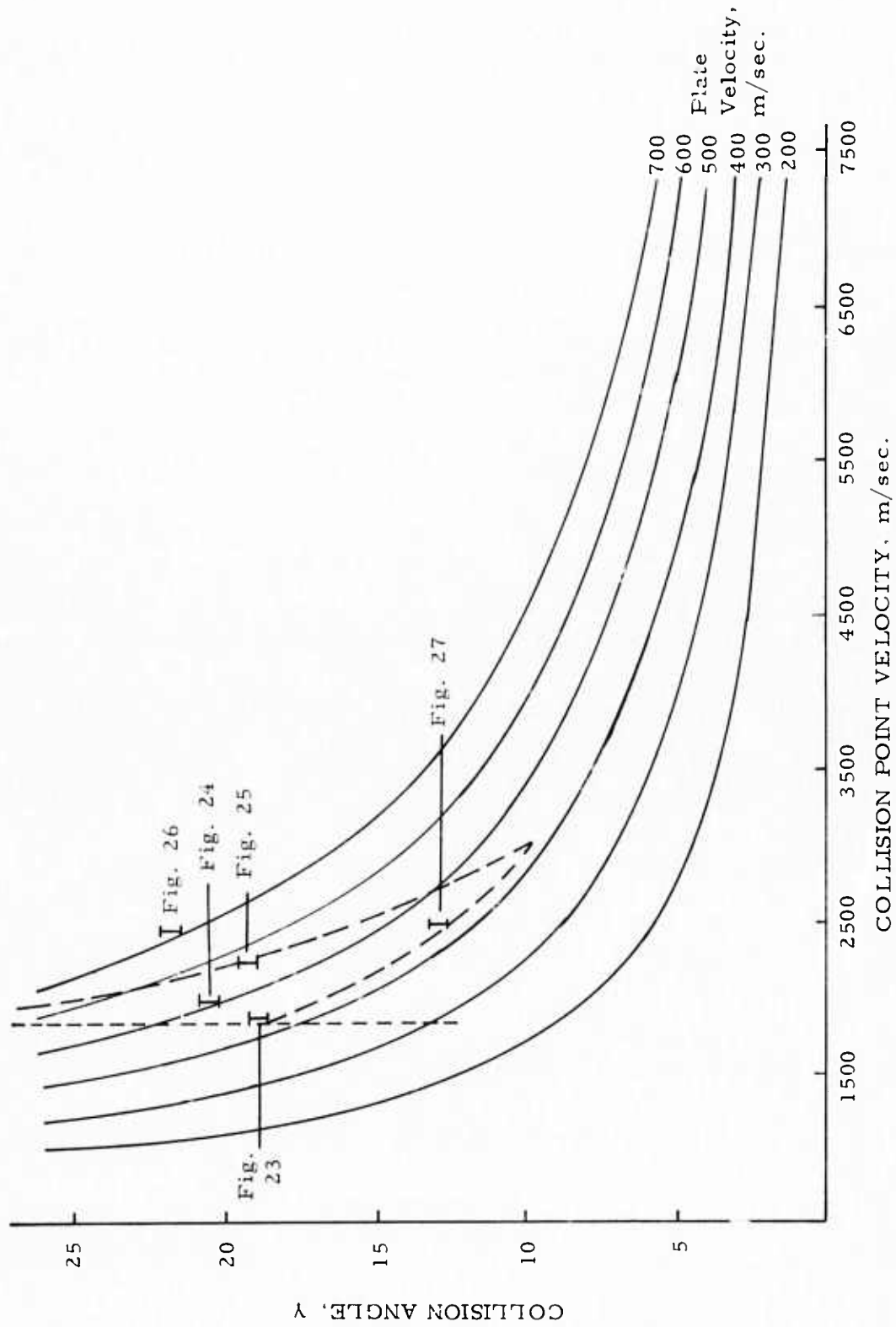
Figure 22. Display giving welding parameters which generated the interfacial conditions seen in Figures 23 through 27.

22
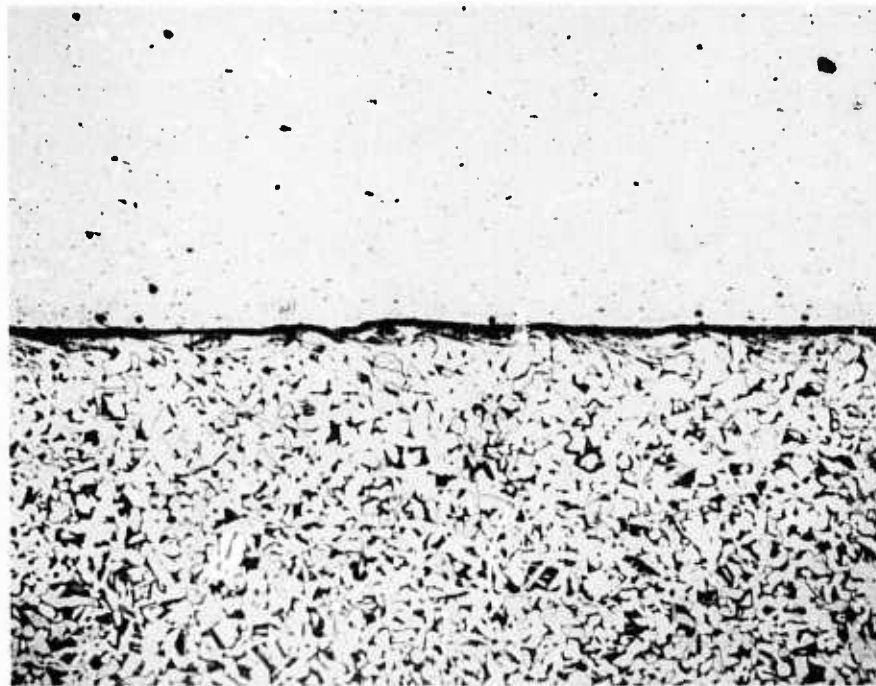
Figure 23. Interfacial conditions resulting from a plate velocity of ∿400 m/sec and a collision point velocity of ∿1800 m/sec (X75).
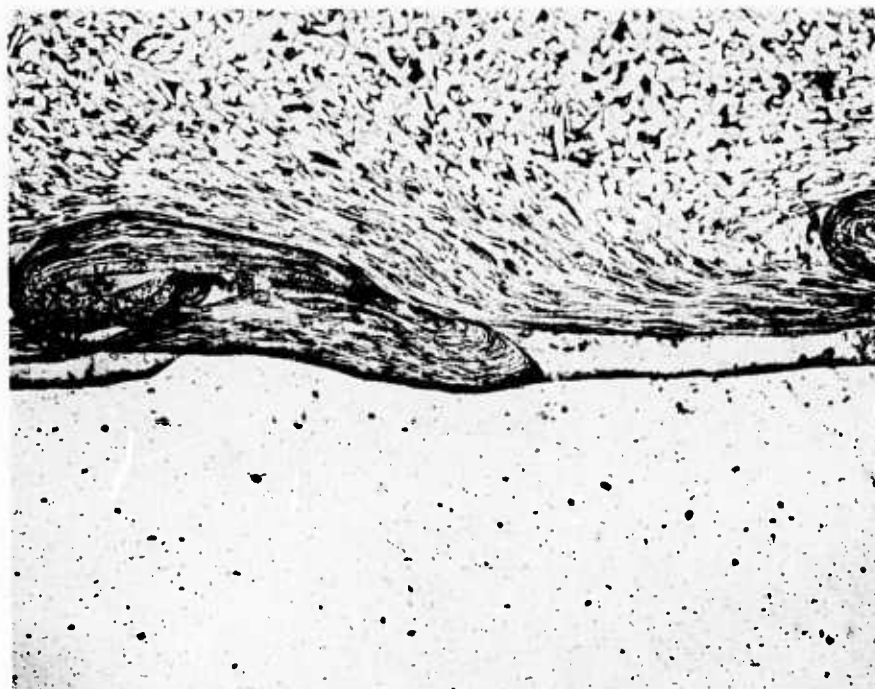
Figure 24. Interfacial conditions resulting from a plate velocity of ∿520 m/sec and a collision point velocity of ∿2000 m/sec (X75).
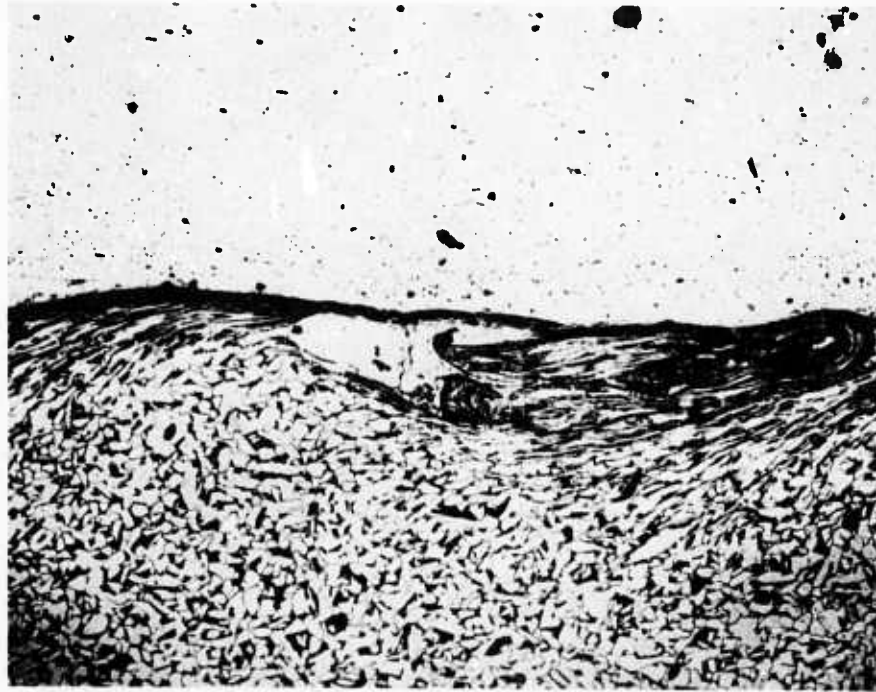
Figure 25. Interfacial conditions resulting from a plate velocity of ∿580 m/sec and a collision point velocity of ∿2250 m/sec (X75).
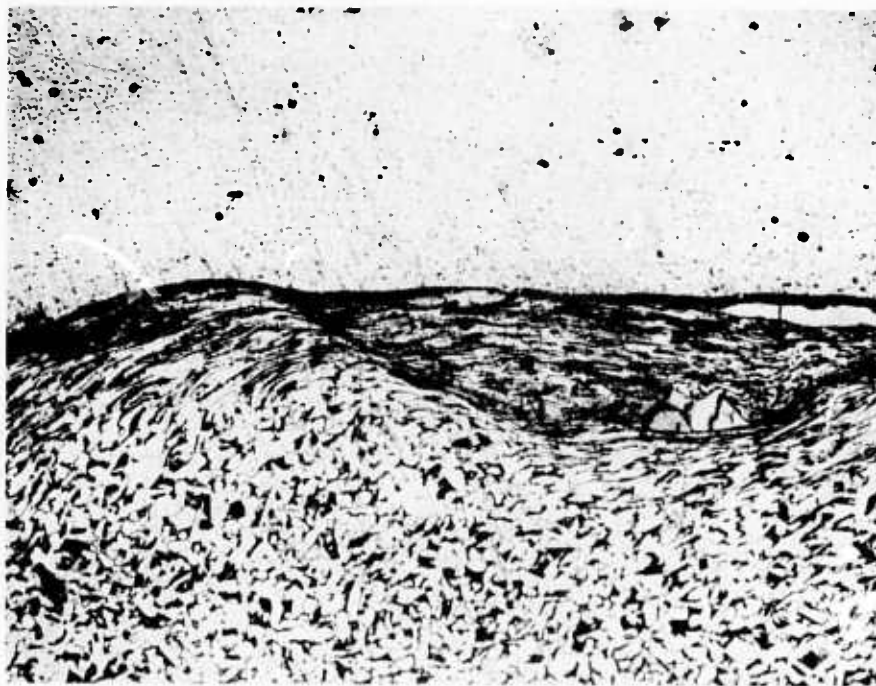
Figure 26. The interfacial conditions resulting from a plate velocity of ∿630 m/sec and a collision point velocity of ∿2350 m/sec (X75).
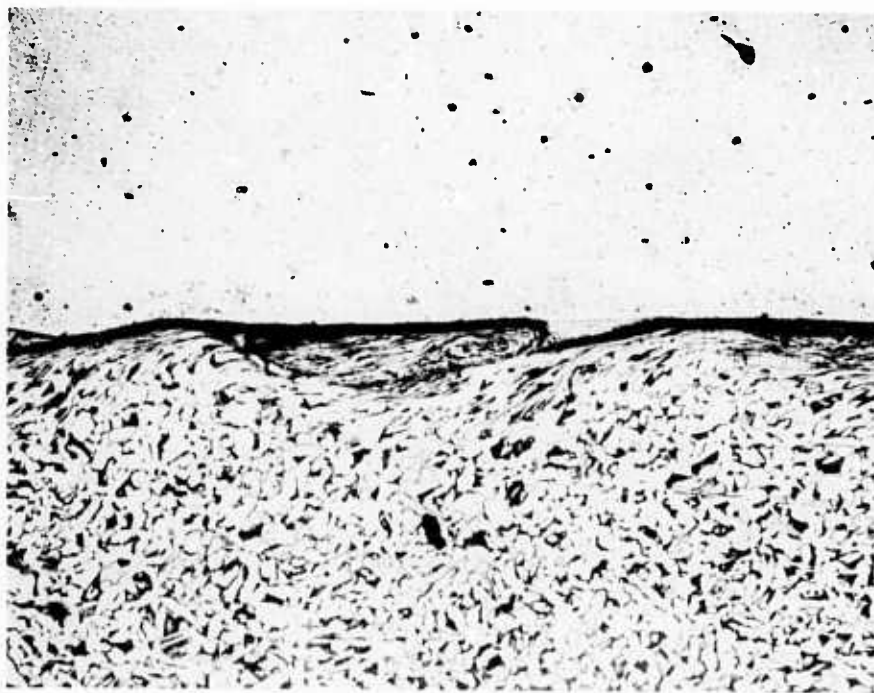
Figure 27. Interfacial conditions resulting from a plate velocity of ∿460 m/sec and a collision point velocity of ∿2500 m/sec.

at the theoretical maximum and that for Figure 26 is well beyond the theoretical maximum. In Figure 27, the smeared-out wave form is again what is expected for a high collision point velocity.

Several conclusions can now be made concerning the techniques used to obtain welding parameters. Those involving the onset of welding conditions—i.e., minimum plate velocity and minimum collision point velocity can be used fairly accurately and consistently even though perhaps not completely understood theoretically. However, the upper parameters limiting explosive welding, in particular, the maximum plate velocity is less understood. Why do welds exist outside the maximum plate velocity limit and why doesn't the interfacial conditions seen in Figure 24 differ more from Figure 25 and 26? Perhaps further experiments would show that the maximum plate velocity falls below even those values in Figure 24. What this seems to lead to is that while the model developed by Wittman (3) can be useful for obtaining welding parameters (Max. V_p) for welds between steel and steel and aluminum-to-aluminum, it fails to fully explain the results of welds between aluminum and steel. Since the Wittman model (3) deals with the thermo-mechanical properties of the metals being welded, either these considerations are too limited in their scope of application or there are other factors which need to be considered. In addition to the theoretical questions raised, more work needs to be done concerning the mechanical properties of the aluminum-to-steel welds.

REFERENCES

1. S.H. Carpenter and R.H. Wittman, *A Preliminary Investigation of Nickel, Steel, and Nickel/Steel Welding,* Center for High Energy Forming, Final Report June 1972, pp. XIV-5 to XIV-16.

2. R.H. Wittman, *The Effect of Explosive Loadings and Heat Treatment on the Mechanical Properties of 6061 Aluminum Alloy Explosive Welds,* Center for High Energy Forming, Final Report June 1972, pp. XIV-7 to XIV-43.

3. R.H. Wittman, *The Influence of Collision Parameters on the Strength and Microstructure of Explosion Welded Aluminum Alloy,* 2nd International Symposium, "Use of Explosive Energy in Manufacturing Metallic Materials of New Properties, Marianske Lazne, Czechoslovakia, October 1973.

4. H. Kolsky, *Stress Waves in Solids,* Dover Publishing Company, New York, 1963.

5. J. Ribovich, R.W. Watson, and F.C. Gibon, *Instrumented Card Gap Test,* AIAA Journal, Vol. 6, No. 7, July 1968, pp. 1260-63.

6. G.R. Cowan, O.R. Bermann, and A.H. Holtzman, *Mechanism of Bond Zone Wave Formation in Explosion-Clad Metals* Metallurgical Transactions; Vol. 2, Nov. 1971, pp. 3145-3155.

7. K. Keller, E. Hornbogen, and A. Burkhardt, *Transition to Turbulent Flow in Crystals,* Z. Metallkde, 58 (1967).

II. DIFFUSION STUDIES IN EXPLOSION WELDED METALS

Faculty Advisor: S. H. Carpenter
Graduate Student: M. D. Nagarkar

The following is a summary of the studies conducted by Mr. Nagarkar in partial fulfillment of the requirements for a Doctor of Philosophy degree from the Chemical Engineering and Metallurgy Department, University of Denver. Mr. Nagarkar is scheduled for graduation in August, 1974.

Introduction

After going through an extensive research and development stage, explosion welding has become a viable commercial process. It has, however, not been adopted as a large scale fabrication or manufacturing process, but in some cases, explosion welding is a suitable substitute for the conventional joining methods. Before going into the main topic of this paper, we shall review briefly the mechanism of explosion welding.

Explosion welding is basically a joining process where an explosive is used to impact two metal plates to be joined. Figure 1 illustrates the basic set-up used for the welding process. There are also other configurations which may be used. To achieve successful welding, two factors are critical: the velocity at which the flyer plate collides, and the angle of collision. The process parameters which control the explosion welding process are:

1. the physical and mechanical properties of the metals to be joined.
2. the type and quantity of explosive used.
3. the initial interface configuration.

Explosion welding results in a solid state metal-to-metal bonding, and normally the weld interface has a wavy or rippled interface, as illustrated in Figure 2. It is also possible to obtain an explosion weld with a straight interface by using a symmetric angled configuration.

The mechanism of wave formation has been extensively studied and the rippled profile is said to be the result of a jetting action at interface. The jet is a mixture of liquid and vapor of the two metal surfaces, thus causing effective removal of surface contaminants such as oxides, nitrides etc. Hence, two virgin metal surfaces are brought in close atomic contact to effect good, metallurgical bonding. The bond strength of explosion welds have often been found to exceed the strength of the parent plates.

One fact which is of significance in explosion welding is the tremendous amount of plastic deformation taking place at the interface as a result of the collision. The extent of deformation is illustrated in Figure 3. The figure shows an explosion weld of two composites made of alternate layers of Cu and Ni. Near the interface the one mil layers have been reduced or enlarged in area by approximately 90%. Note, even with the extreme cold working near the interface, 10 mils either side of the interface the material appears undisturbed. Measurements made of the change in the interface length in our studies the increase in the length was found to be approximately 133%. These measurements along with Figure 3 give indications of the intense plastic deformation and metal flow occurring at the interface. This effect has an important bearing on the observed diffusion results, which will be dealt in detail later.
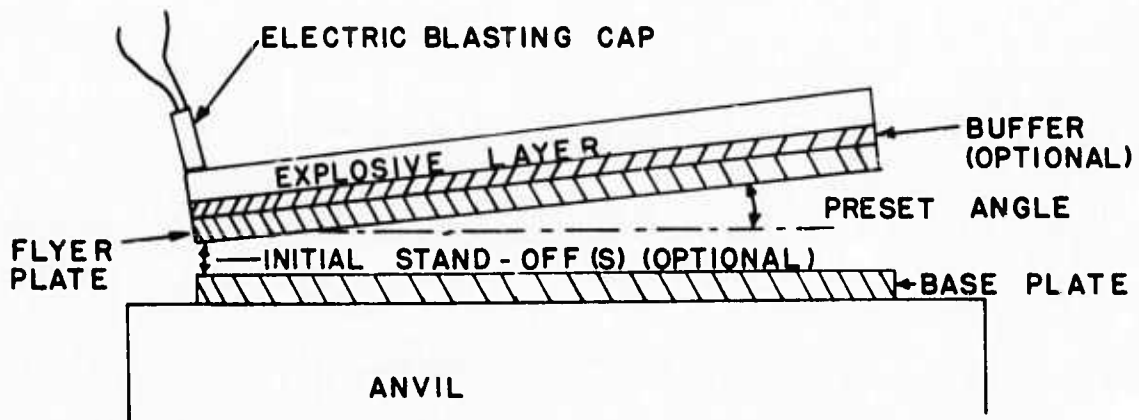
Figure 1A. Preset Angle Standoff Explosion Welding Configuration.
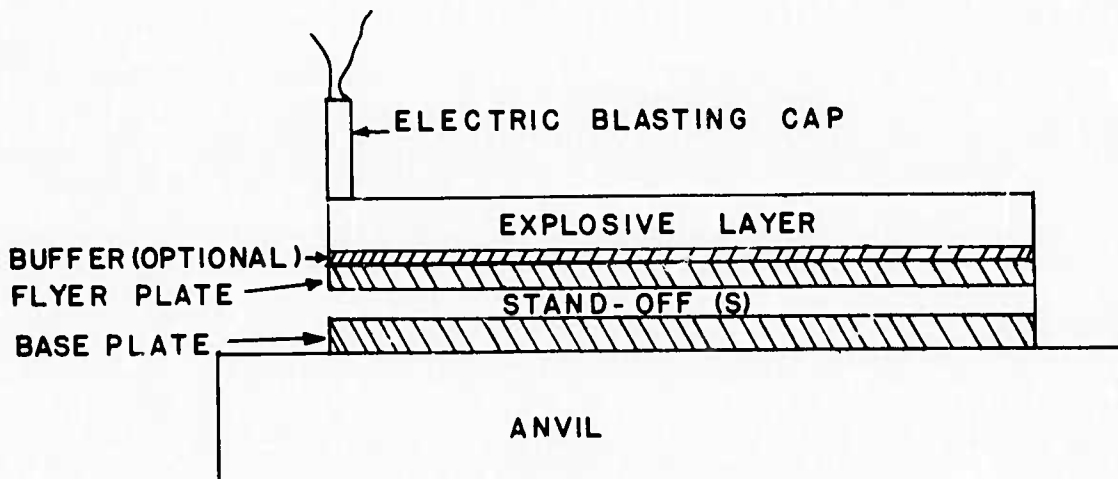
Figure 1B. Parallel Plate Standoff Explosion Welding Configuration.
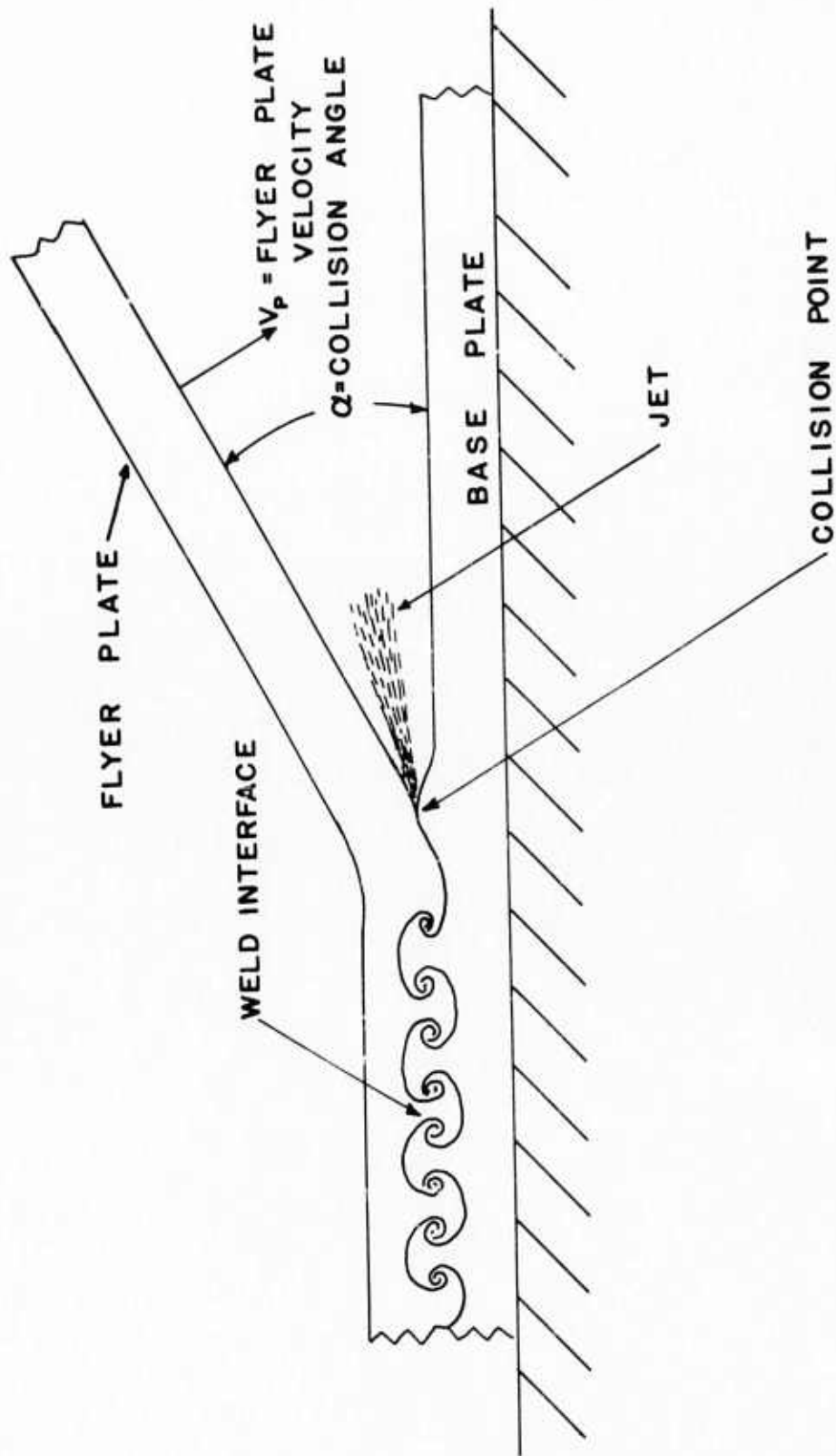
Figure 2. Sketch illustrating an Oblique Collision of Metal Plates during a typical Explosive Welding Operation.

30
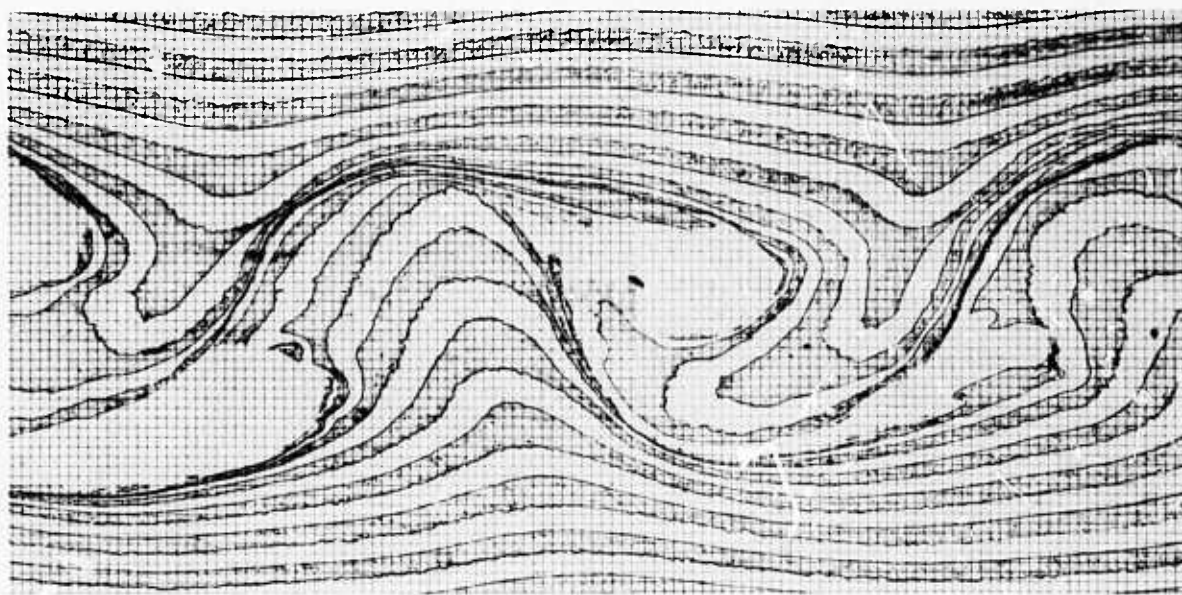
Figure 3. Explosion weld interface of welded composites fabricated of alternate layers of 1 mil Cu and Ni. Each square 0.0005" x 0.0005". (With permission of R.H. Wittman).

One unique advantage of explosion welding over other conventional joining techniques is its ability to weld or clad a variety of combinations of metals. Even such hard to join metals, such as, aluminum and steel, or lead and steel, have been successfully bonded. The success of any welding operation is judged by its ability to form a metallurgical bond between the two metals and to produce a joint of the desired strength. Equally important is the performance of the weld under service conditions where extraneous factors, such as, temperature, stress, strain etc. come into play.

When explosion welding brings into intimate contact two dissimilar metals at the interface there is a sharp transition from one metal to the other. Under the influence of temperature, depending on the metals in the couple, reactions which could occur would include:

1. Formation of a solid solution resulting from diffusion across the interface.
2. The development and growth of new phases or intermetallic compounds at the interface.

These diffusion reactions will be governed by:

1. The duration and magnitude of the service temperatures.
2. The amount of plastic deformation and hence, the amount of strain energy at the interface.
3. The defect density and defect structure at the interface.

Explosion welding is a dynamic process which involves high pressures and temperatures of short duration and a considerable amount of plastic deformation at the weld interface. The present investigation was directed towards determination of the effects such a welding process would have on the diffusion kinetics at the interface.

Experimental

The material used in this study were copper and nickel. selected mainly on account of their mutual unlimited solid solubility. The raw material was obtained in the form of commercially roll-bonded copper-nickel strips from Texas Instruments, Attleboro. The diffusion couple was prepared by explosively welding the Cu-Ni composites to one another. and the final sample had a configuration shown in Figure 4.

The weld was prepared by using parallel plate arrangement with a standoff equal to the thickness of the cladder plat   Each layer is 50 mil thick.

The weld piece had three interfaces:

1. A roll-bond interface in the cladder plate
2. An explosion weld interface
3. A roll-bond interface in the base plate

Specimens for diffusion annealing were cut from this weld piece and thus it was possible to compare the diffusion characteristics in the roll-bonded interfaces and the explosion weld interface. The specimens were annealed at 500°, 750°, 900°. and 975°C for 10 hours in a vacuum furnace. These temperatures roughly correspond to 0.6, 0.7, 0.8, and 0.9 respectively of the melting temperature of copper. Plain roll-bonded Cu-Ni composite specimens were also annealed at the same time along with the explosion welded specimens.

32

Ni

Interface 1

Cu

Interface 2

Ni

Interface 3

Cu
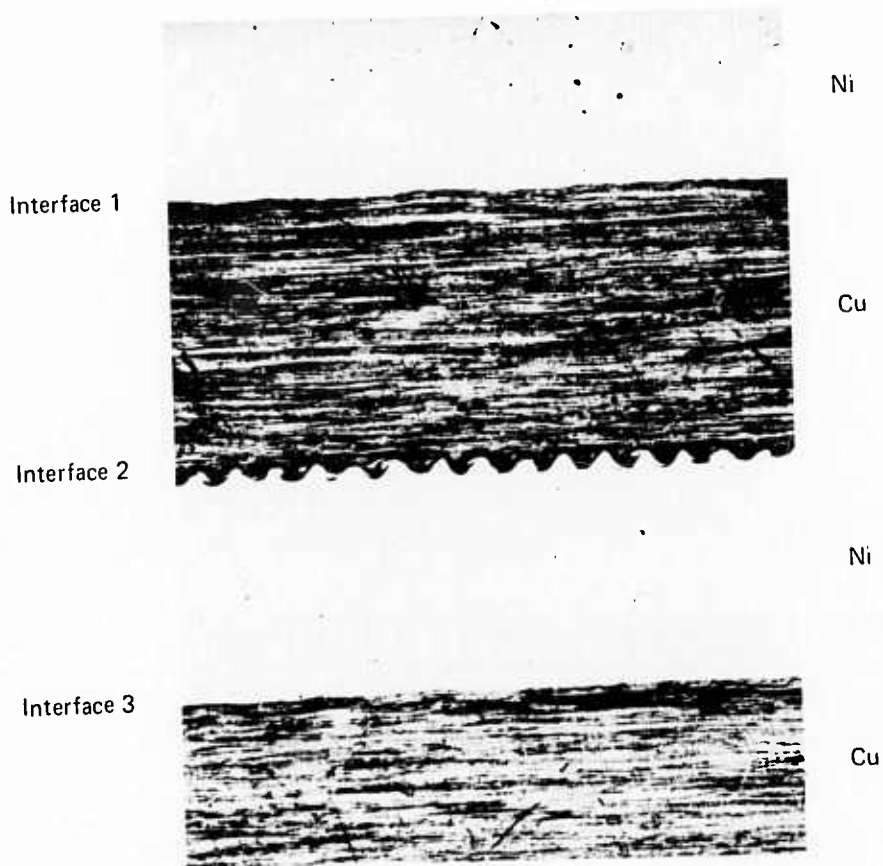
Figure 4. Photomicrograph of an explosion welded sample fabricated from roll-bonded composite material. Interface 1 – Roll Bond. Interface 2 – Explosion Weld. 3 – Roll Bond.

Magnification 30X

33

Diffusion measurements were made using the electron microprobe and the width of the diffusion zone determined.

Results And Discussion

Diffusion coefficients were calculated using a computer program to apply the Boltzman-Matano analysis. The relationship of diffusivity with temperature is shown plotted in Figure 5. The diffusion data for the specimen explosively welded at an higher explosive loading is plotted in Figure 6. These figures illustrate the temperature dependence of diffusivity across the trough and crest section of the explosively welded interface, and also in the roll-bonded interface of the cladder plate and the base plate. For sake of comparison, diffusion coefficient data from plain roll-bonded specimen and data from the experiments of Anand, Murarka, and Agarwala (1) are also plotted in the same graph. To determine the best fit for the line through the experimental points, the least square method of analysis was used. From these plots, frequency factors and activation energies were calculated, which are listed in Table 1.

TABLE 1
ACTIVATION ENERGIES AND FREQUENCY FUNCTIONS

Explosive Loading g/cm^2	Copper-Nickel Interface	Frequency Factor, D_0 cm^2/sec	Activation Energy Kcal/mole
1.24	Cladder plate roll-bond	$5.09 \times 10^{-2} \pm 18\%$	$51 \pm 2.5\%$
	Base plate roll-bond	$5.84 \times 10^{-2} \pm 18\%$	$48 \pm 2.5\%$
	Trough: Explosion weld	$1.09 \times 10^{-4} \pm 20\%$	$36.4 \pm 2.0\%$
	Crest: Explosion weld	$2.53 \times 10^{-4} \pm 20\%$	$38.7 \pm 2.0\%$
None	Plain roll-bond	$1.89 \times 10^{-1} \pm 22\%$	$53 \pm 3.5\%$
None	Literature (reference 14)	7.24×10^{-1}	61
1.86	Cladder plate roll-bond	$1.56 \times 10^{-2} \pm 19\%$	$50.3 \pm 2\%$
	Base plate roll-bond	$6.69 \times 10^{-3} \pm 18\%$	$47.8 \pm 2.5\%$
	Trough: Explosion weld	$1.43 \times 10^{-4} \pm 20\%$	$35.7 \pm 2.0\%$
	Crest: Explosion weld	$2.96 \times 10^{-4} \pm 20\%$	$37.9 \pm 2.0\%$
1.24	Cladder plate roll-bond (Ni-to-Cu)	$1.70 \times 10^{-1} \pm 18\%$	$54 \pm 3.5\%$
	Base plate roll-bond	$1.1 \times 10^{-1} \pm 18\%$	$52 \pm 3.5\%$
	Trough: Explosion weld	$2.01 \times 10^{-3} \pm 20\%$	$40.2 \pm 2.0\%$
	Crest: Explosion weld	$4.33 \times 10^{-3} \pm 20\%$	$42.5 \pm 2.0\%$

To examine the influence of nickel impacting on copper, a nickel on copper explosion weld was also made. The results of the diffusion measurements in this specimen are plotted in Figure 7.

Microhardness Measurements

Several investigators (2,3) have reported general increase in hardness in explosion welded metals, and traverses made across the Ni-Cu-Ni-Cu explosion welded composite by the author also showed a similar phenomenon. The results are plotted in Figure 8 and Figure 9. After explosion welding, increased level of hardness is noted in both the copper and nickel components of the cladder and the base plate. Also at the explosion weld interface a sharp increase in
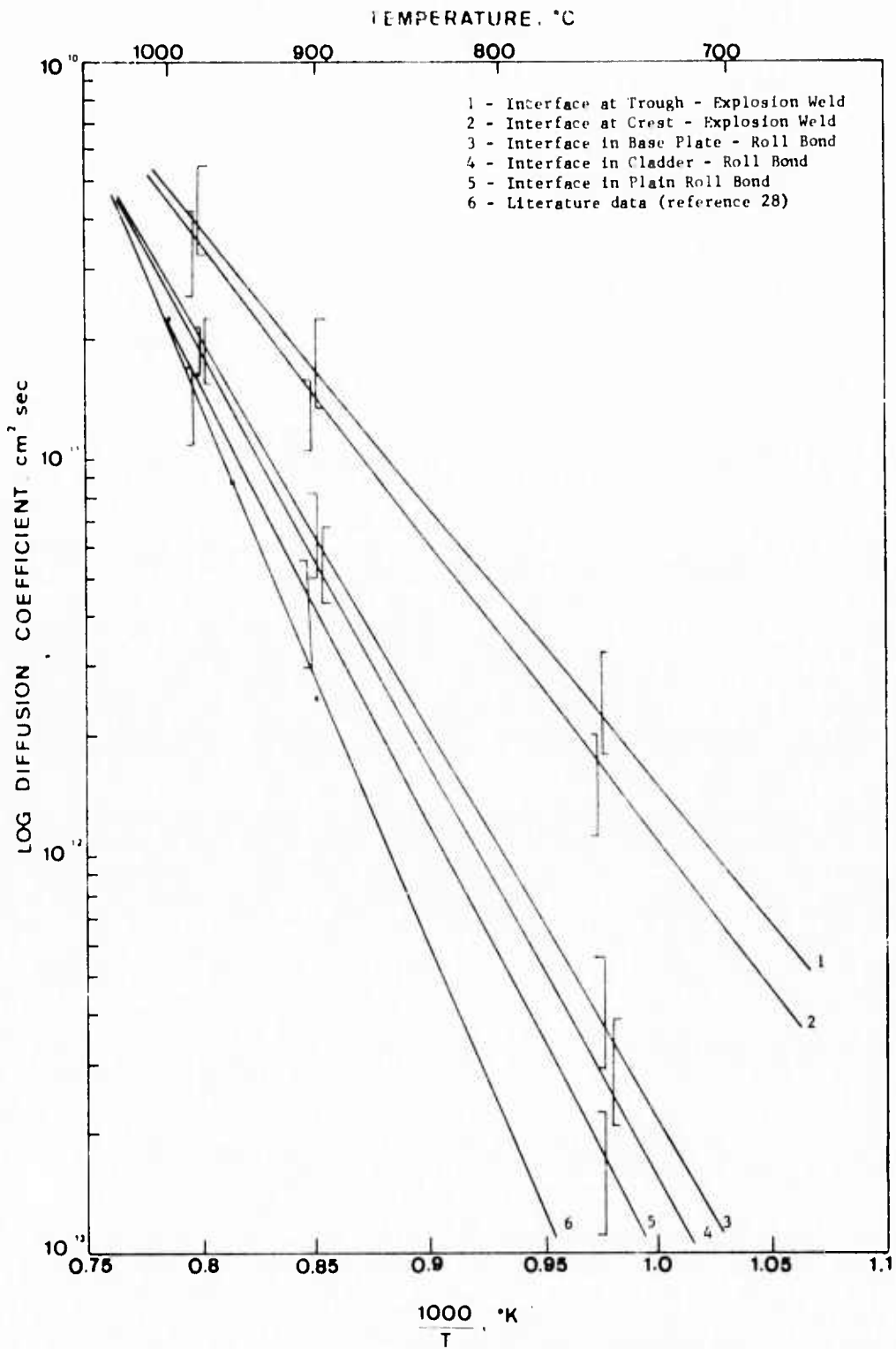
Figure 5. Diffusion coefficients for copper as a function of temperature at 50 atomic per cent copper in copper-nickel system. Copper-to-nickel specimen explosion welded with 1.24 g/cm.² loading.

35
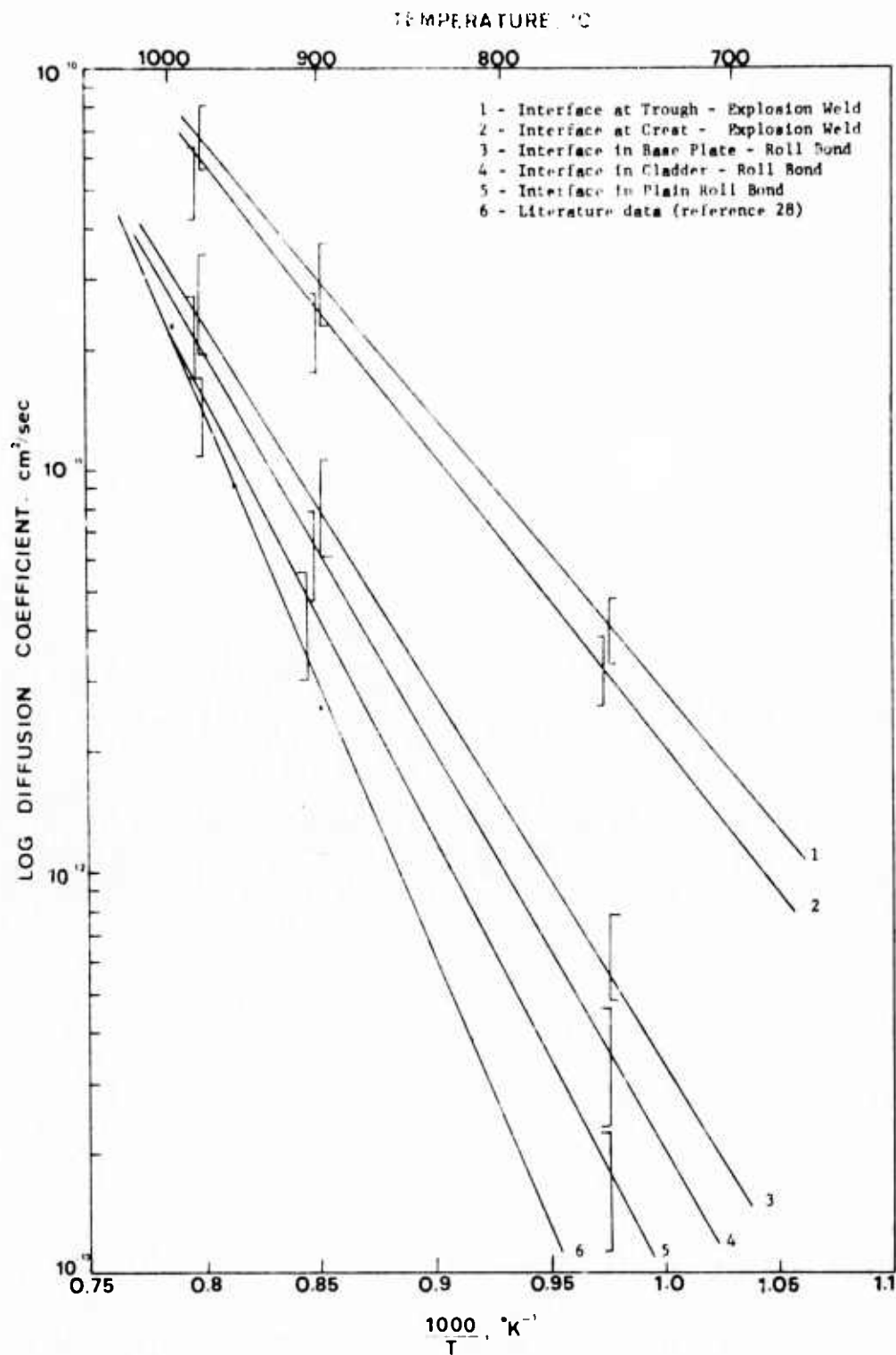
Figure 6. Diffusion coefficients for copper as a function of temperature at 50 atomic per cent copper in copper-nickel system. Copper-to-nickel specimen explosion welded with 1.86 g/cm.^{2} loading.
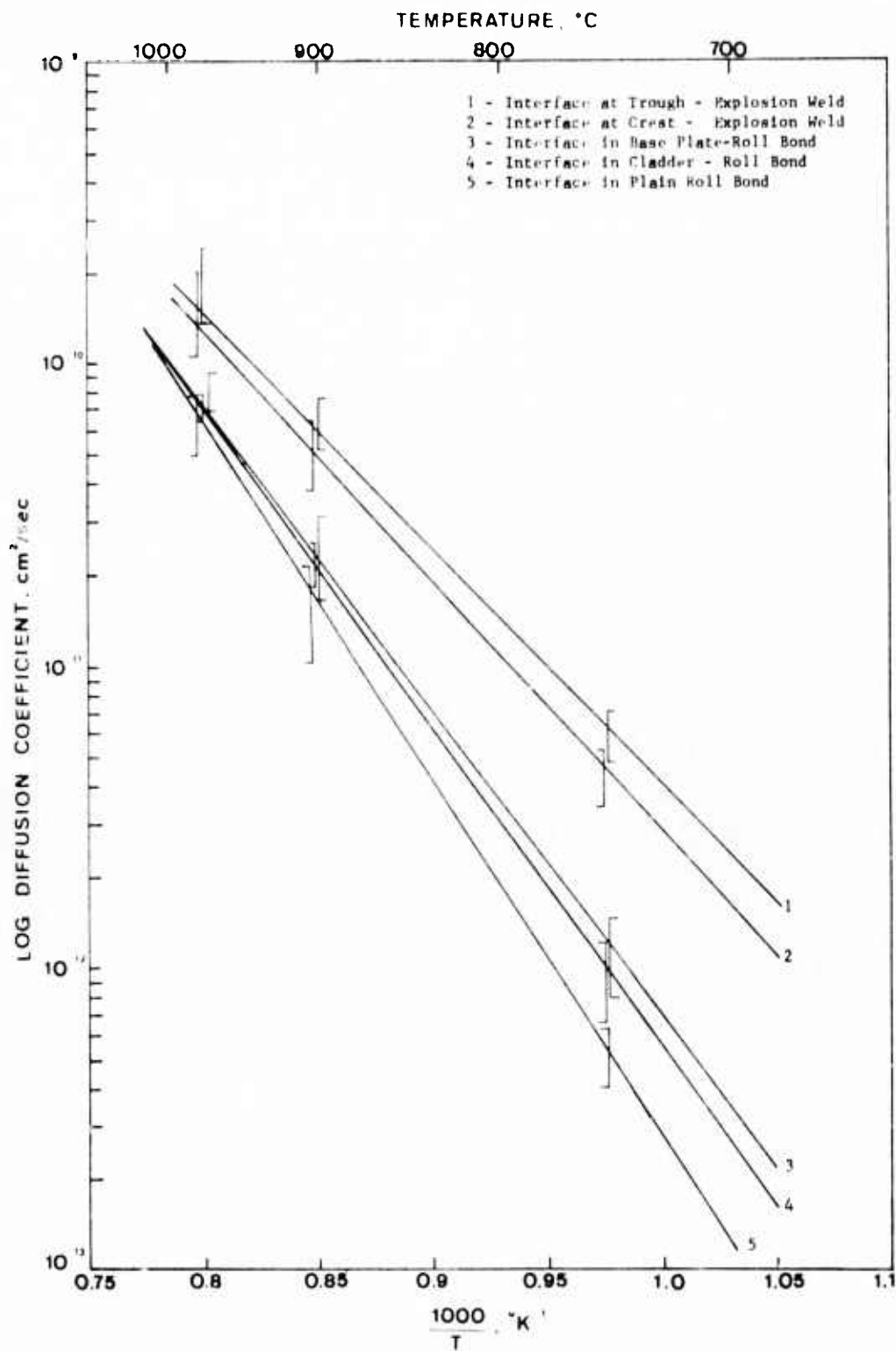
Figure 7. Diffusion Coefficients for copper as a function of temperature at 80 atomic per cent copper in copper-nickel system. Nickel-to-copper specimen explosion welded with 1.24 g/cm.² loading.
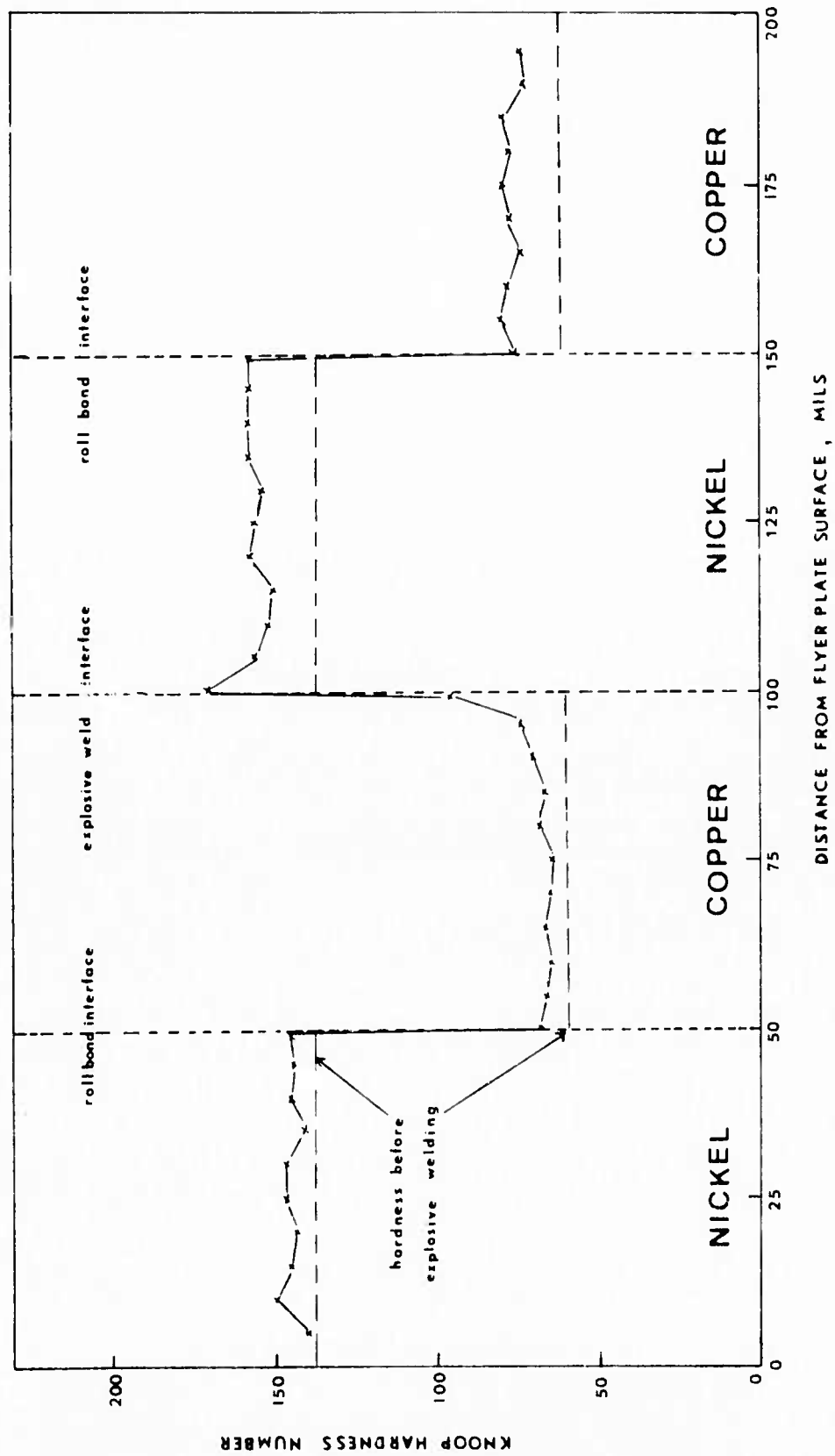
Figure 3. Hardness Profile for Ni-Cu-Ni-Cu Explosion Welded Specimen: As-Welded Condition.

38
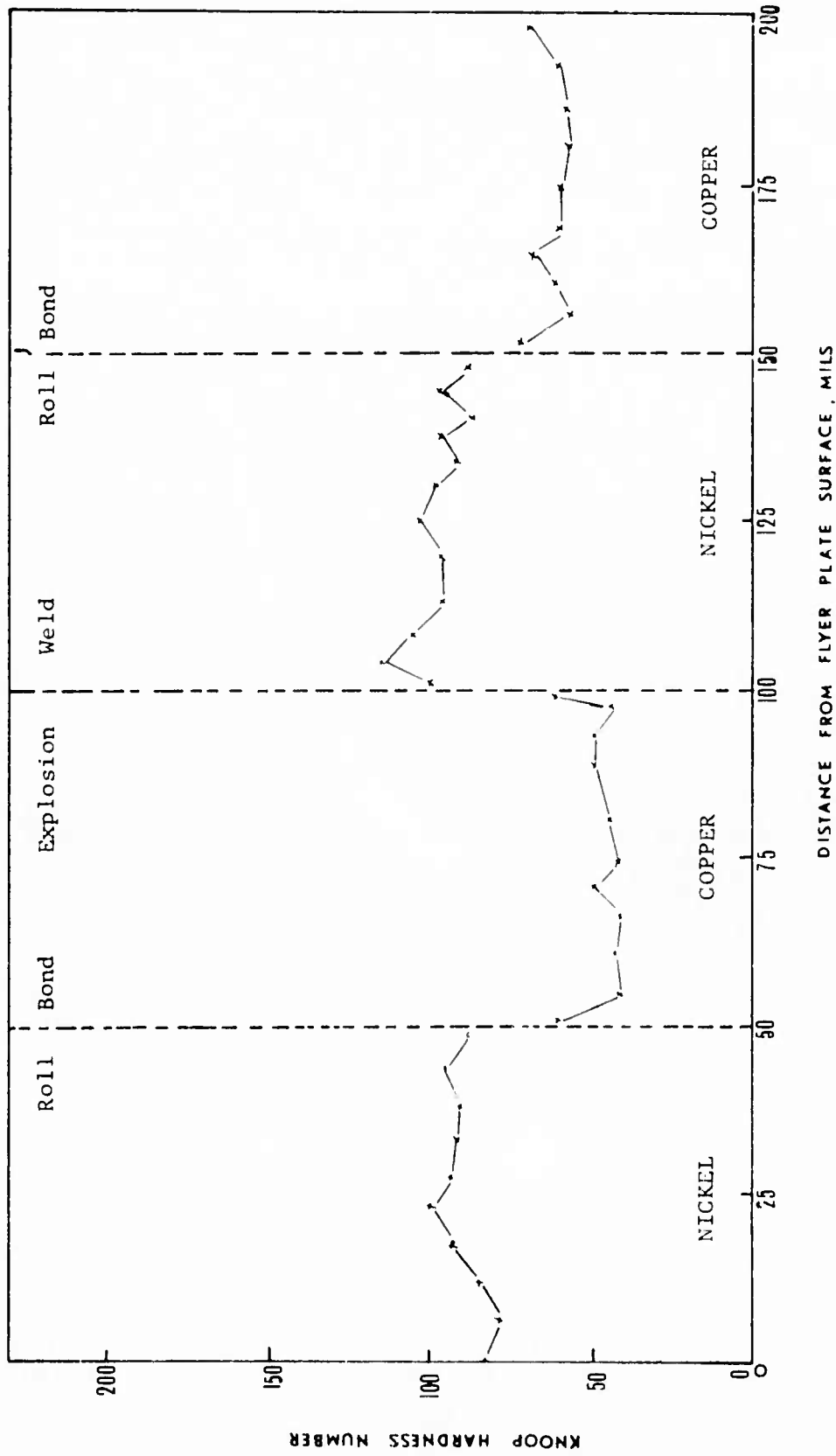
Figure 9. Hardness Profile for Ni-Cu-Ni-Cu Explosion Welded Specimen: After 975° C Anneal.

39

hardness is noticeable, which is possibly due to shock hardening as well as localised work-hardening as a result of severe plastic flow at the weld interface. Shock hardening in metals has been attributed to the production of a very high density of dislocations and a probable high density of point defects. The point defects are said to cause hardening by interaction with dislocations, producing a high density of jogs.

The hardness profile also shows a higher level of hardness in the base plate in comparison to the cladder. It is likely that this is due to additional shock hardening resulting in the base plate by the impact of the cladder. In Figure 9 the hardness profile after the 975°C anneal is plotted. It is interesting to observe that the hardness is still higher than the cladder even after annealing. The hardness data offers an interesting correlation with the diffusion results, which will be discussed later.

Discussion on Diffusion Results

The following results of significance emerge from the diffusion experiments as judged from the activation energies data:

1. The activation energies of diffusion across the explosion welded interface, both crest and trough, are in the range of 36.5 to 38.0 Kcals per mole. Then energy values are substantially lower than the activation energy of 53 Kcals per mole for diffusion across the plain roll bonded interface. These results indicate enhanced diffusion across exp. welded interface, even when a higher explosive loading is used or when nickel is explosion welded on to copper.

2. Lower activation energy seems to be required for diffusion across the trough than the crest in all the three specimens.

3. The activation energies in all the roll-bonded interfaces, viz., in the cladder plate, the base plate and in plain roll-bonded material, are in the range of 48 to 53 Kcals per mole. The results suggest that there is a substantial difference in the diffusion rates across these three roll-bonded interfaces.

4. On close comparison of the diffusion in base plate and the cladder plate, the former has consistently lower activation energies in all the three exp. welded specimens. The microhardness data on the as-welded condition and at 975°C anneal appears to support these diffusion results. In the as-welded condition the level of hardness is higher in the base plate than the cladder, and similar difference is noted even after annealing to 975°C.

Diffusion Across the Explosion Weld Interface

During the course of carrying out microprobe traverses for measuring diffusion in explosion welded specimens it was necessary to consider the wavy or rippled nature of the interface. The wave pattern had distinct trough and crest portions. Traverses were made perpendicular to the interface, five each across the trough and the crest. The results of diffusion measurements indicate slightly enhanced diffusion across the trough as compared to the crest portion of the wave. The difference is consistent even when different explosive loadings are used. It is possible that the mechanism of wave formation, as illustrated in Figure 2, creates different conditions for diffusion in the crest and the trough.

It was first suspected that the enhanced diffusion observed in the explosion welds could be due to the different geometry of its interface. The explosion weld interface in the specimens had a wave profile whereas the roll-bonded interface was planer. By using a symmetric angled configuration a copper-nickel explosion weld with a straight interface was prepared. The nature of the interface is shown in Figure 10. Test pieces from this specimen were annealed at 750°C, 900°C, and 975°C for ten hours under similar conditions as other diffusion specimens. Diffusion measured in this specimen once again exhibited higher diffusivity in the explosion weld even with a straight interface as compared to the roll-bonded specimens. The results clearly showed that the diffusion enhancement was not due to any geometrical effects at the explosion welded interface.

It is, therefore, obvious that the explosion welding process creates certain conditions at the interface which favorably assist diffusion to proceed at a higher rate.

Optical Metallography

The explosion welded specimens and plain roll-bonded specimens were together subjected to diffusion anneal at four different temperatures, namely, 500°C, 750°C, 900°C and 975°C for ten hours. The microstructural changes occurring as a consequence of these annealing treatments were studied with the aid of optical metallography. Figures 11 to 14 show photomicrographs of both the specimens in the as-welded condition and after each step of annealing treatment. The micrographs in Figure 11 are of a section of the explosion welded specimen. The copper component of the weld composite has been etched to reveal the microstructure and it appears sandwiched between two nickel layers. The copper-nickel roll-bonded interface of the cladder plate appears in the top part of the picture and the explosion welded interface in the lower part.

In the as-welded condition, Figure 11(a), the microstructure is typical of hot-rolled copper. The explosion welded interface has the characteristic wavy profile.

In Figure 11(b), after a ten-hour anneal at 500°C, the rolled-structure of the as-welded condition has completely disappeared and appearance of new, small grains is noted. In some of the grains annealing twins can be seen.

Figure 11(c) depicts the microstructure of copper in the explosion welded specimen after annealing at 750°C. Completely recrystallized grains appear and the size of the grains is much larger than those seen after the 500°C anneal, suggesting occurrence of grain growth.

After the 900°C anneal excessive grain growth is observed in Figure 11(d). Smoothing out of the ripple or wave pattern of the explosion weld interface is noticed. An enlarged view of the explosion weld interface at 150X magnification is shown in Figure 12(a). Small voids or pores are seen to form in the copper side of the interface.

The photomicrograph in Figure 11(e) of specimen annealed at 975°C shows substantial flattening out of the wave pattern. Voids appear at both the explosion weld interface and the roll-bonded interface in the cladder plate. At higher magnification of 150X in Figure 12(b), the interface can be seen to be completely lined with voids.

41

Roll Bond

Explosion
Weld

Figure 10. Photomicrograph of copper-to-nickel explosion welded
specimen with straight interface.   Magnification 30X

Nickel

Copper

Nickel
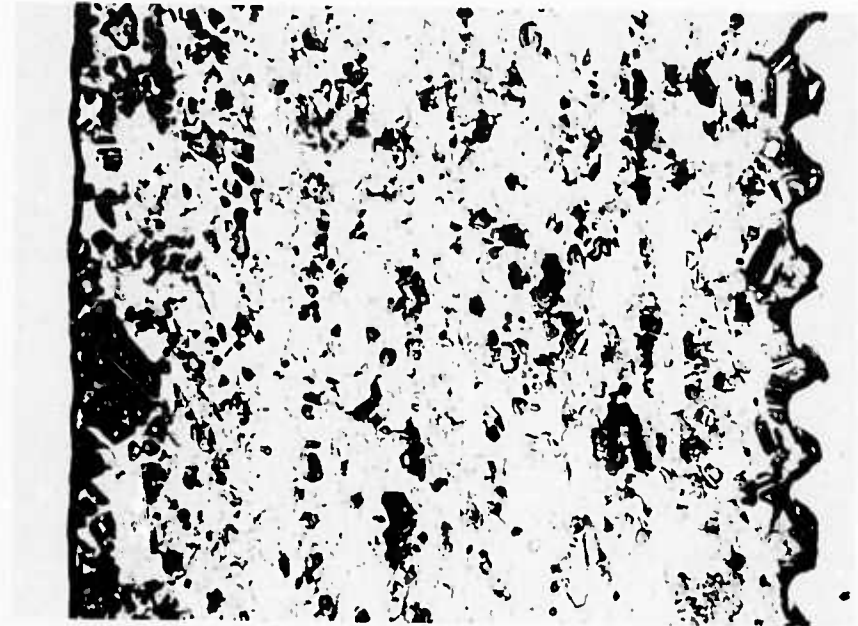
(b) After 500°C anneal   Magnification 75X

(a) As welded

Figure 11. Photomicrograph of copper-nickel explosion welded specimen.

43
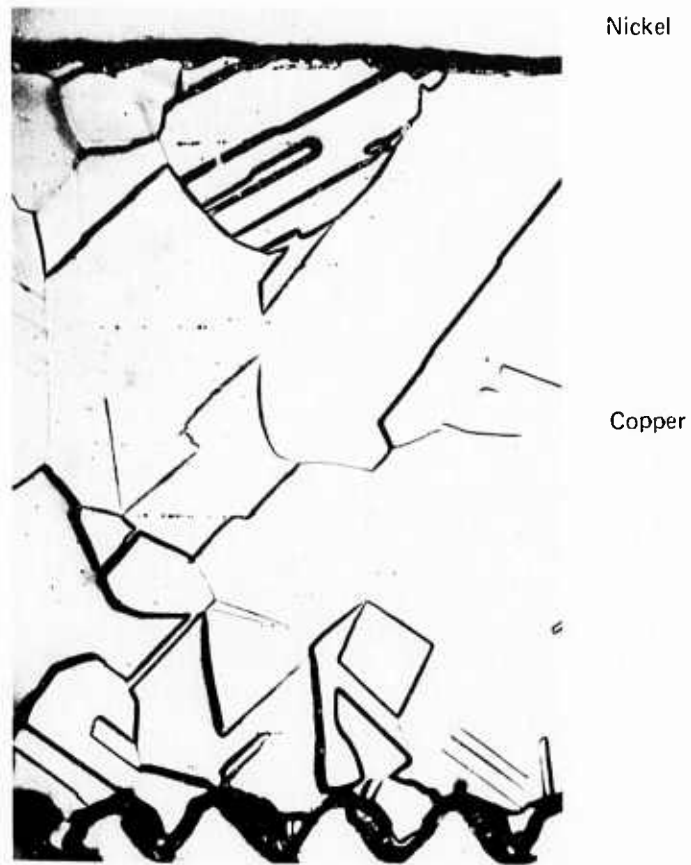
Nickel

Copper

(c) After 750°C anneal

Figure 11. (Continued)   Magnification 75X

44

Nickel

Copper

Nickel

(e) After 975°C anneal

(d) After 900°C anneal

Magnification 75X

Figure 11. (Continued)

45

Copper

Nickel

(a) After 900°C anneal
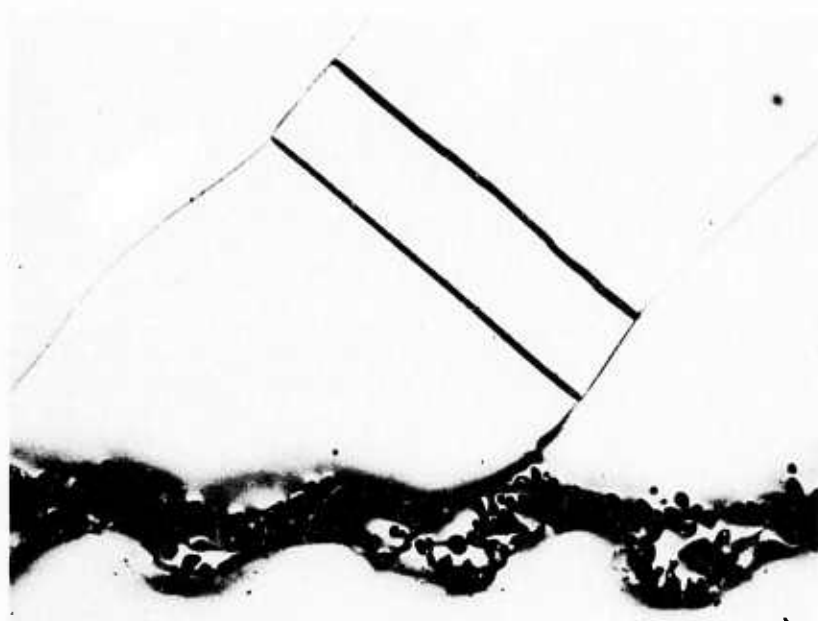
Copper

Nickel

(b) After 975°C anneal

Figure 12. Photomicrographs of copper-nickel explosion welded specimens showing void formation at the interface.   Magnification 150X

Figures 13 and 14 are photomicrographs of plain roll-bonded copper-nickel couple subjected to the same annealing treatment as the explosion welded pieces. Here again the copper side of the couple has been etched. The general changes in the microstructure after the isochronal anneals follows a similar pattern as the explosion welded specimens. The hot-rolled structure of the as-welded condition in Figure 13(a), is completely replaced by new recrystallized grain structure at 500°C in Figure 13(b).

After annealing at 750°C for ten hours, complete recrystallization has occurred in both the roll-bonded and explosion welded specimens. There is also a significant difference in grain size from that noted in specimens annealed at 500°C, which suggests occurrence of a rapid and tremendous grain growth between 500°C and 750°C annealing temperatures. There appears to be little difference between the average grain size of the roll-bonded and explosion welded specimens. The microstructure in Figures 13(d) and 13(e) indicate abnormal grain growth during the 900°C and 975°C anneal. At 150X magnification in Figures 14(a) and 14(b), void formation in the diffusion zone is more clearly revealed.

The results of optical metallography show that on a microscopic scale there is not much difference in the changes in microstructure between the explosion welded and the roll-bonded specimen following the isochronal anneals. The higher diffusivity noted across the explosion welded interface is, therefore, due to the different defect structure developing right at the interface, which could not be revealed by optical microscopy. Some idea of this defect structure can be gained on close examination of the nature of the weld interface. During the welding process, high pressures are generated causing intense plastic deformation, to the point of hydrodynamic flow, of the mating metal surfaces. The intensity of deformation has already been shown in Figure 3. Such excessive plastic deformation can reasonably be expected to cause extensive changes in the defect structure at the interface. Transmission electron microscopy studies (4) of the explosion welds have estimated dislocation densities on the order of 10^{11} dislocations cm^{-2} at the interface. The creation of the high dislocation density and metal flow at very high strain rates will generate an extremely high concentration of vacancies, very likely in excess of the thermal equilibrium concentration.

Defects in the crystal lattice play an essential role in the diffusion process in solids. Their presence in large numbers contributes significantly to diffusion enhancement. However, the fact remains that as the temperature is raised the defects too become mobile like atoms, and diffuse through the lattice and ultimately disappear at suitable sinks. But the higher diffusivity measured in explosion weld interface suggests that some type of thermally stable defect structure exists at the interface even at very high temperatures. Evidence of such a stable defect structure has been previously reported by Wittman. In his study of the effects of heat-treatment on the mechanical properties of explosion welded 6061 Al alloy, Wittman (5) found that the high rate deformation via explosion welding was more effective in extending the mechanical properties than conventional deformation following post-welding heat-treatments. Comparison was made following isochronal anneals up to 750°F, between the weld tensile strength of explosion welded alloy and the ultimate strength of cold-reduced alloy. Both the materials possessed the same initial hardness and strength prior to annealing. It was found that the explosion welded specimen retained a higher level of strength than the cold-rolled material, the effect being more pronounced when the material was heat-treated to higher temperatures of anneal. The retention of explosion weld strength even following anneals at high temperatures was attributed to hardening by likely interaction of precipitated solute atoms and stable dislocation networks.

47
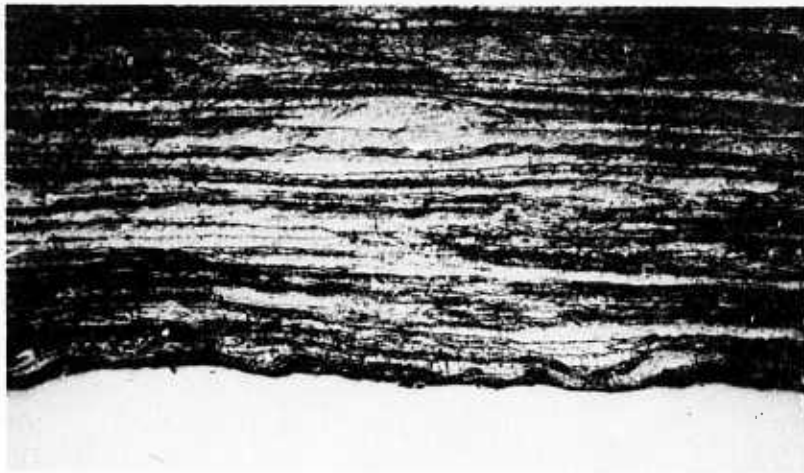
Copper

Nickel

(a) As welded
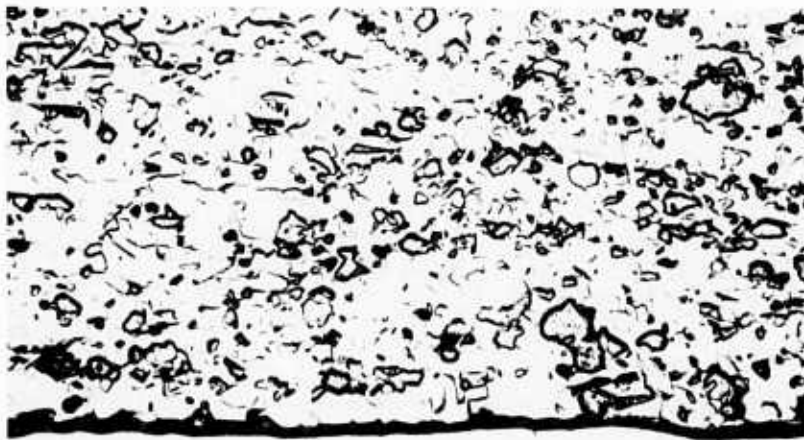
Copper

Nickel

(b) After 500°C anneal
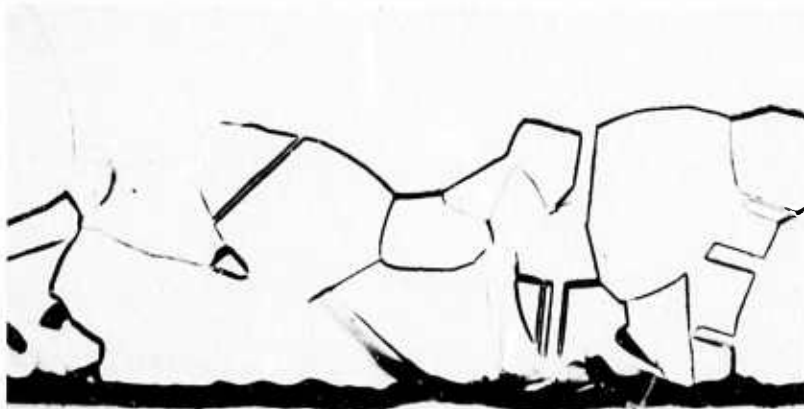
Copper

Nickel

(c) After 750°C anneal

Figure 13. Photomicrographs of plain roll-bonded specimen   Magnification 75X

48
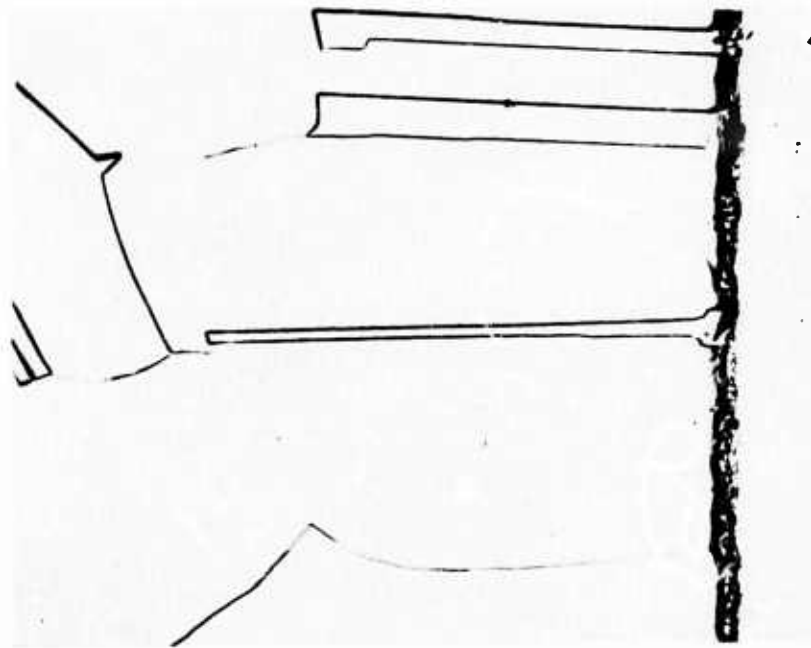
Copper

Nickel

(d) After 900°C anneal

(e) After 975°C anneal

Magnification 75X

Figure 13. (Continued)

49
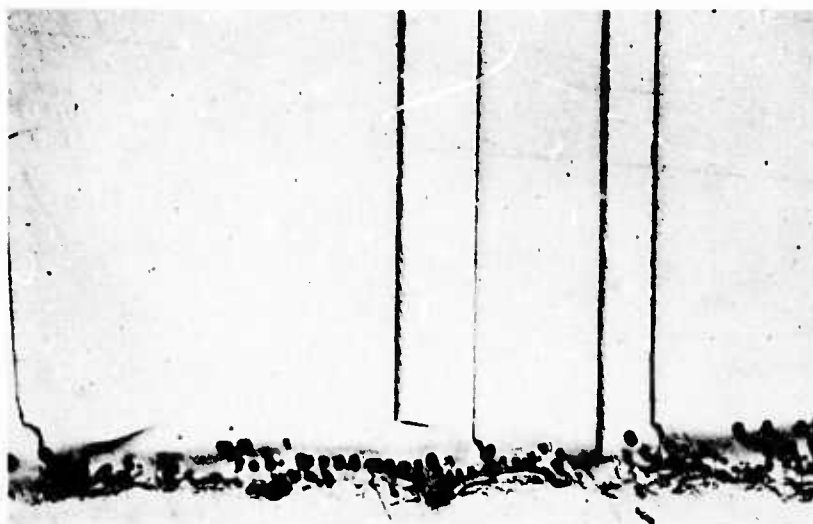
Copper

Nickel

(a) After 900°C anneal
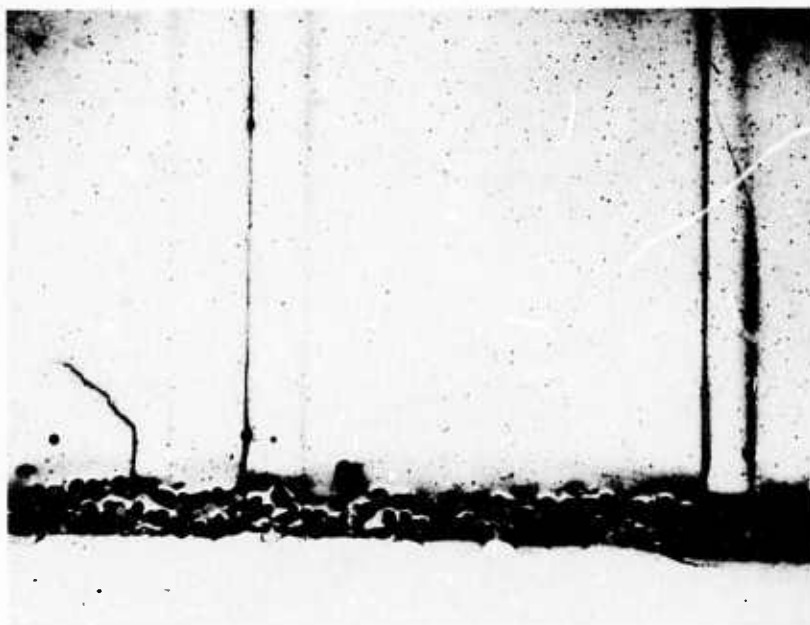
Copper

Nickel

(b) After 975°C anneal

Figure 14. Photomicrographs of copper-nickel roll-bonded specimens showing void formation at
the interface.   Magnification 150X

To examine if such a thermally stable defect structure was also present in the annealed copper-nickel explosion welded specimens in this study, transmission electron microscopy was carried out on thin foils prepared from the weld interface area. By using the ion-bombardment technique, it was possible to obtain thin foils from regions well within the diffusion zone. It was also deemed necessary to examine the microstructure developing in the plain roll-bonded material for effective comparison.

Transmission Electron Microscopy

Figure 15(a) is a transmission electron micrograph of a section in the copper side of the copper-nickel explosion welded specimen in the as-welded condition and prior to annealing. The area shown in the micrograph is about 19 microns from the weld interface. A very dense network of dislocations can be seen. The dislocations appear in dense tangles and do not seem to be arranged in any definite cellular pattern. Similar dislocation densities have been observed by others in explosion welded interfaces. They estimate the density to be as high as 10^{11} dislocations cm^{-2}.

Figure 15(b) also characterizes a specimen in the as-welded condition, but depicts the substructure away from the weld interface. The area is approximately 1 millimeter away from the weld interface and is at the copper-nickel roll-bond interface of the cladder plate. The substructure reveals what appears to be mechanical twins in a matrix containing dislocations, similar to those observed by other workers.

After subjecting the explosion welded couple to diffusion anneal of 500°C for ten hours, the changes in substructure of an area 25 microns from the interface can be seen in Figure 15(c). The dislocation density is still very high, even when the material has been heated to a temperature close to half its melting point. The electron micrograph reveals dislocation tangles and loops. Their presence of loops in the explosion welded metal even after annealing to 500°C is of significance to note.

The microstructure of plain roll-bonded specimen after the 500°C anneal in Figure 15(d) is, however, totally different to that found in explosion welded specimen. There is evidence of recrystallization and the dislocation density is low. Average subgrain size is about 0.25 microns and the boundaries seem well-defined.

Figure 15(e) of the explosion welded specimen shows a significant change in the substructure after the 750°C anneal. The dislocation density is still high in some of the grains but annealing has resulted in some recovery and recrystallization. The dislocations are rearranged in subgrain boundaries. In comparison, in Figure 15(f), the plain roll-bonded material exhibits much larger subgrain size of about 0.5 microns, with a greater percentage of recrystallized grains.

The difference in the substructure at the explosion welded interface and the roll-bonded material is even more significant at 900°C and 975°C, as seen in Figures 15(g-j). In the former, it is quite unique to find the presence of a large number of dislocations even after annealing to such high temperatures. Dislocations appear to be trapped in sub-boundary walls. The roll-bonded specimen, however, presents a well-annealed structure with a low dislocation density.

(a) Copper-Nickel explosion welded specimen is as-welded condition. Area shown is within diffusion zone and 0.019 mm. from the weld interface.

(b) Copper-Nickel explosion welded specimen in as-welded condition. Area shown is 1 mm. away from the interface and close to the cladder-plate roll-bond interface.

Figure 15. Transmission electron micrographs of copper.
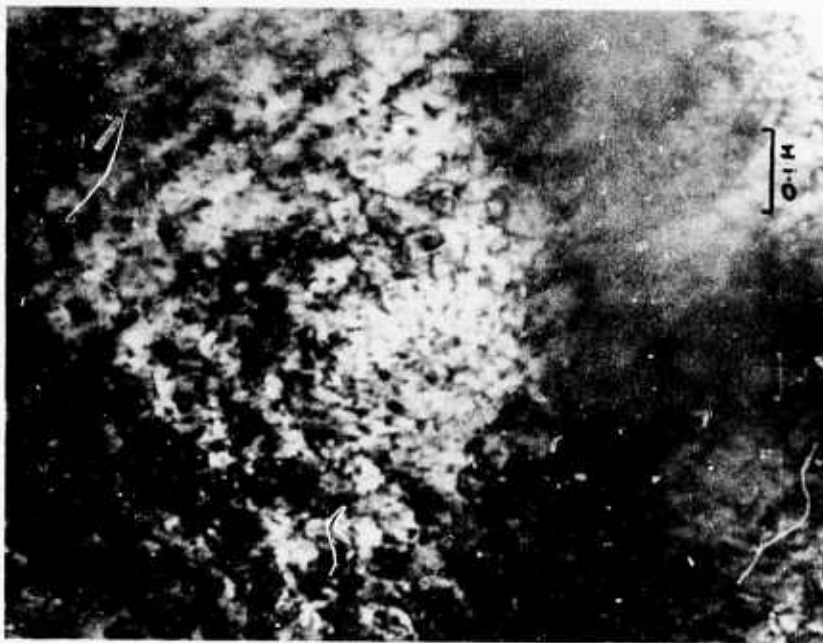
(c) Copper-Nickel explosion welded specimen after annealing at 500°C for 10 hours. Area shown is 0.025 mm. from the nickel side of the interface.

(d) Copper-Nickel roll-bonded specimen after annealing at 500°C for 10 hours.

Figure 15. (Continued)

(e) Copper-Nickel explosion welded specimen after annealing at 750°C for 10 hours. Area shown is 0.020 mm. from the nickel side of the interface.

(f) Copper-Nickel roll-bonded specimen after annealing at 750°C for 10 hours.

Figure 15. (Continued)
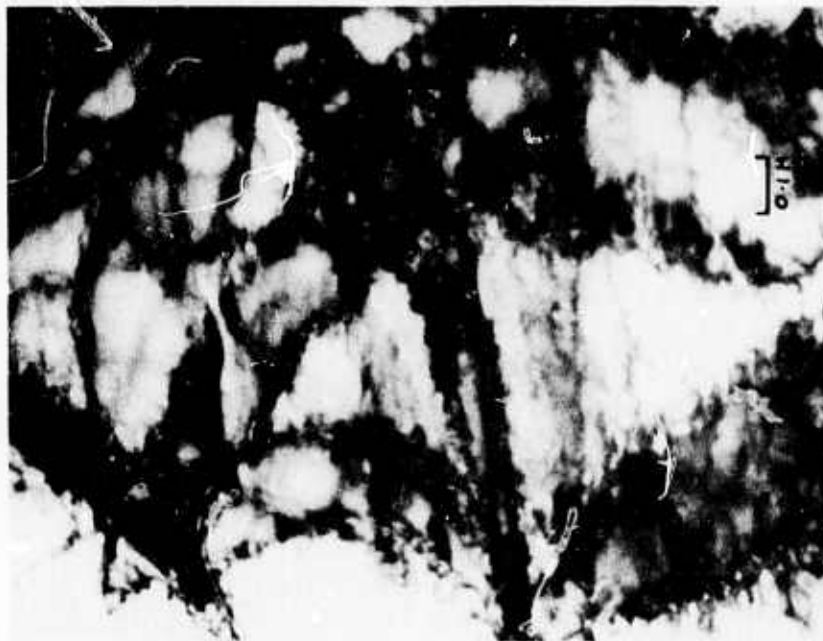
(g) Copper-Nickel explosion welded specimen after annealing at 900°C for 10 hours. Area shown is 0.025 mm. from the nickel side of the interface.

(h) Copper-Nickel roll-bonded specimen after annealing at 900°C for 10 hours.

Figure 15. (Continued)

(i) Copper-Nickel roll-bonded specimen after annealing at 975°C for 10 hours.

(i) Copper-Nickel explosion welded specimen after annealing at 975°C for 10 hours. Area shown is 0.018 mm. from the nickel side of the interface.

Figure 15. (Continued)

The results of transmission electron microscopy indicate strongly the existence of a thermally stable defect structure at the explosion welded interface.

In conclusion, it can be stated that the enhanced diffusion observed in the explosion welded specimens, is due to the unique defect structure created by the welding process at the interface, and its stability even at high temperatures contributes to the diffusion process.

REFERENCES

1. M.S. Anand, S.P. Murarka, and R.P. Agarwala, J. Appl. Phys., *36* 3860 (1965).

2. A.H. Holtzman and G.R. Cowan, *"Bonding of Metals with Explosives,"* Welding Research Council Bull. No. 104, 6 (1965).

3. B. Crossland and J.D. Williams, Met. Rev., *15*, 79 (1970).

4. L. Trueb, Trans. AIME, *242*, 1057 (1968).

5. R.H. Wittman, in *"Metallurgical Effects at High Strain Rates,"* AIME, New York, 669 (1973).

III. EXPLOSIVE FORMING OF SPHERICAL GORE SEGMENTS

Faculty Advisor: W. G. Howell
Graduate Student: B. C. Patel

The following is a summary of the studies conducted by Mr. Patel in partial fulfillment of the requirements for the degree of Master of Science in the Mechanical Engineering Department, University of Denver.

One of the attractive applications of explosive forming is the forming of spherical gore segments. These gore segments are sections of a hemispherical or spherical tank and have equal curvature in all directions. It would be extremely difficult to form a hemisphere from a large welded blank using a single explosive shot. One of the problems would be designing of forming-tooling and handling equipment for an extra large blank: For example, to form a 60 foot diameter hemisphere using a single shot would require a 5652 sq. ft. blank (about a 75-ft. x 75-ft. metal piece). The hemisphere is, therefore, fabricated using gore segments. These gore segments are first formed individually using explosives and then fastened together by welding or riveting to form a complete sphere.

Under the ARPA Program, the feasibility of explosively forming 118.5-ft. diameter, 1.5 in. thick, 6061 T6 Aluminum L.N.G. (liquid nitrogen gas) spherical storage tank, was to be demonstrated. The well-known engineering technique of scale model tests was employed.

Figure 1 shows the 59.25-ft. radius L.N.G. spherical tank. The largest circumference in the horizontal plane is divided in ten equal parts, each 37.2-ft. long. There are two polar caps, each with a solid angle of 40° at the center of the sphere. Base diameter of the polar cap is 40.54-ft. and it is 3.55-ft. high. The great circles in the vertical plane are divided into ten equal parts, each 14.47-ft. wide. The sphere is thus partitioned as shown in Figure 1. The largest gore segments (adjacent to the equator) are 37.2-ft. x 14.47-ft. x 36.14-ft. x 14.47-ft. The smallest gore-segs adjacent to the polar caps are 20.82-ft. x 14.47-ft. x 12.75-ft. x 14.47-ft. There are altogether 100 gore segments and two polar caps. The full scale gore segment would be 16-ft. x 40-ft. x 1.5-ft. with radius of curvature of 59.25-ft. This would allow trimming and finishing the gore segments to the required size.

A scale of 1:8 was used for scale model testing. The size of the workpiece was thus 2-ft. x 5-ft. x 0.1875-in. with a radius of curvature of 7.5-ft. A ten-piece concrete die was to be used. Each of the ten pieces was 2-ft. long and 6-in. wide; when mounted together, the die would have a 2-ft. x 5-ft. forming surface with a radius of curvature of 7.5-ft. along the 2-ft. length. Along the 5-ft. length, the radius of curvature of 7.5-ft. was approximated by ten 6-in. segments with an angle of 176° between any two adjacent segments. A two-piece die (instead of ten-piece) was used in the scale model tests on the grounds that if a 2-ft. x 1-ft. x 0.1875-in. gore segment could be formed on a two-piece die, then it would be possible to form a 2-ft. x 5-ft. x 0.1875-in. gore segment on a ten-piece die. The 2-ft. x 1-ft. x 0.1875-in. thick 6061-T6 aluminum workpiece was formed in four tests on a two-piece reinforced concrete die with steel armour on the forming surface and in three tests on a bare concrete die. The steel armour reinforced concrete die is shown in Figure 2. The workpiece was constrained at two places. The forming test set up is shown in Figure 3.
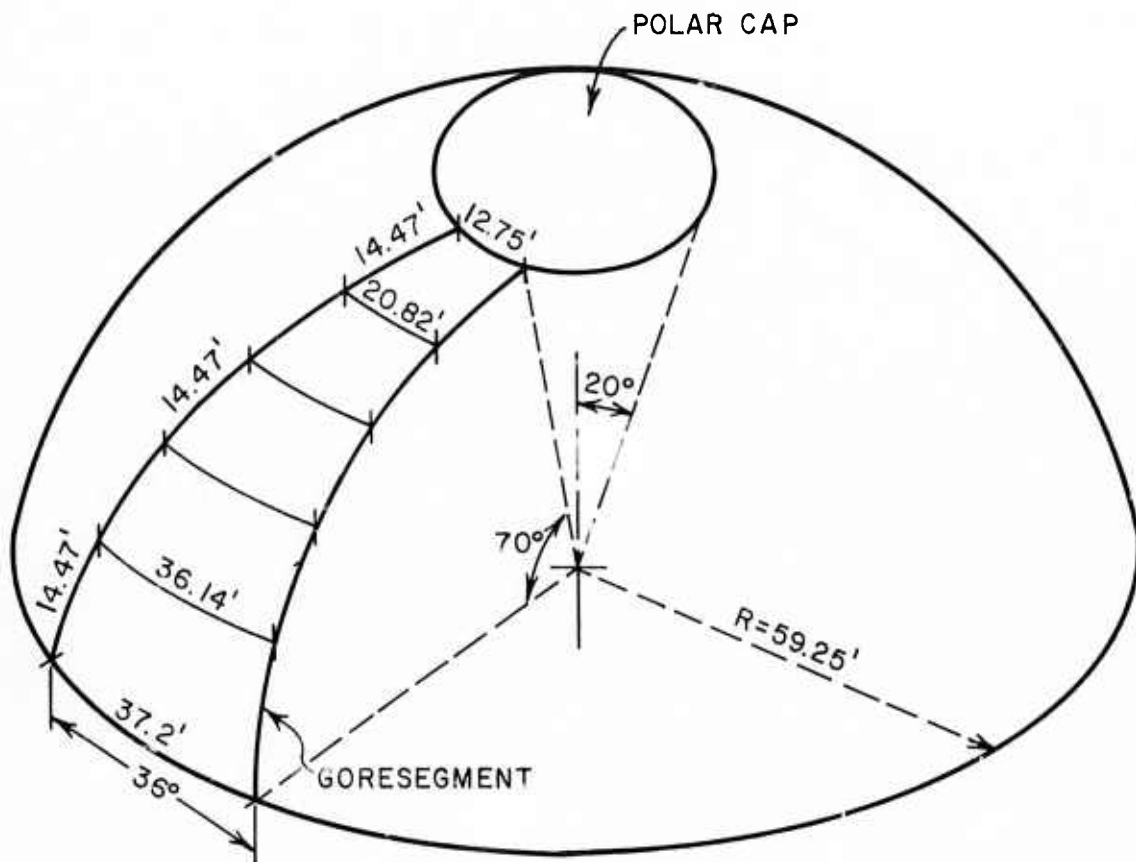
Figure 1. Hemispherical Tank fabricated by using 50 gore segments and one polar cap.

3/8" All threaded rod & nuts

9"

4°

176°

4°

END – VIEW

1/2" Tubing

Two Re-Bars in each seg.

All thread rod

2.25'

Steel Armour 0.375"

CONCRETE

R=7.5'

FRONT – VIEW

1/2" Tubing

Re-Bars

6"

6"

TOP – VIEW
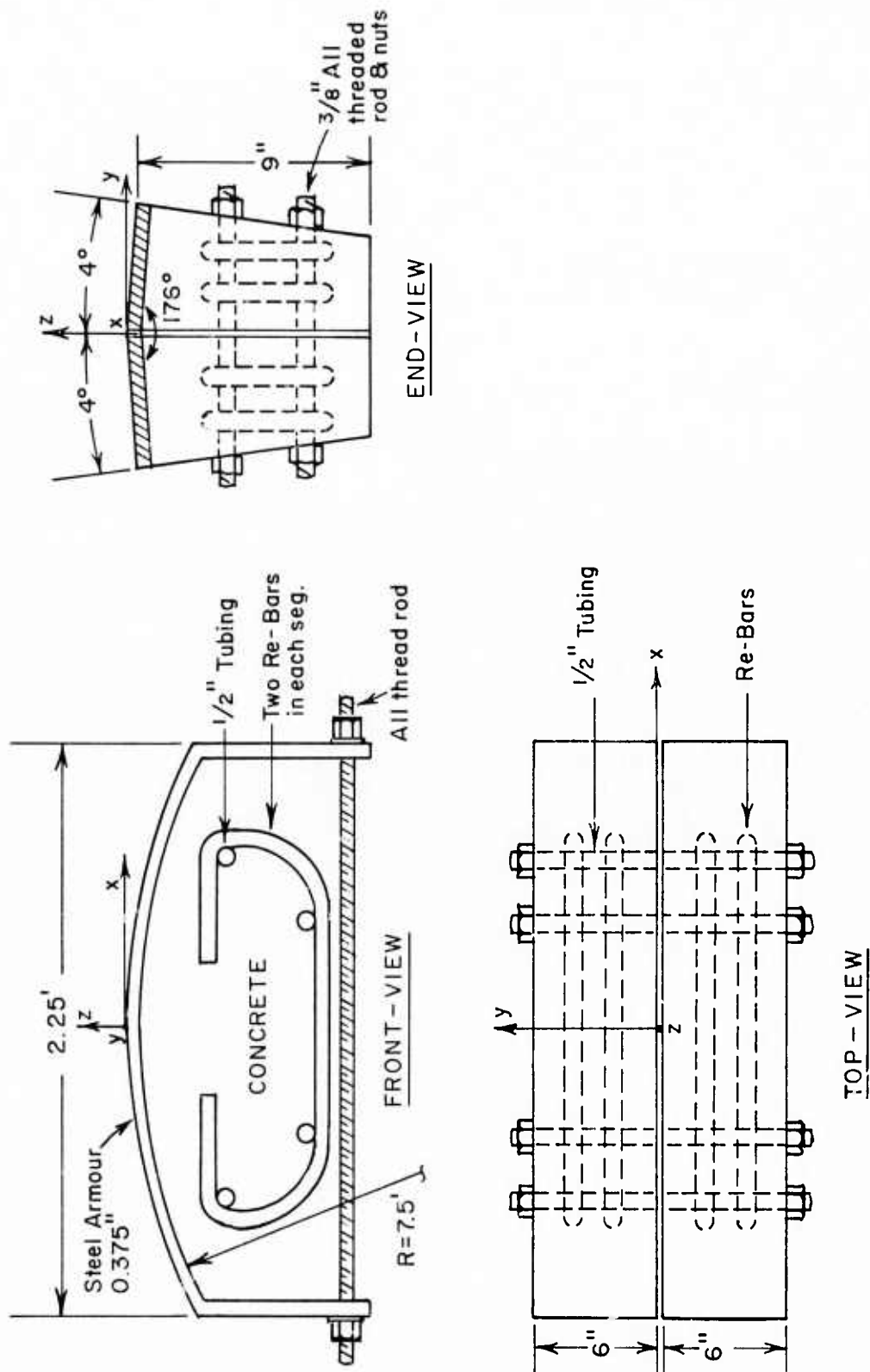
Figure 2. Two-piece steel armoured reinforced concrete die
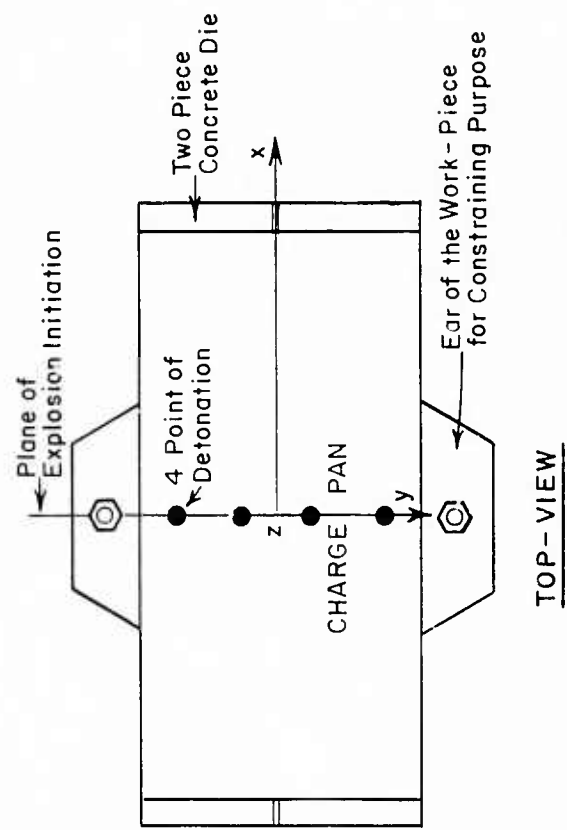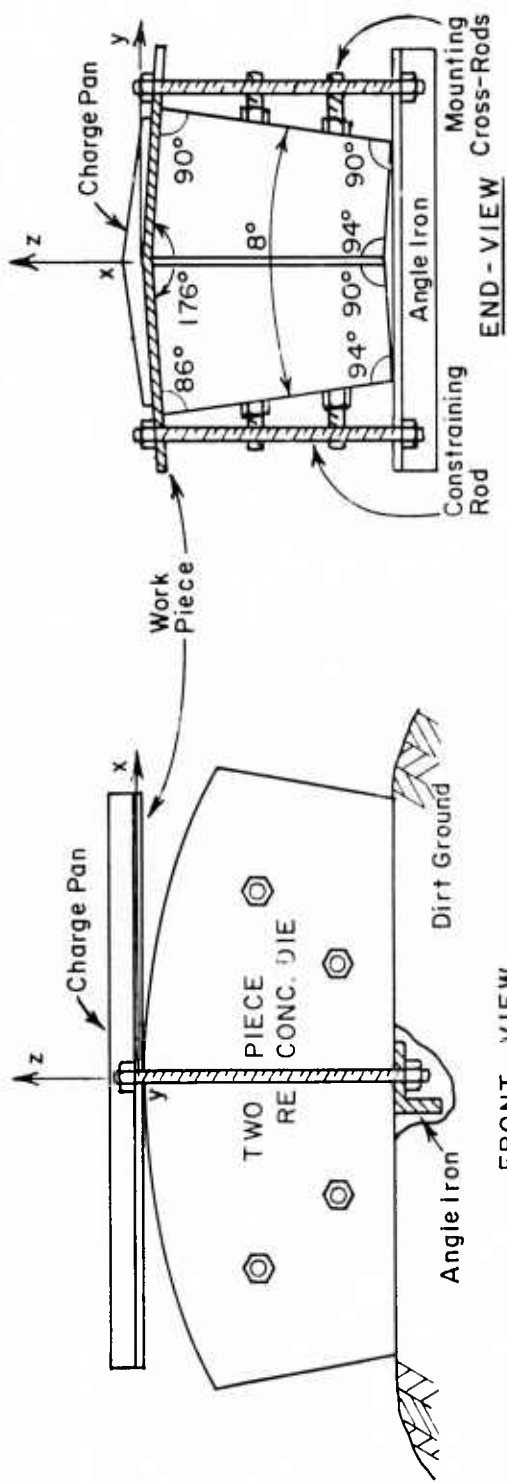
Figure 3. Forming test set-up

There were seven forming tests done. Tests 1 through 4 were done on steel-armoured concrete die; Tests 5, 6, and 7 were done on a bare concrete die. Ireco was used as an explosive charge on all tests except Test 4 in which free-running dynamite was used. On each test a layer of explosive (approximately 2-ft. x 1-ft. x 3/8-in. which weighed about 2,000 gms was used. On each test shot, the concrete die was destroyed. On the last two tests, a 1.5-in. standoff distance was used. On Test 4 and Test 5, momentum traps (lead and aluminum respectively) were used in an attempt to prevent the workpiece from getting a negative radius of curvature. The two kinds of explosives used had the following properties:

Ireco: DBA-10HV, density = 1.35 gms/cm^3 detonation velocity = 3800 m/sec., heat of detonation = 1350 cal/gm. Gurney constant = 1722 m/sec. (for plane detonation) and 1600 m/sec. for grazing or tangential detonation. Ireco was used at a temperature of about 95°F.

Forty percent free-running dynamite: density = 0.85 gm/cm^3 detonation velocity = 1750 m/sec. Gurney constant = 340 m/sec.

The concrete die was set on level ground. On all the test shots except for Test 4, the plane of explosion initiation was along the 1-ft. width of the blank as shown in Figure 3.

In Test 1, the workpiece did not have any radius of curvature and was torn into four pieces as a result of 2200 gms. ireco fired on a steel-armoured concrete die.

In Test 2, the result was better; the workpiece received a radius of curvature of 17.75-ft. as a result of firing 2000 gms. or ireco on a steel-armoured, reinforced concrete die with a forming suface radius of curvature of 7.5-ft. It was inferred that this resulting higher radius of curvature of 17.75-ft. from an initial radius of curvature of 7.5-ft. was caused by the springback in the workpiece. Two factors contribute to this springback in the workpiece. Two factors contribute to this springback. One is the rebound velocity that results from the collision between the moving metal blank and the die surface; the other is the proportion of elastic strain present in the total deformation. The higher proportion of elastic strain would cause higher springback. At this point no attempt was made to manipulate the proportion of elastic strain. The velocity of rebound is proportional to the terminal velocity with which the blank strikes the die surface and the coefficient of restitution between the blank material and the material of the die. The coefficient of restitution is defined as the ratio of the rebound velocity to the impact velocity. At this point no attempt was made to manipulate the amount of rebound. Instead, a different approach was taken.

Based on the results of Test 2, an initial radius of curvature of 4.66 feet was determined to achieve a resulting radius of curvature of 7.5-ft.; see Figure 4. Therefore, in Test 3, all parameters were unchanged from Test 2 except that the die surface had a radius of curvature of 4.66-ft. along its length. The results of this shot were encouraging. The corners and edges of the workpiece were cracked and torn during the forming test. After removing the damaged edges, the workpiece measured 17-1/2-in. x 11-1/2-in. It had some thinout away from the center line. The resulting radius of curvature along its length was 6.26-ft. The radius of curvature along its width was 22-ft. The resulting gore segment of forming Test No. 3 is shown in Figures 5 through 9.

$$TAN \frac{\theta_o}{2} = Sin \frac{\theta_o}{2} \text{ for small } \theta_o/2$$

$$Sin \frac{\theta_o}{2} = \frac{0.5}{7.5} = \frac{\Delta_o}{1} = \tan \frac{\theta_o}{2} \therefore \Delta_o = 0.0677$$

$$Sin \frac{\theta_A}{2} = \frac{0.5}{17.75} = \frac{\Delta_A}{1} = \tan \frac{\theta_A}{2} \therefore \Delta_A = 0.0282$$

$$\delta_S = \Delta_o - \Delta_A = \text{Spring Back}$$

$$\Delta_D = \Delta_o + \delta_S$$

$$= \Delta_o + \Delta_o - \Delta_A$$

$$\Delta_S = 2\Delta_o - \Delta_A = 0.1072$$

$$Sin \frac{\theta_D}{2} = \frac{0.5}{R_D} = \frac{\Delta_D}{1} = \frac{0.1072}{1}$$

$$R_D = \frac{0.5}{0.1072} = 4.66$$

Take $R_D = 4'\text{-}8''$

New Radius of Curvature = $4'\text{-}8''$

Figure 4. Method to compute a new radius of curvature.
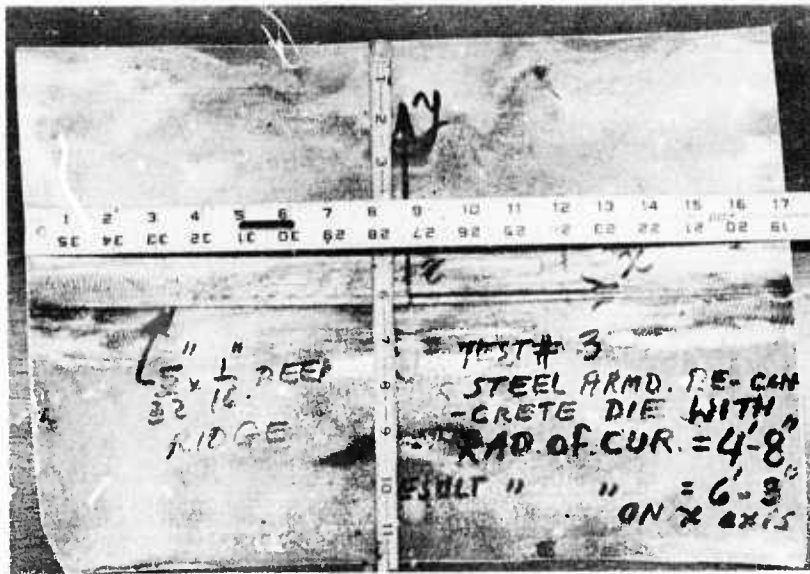
Figure 5. Gore Segment formed in Test 3. Inside view.

Figure 6. Gore Segment formed in Test 3. Outside view.
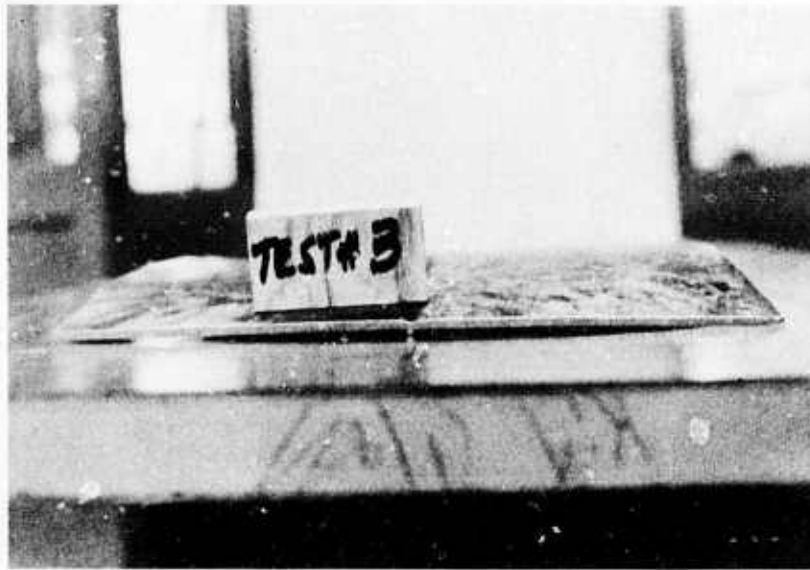
Figure 7. Gore Segment formed in Test 3. End view.
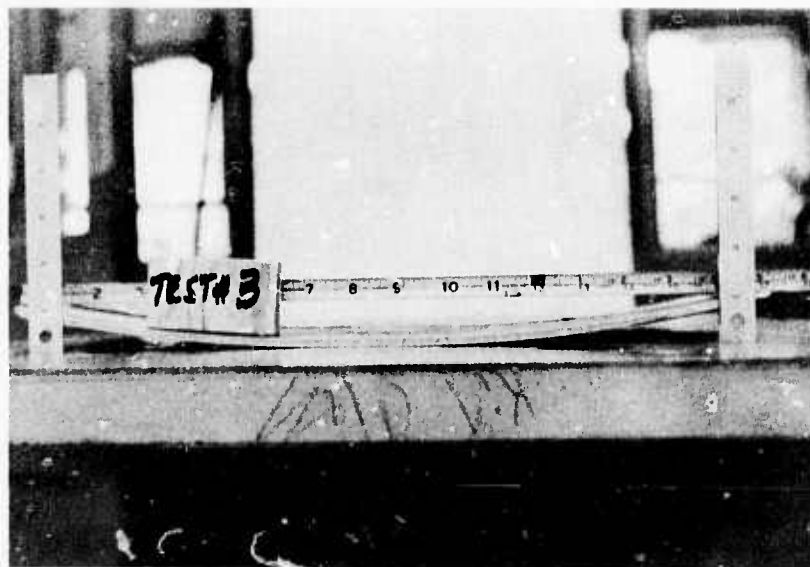
Figure 8. Gore Segment formed in Test 3. Side view.
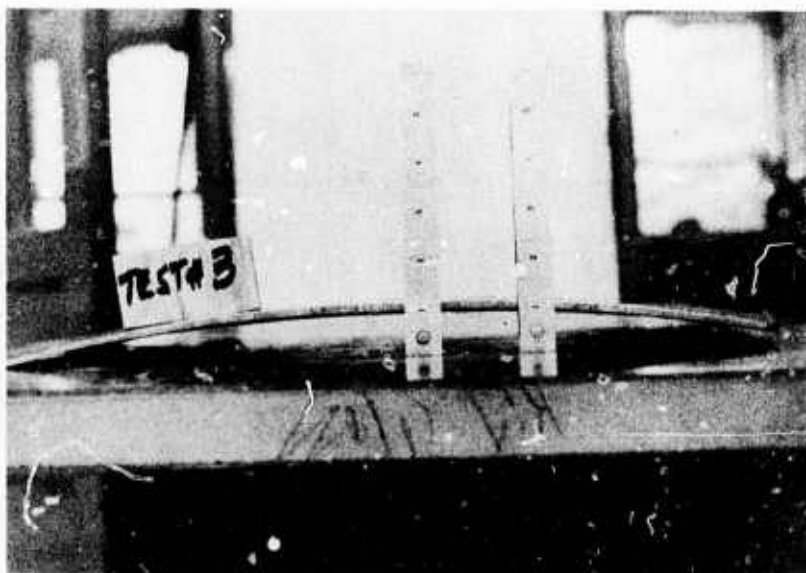
Figure 9. Gore Segment formed in Test 3. Side view.

In Test 4, an idea of a momentum trap was introduced. A 2-ft. x 1-ft. x 1/8-in. lead sheet was glued on the top of the 2-ft. x 1-ft. x 3/16-in. 6061 T6 aluminum workpiece. The idea here was that the compression shock wave from inside the workpiece passes through the interface and into the lead sheet. When reflected from the outer (upper) boundary surface this shock wave becomes a tensile shock wave and causes the lead sheet to fly away leaving the workpiece on the die. The objective was to produce a workpiece having a radius of curvature closer to that of the die by reducing the springback in the workpiece. The result was not good. The workpiece had a resulting radius of curvature of 24-ft. in the opposite direction.

In Test 5 the forming shot was fired on a bare reinforced concrete die, thus reducing the coefficient of restitution between the blank material and the material of the die surface. This lower coefficient of restitution would lower the rebound velocity of the workpiece and consequently reduce the springback in the workpiece. In this test a 2-ft. x 1-ft. x 3/16-in. 6061-T6 aluminum momentum trap was glued on the top of the workpiece. The result was not good. The momentum trap did not fly away, instead it was stuck together with the workpiece. The combination had a radius of curvature of 16.5-ft.

In Test 6 no momentum trap was used. The shot was fired on a bare reinforced concrete die. A 1/4-in. masonite pan, 3/8-in. deep containing a 3/8-in. layer of ireco was held 1.5 inches above the top of the workpiece. This standoff of 1.5-in. was provided for the explosive charge to reduce the impact velocity of the workpiece when it strikes the die. This reduction in impact velocity would reduce the rebound velocity and consequently would reduce the springback in the workpiece. The result was not good. The workpiece edges were torn and it flew to about 15-ft. away from the die. It has a resulting radius of curvature of 20-ft.

It was concluded that in the previous tests, the greater amount of explosive charge (about 2000 gms of ireco) was causing higher impact velocity and consequently higher springback in the workpiece.

It was decided that in Test 7 only about 1600 gms. of ireco should be used and held 1.5-in. above the top of the workpiece. Ireco has a critical layer thickness of 3/8-in.; if it is thinner than this, the charge would not detonate. Part of the charge pan surface was blocked out with 3-in. diameter 1/2-in. thick aluminum and wooden blocks to produce a charge thickness of 3/8-in. This forming shot was fired on a bare-concrete die with 1690 gms. of ireco. The charge did not detonate. The test program was terminated at this point.

In three tests, the resulting radius of curvature was about 18 feet with the die radius of curvature of 7.5-ft. The results of Test 3 were encouraging; the resulting radius of curvature of 6.25-ft. with the die radius of curvature of 4.66-ft. More testing using the approach of Test 3 appears to be justified. As an alternative to the approach used in Test 3, a lesser amount of explosive than 2000 gms of ireco should be used with and without standoff of the charge. Different types of explosive which would give lower impact velocity to the workpiece should be tested. The forming die should be redesigned. The die should be such that it is less time consuming to make and is useable for more than one test. Also, the die surface should have the required radius of curvature in both directions that is, along its length and along its width (along the x and y directions). The die used for the tests reported have had the required radius of curvature in the x-direction (i.e. along its 2-ft. length). The radius of curvature in the y-direction

(i.e. along its 1-ft. width) was approximated by two 6-in. wide flat surfaces making an angle of 176°. In the redesigned die this angle should be eliminated. The idea of using explosives to form the gore segments is very attractive; it would therefore be worthwhile to do further testing in this direction.

IV. EXPLOSIVE THERMOMECHANICAL PROCESSING OF BETA III TITANIUM ALLOY

Faculty Advisor: R. N. Orava
Graduate Student: M. B. de Carvalho

The following is a summary of the studies conducted by Mr. de Carvalho in partial fulfillment of the requirements for the degree of Master of Science from the Chemical Engineering and Metallurgy Department, University of Denver. His thesis is dated November, 1973.

The objectives of this investigation were: to assess the explosive formability of Beta III titanium; to determine the relative influence of explosive forming and more conventional deformation processing on the terminal properties of this alloy; to establish whether the combination of explosive forming or explosive shock loading, and appropriate thermal treatments is an effective technique for strengthening Beta III titanium over and above the normal precipitation-hardened state; and to provide a mechanistic interpretation of the results obtained.

Beta III titanium (nominally 11.5% Mo, 6% Zr, and 4.5% Sn by weight) is a beta-isomorphous (BCC) stabilized titanium alloy which, on aging after solution treatment will develop an omega and/or alpha phase precipitate depending on the aging temperature. The material was received in the solution treated ($1325^{\circ}F$) condition, and subsequent aging for 8 h at $900^{\circ}F$ yielded basically an alpha precipitate as the strengthening phase.

The material was cold-rolled, explosively stretch-formed unidirectionally, or explosively plane-wave shock loaded (317 kbar) to the same effective strain of 28% in the solution treated ($1325^{\circ}F$) condition. Room-temperature tensile tests disclosed that Beta III in the solution treated state is more susceptible to work hardening by rolling than by shock loading or explosive forming, with the latter being least effective. After aging at $900^{\circ}F$ for 8 h, however, the shock-loaded samples had the highest strengths, and concomitantly, lowest ductilities.

The effect of shock thermomechanical processing (TMP), then, was to raise the yield strength from 200 ksi in the solution-treated and aged material to 222 ksi in the solution treated, shocked, and aged condition. This 10% improvement in strength was accompanied by a reduction in total elongation from 4.8% to 1.7% and in reduction in area from 11.5% to 1.7%. One of the interesting aspects of the findings was the failure of the explosively TM-processed material to reach thermally treated (solution treated and aged) strengths, i.e. 185 ksi versus 200 ksi, in addition to also having lower tensile ductility.

A microstructural characterization was performed in an attempt to explain these observations. Firstly, it was found that no strain- or pressure-induced martensite existed in the deformed alloy. The x-ray lines present were all identified as BCC beta phase, with the exception of a trace of HCP omega phase formed during quenching from the solutionizing temperature.

Supplementary tensile tests were then carried out to determine the strain-rate dependence of the work-hardening rate, and to compare surface deformation traces with internal features. The former revealed that an increase in the rate of strain lowers the work-hardening rate, and accordingly accounts, at least in part, for the fact that the static yield strength of explosively

formed material is lower than that of its cold-rolled counterpart. Moreover, from the examination of deformation markings, it was shown that the twin density increases with increasing strain rate. It was concluded, therefore, that twins are less effective obstacles to subsequent slip than dislocations in the BCC matrix of the Beta III alloy.

This factor, along with the results of structure characterization by transmission electron microscopy, and a qualitative x-ray line broadening analysis, led to the following interpretation of the results of the forming and shock-loading studies. Firstly, in the as-deformed state, the cold-rolled material has a higher terminal strength than after explosive forming due to a lower twin density in the former. Whereas shock loading introduces a high density of twins, it also generates a denser and finer dislocation substructure than explosive forming. Hence, the strength is intermediate between the two. That the strength of shocked material surpasses that of the cold-rolled control after aging is thought to be due to the presence of a finer precipitate structure created by nucleation on the finely dispersed shock-induced dislocation substructure, aided by the much higher excess vacancy concentration produced by shock deformation.

Beta III titanium exhibits excellent explosive formability in the solution treated condition, consistent with its good cold-forming characteristics. However, this attractive property is almost completely destroyed even after only 10 min aging at 900°F. Moreover, predeformation aging did not appear to have any favorable influence on TMP strengthening for the conditions examined.

V. FREE FORMING OF INFINITE PLATES UNDER ARBITRARY CHARGE DISTRIBUTION

Faculty Advisor: M. Kaplan
Graduate Student: S. Aku

The following is a summary of studies conducted by Mr. Aku in partial fulfillment of the reqirements for a Doctor of Philosophy Degree from the Mechanical Engineering Dept., University of Denver.

Introduction

Much of the work done in explosive forming has been associated with the production of domes. This study was initiated in an attempt to develop some understanding of the general area of explosive forming of plates so that techniques for forming a wider variety of shapes could be developed. It is believed that the developed techniques might find applications in underdeveloped nations with limited capital available for investment in heavy equipment.

Because of the complexities involved in the general explosive forming problem, some simplifications were introduced. The study was limited to infinite plates and to explosions in air. In the first part of the study, the response to a single point charge is determined. This is then expanded to include the response to an arbitrary distribution of charge and finally the inverse problem is examined, i.e., the distribution of charge necessary to produce a specified shape.

Response to a Point Charge

The pressure time history at the plate surface produced by the charge was determined using acoustic theory and assuming that the wave is locally an oblique plane wave. An exponentially decaying pressure time history was used. Allowing for wave reflections and the rigid motion of the plate, the initial velocity of the plate (the velocity when the pressure decays to zero) was found.

That part of the velocity which was used to deform the plate elastically was removed in order to find the initial velocity used to produce permanent deformations. The resulting corrected velocity distribution produced by a .938 charge of Detasheet acting on a .035" thick steel plate is shown in Figure 1, for different standoffs.

In order to calculate the plastic deformation produced by the corrected initial velocity v_c it was assumed that at the radius where $v_c = 0$ the plate was simply supported. The ensuing analysis was a modification of Jones' treatment[1] of a simply supported plate under a uniform initial velocity field. The basic assumption was that the plate deformed in two stages. In the first stage, following detonation a plastic hinge moved inward from the simple support to the center of the plate as the plate moved down and the deformation was due primarily to bending, although a correction to account for stretching was made. In the second stage, which initiated when the plastic hinge reached the center of the plate and continued until the plate had come to rest, deformation was a result of stretching (membrane forces) and bending effects were ignored. The final plate deflection was given as an infinite series in the Bessel Function J_0. It was found that the series could be truncated after the fifth term without significant loss in accuracy. The resulting deflection curve for a .938 gm Detasheet charge is shown in Figure 2 at standoffs of .75" and 1.25" and compared with experimental results.
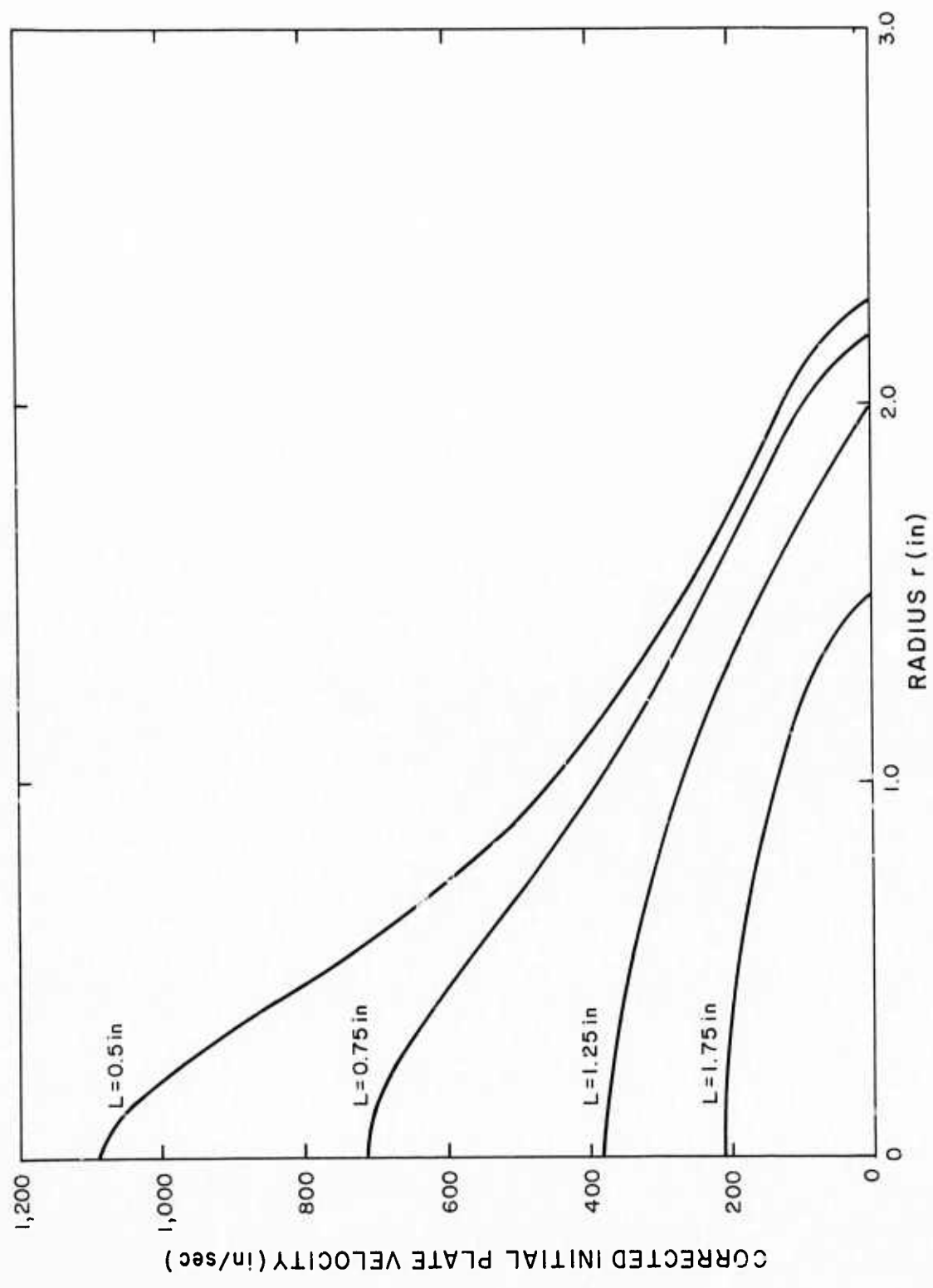
Figure 1. Corrected initial velocity distribution for .938 gm point charge for various standoff distances.
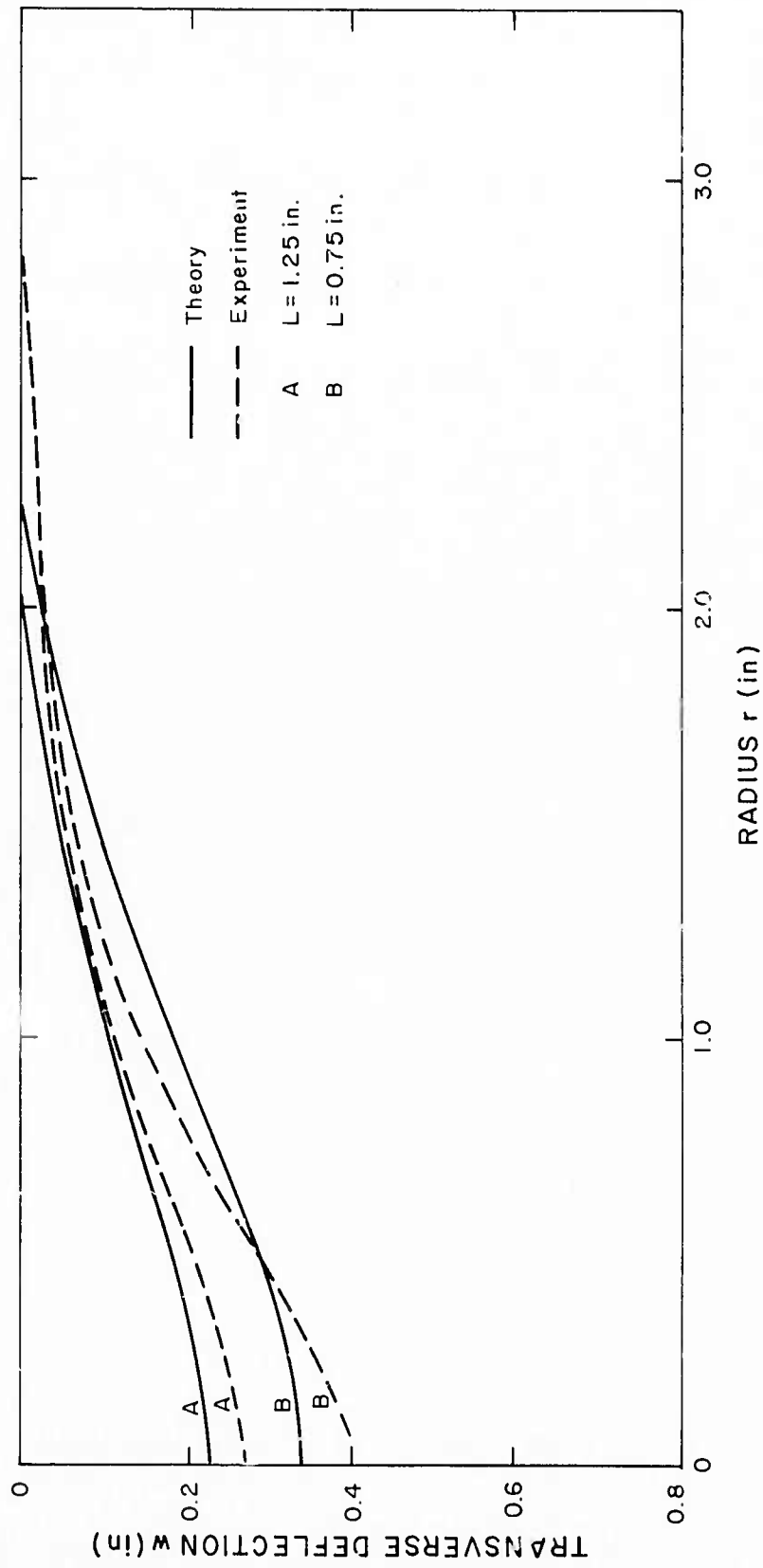
Figure 2. Deflection curves due to .938 gm point charge for standoff distances of 0.75 in. and 1.25 in.

The analysis developed for the point charge was also valid for all axi-symmetric velocity distributions where the initial velocity was a maximum at the center of the plate and decreased monotonically to zero. A more general axi-symmetric initial velocity, such as that produced by a ring charge (Figure 3), was also handled by a modification of the analysis. In particular, independent solutions were developed for the regions defined by $0 \leq r \leq r_0$ and $r_0 \leq r \leq b$ where r_0 and b were the radii at which the velocity was respectively maximum and zero.

Response to an Arbitrary Charge Distribution

One of the results of the single point charge study was that the final deformation of the plate was very nearly proportional to the corrected initial velocity distribution. This was demonstrated both analytically and experimentally. Since the initial velocity produced by general charge distributions can be readily calculated, while the problem of analytically determining the plate response is extremely difficult, an experimental program was conducted to determine if there was any simple relationship between the corrected initial plate velocity and final plate deflection in the general case.

The charge configuration in the four tests conducted is shown in Figure 4. As with the single point charge, it was found that the corrected initial velocity and the final deflection were nearly proportional in all cases. In order to calculate the amplitude of the deflection from the initial velocity, the following technique was used. At the point of maximum velocity, a lower bound estimate of the deflection was made by using the axi-symmetric theory with the velocity along the direction for which the energy delivered to the plate was a minimum. Similarly, an upper bound estimate was made, and the final deflection was taken to be the average of the two. A typical result of the deflection calculated from the corrected initial velocity is shown in Figures 5 and 6 and compared with experimental data.

The Inverse Problem

The inverse problem requires the determination of the charge distribution required to produce a given plate deflection. In order to simplify the problem the charge distribution was limited to point charges placed at the nodal points of a predetermined rectangular grid located some distance from the plate surface. With some further approximations the problem was reduced to the solution of n linear algebraic equations in n unknowns.

An example of the type of result obtained is shown in Figure 7. There, the deflected shape was chosen to be that obtained experimentally from three point charges (Case b, Figure 4).

Conclusions

The study showed that it is possible to predict, at least to a first approximation, the charge distribution necessary to produce relatively complex shapes in infinite plates. The techniques developed can also be used to predict the damage produced by an explosive charge. In order to be able to actually produce complex shapes economically, the techniques must be expanded so that a variety of finite boundary conditions can be accounted for.
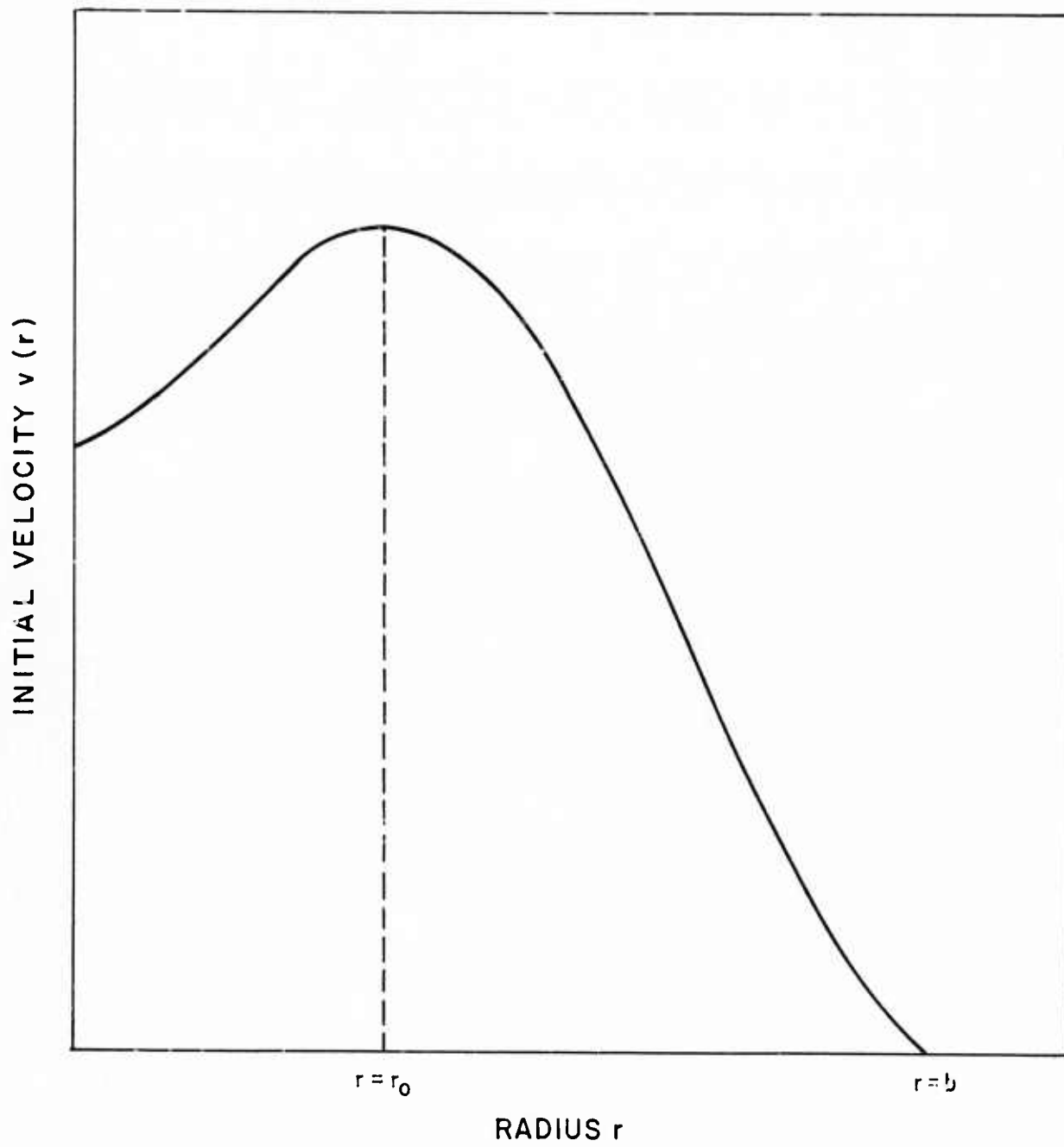
Figure 3. Diagram showing more general axi-symmetric initial velocity distribution.
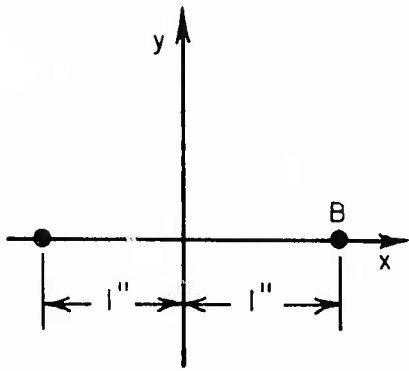
(a) Two point charges
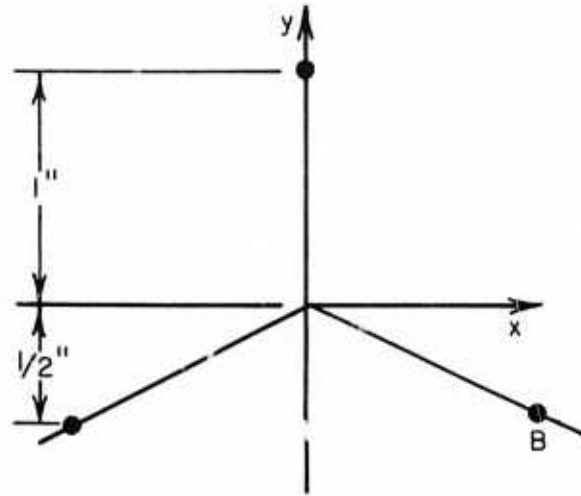
(b) Three point charges
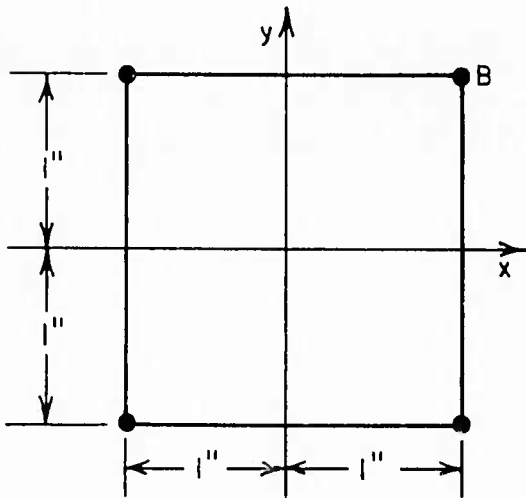
(c) Four point charges
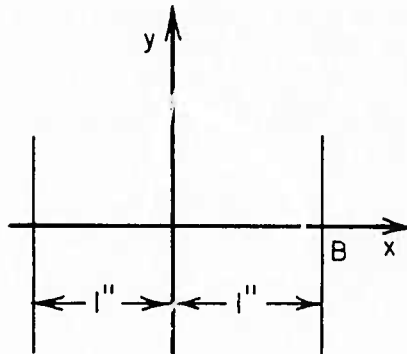
(d) Two line charges

Figure 4. Diagram showing position of charges in multiple charge experiments.
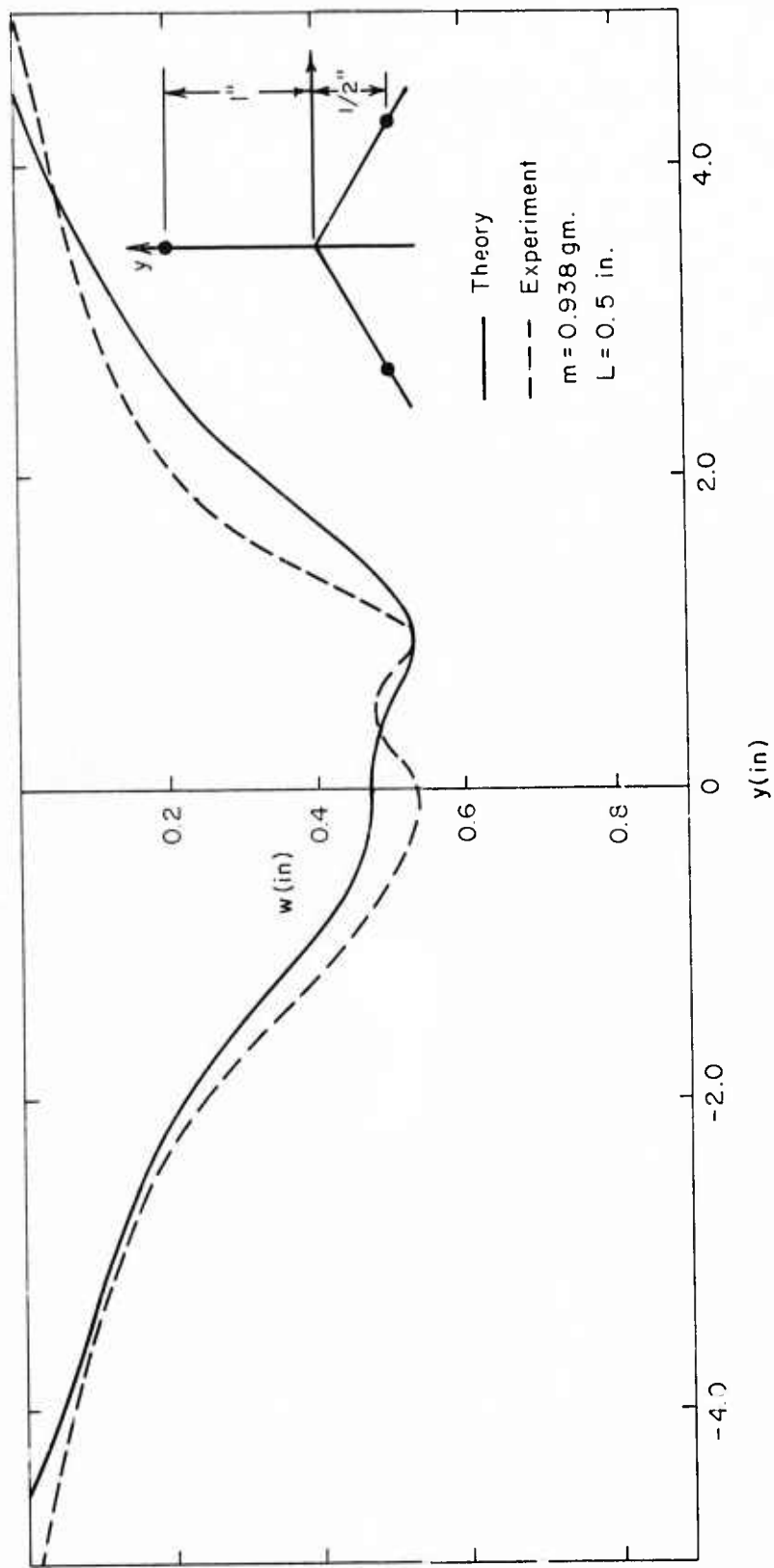
Figure 5. Curves of transverse deflection w along the y axis due to three equal point charges.
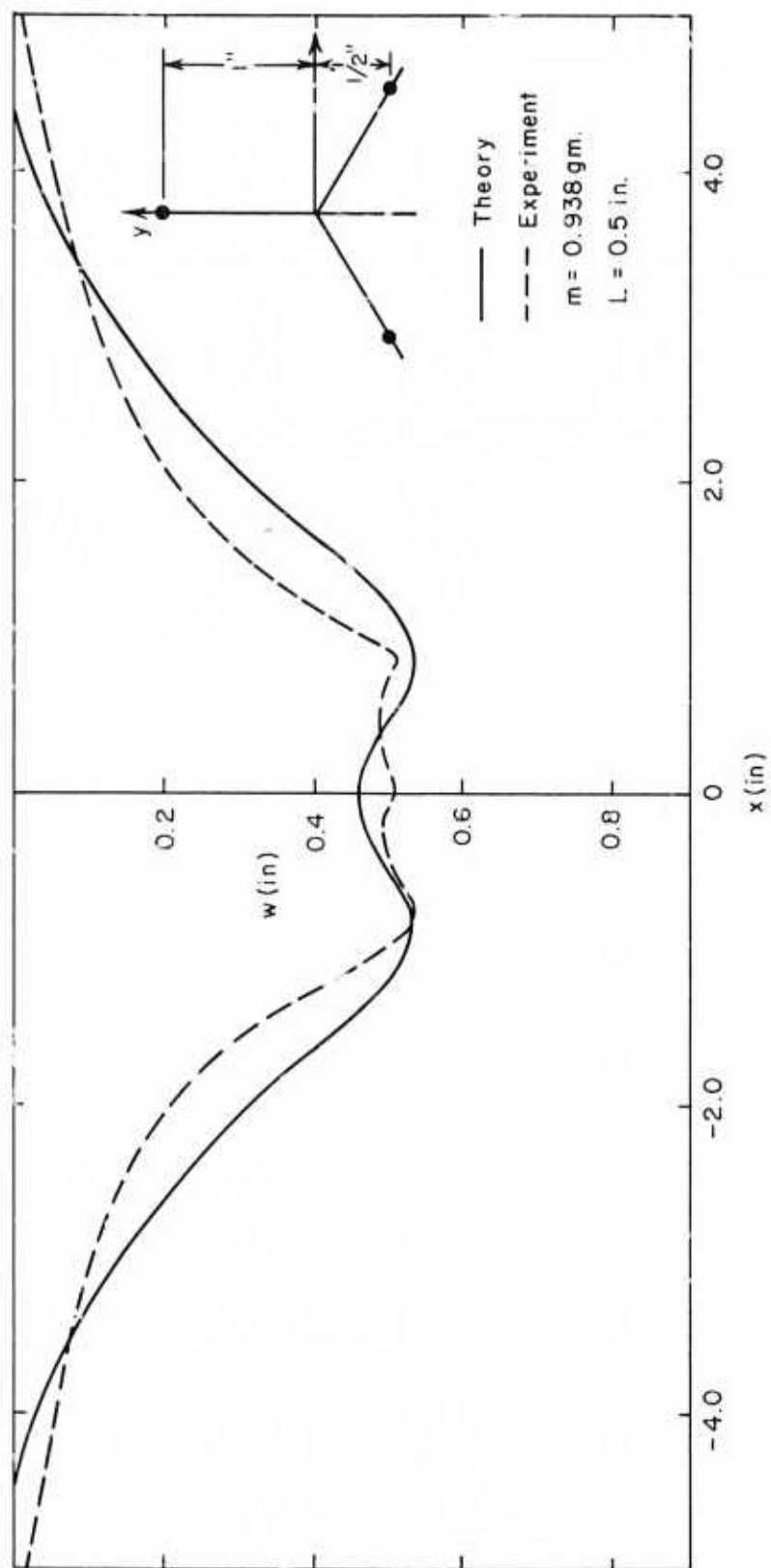
Figure 6. Curves of transverse deflection w along the line y = −0.5 in. due to three equal point charges.
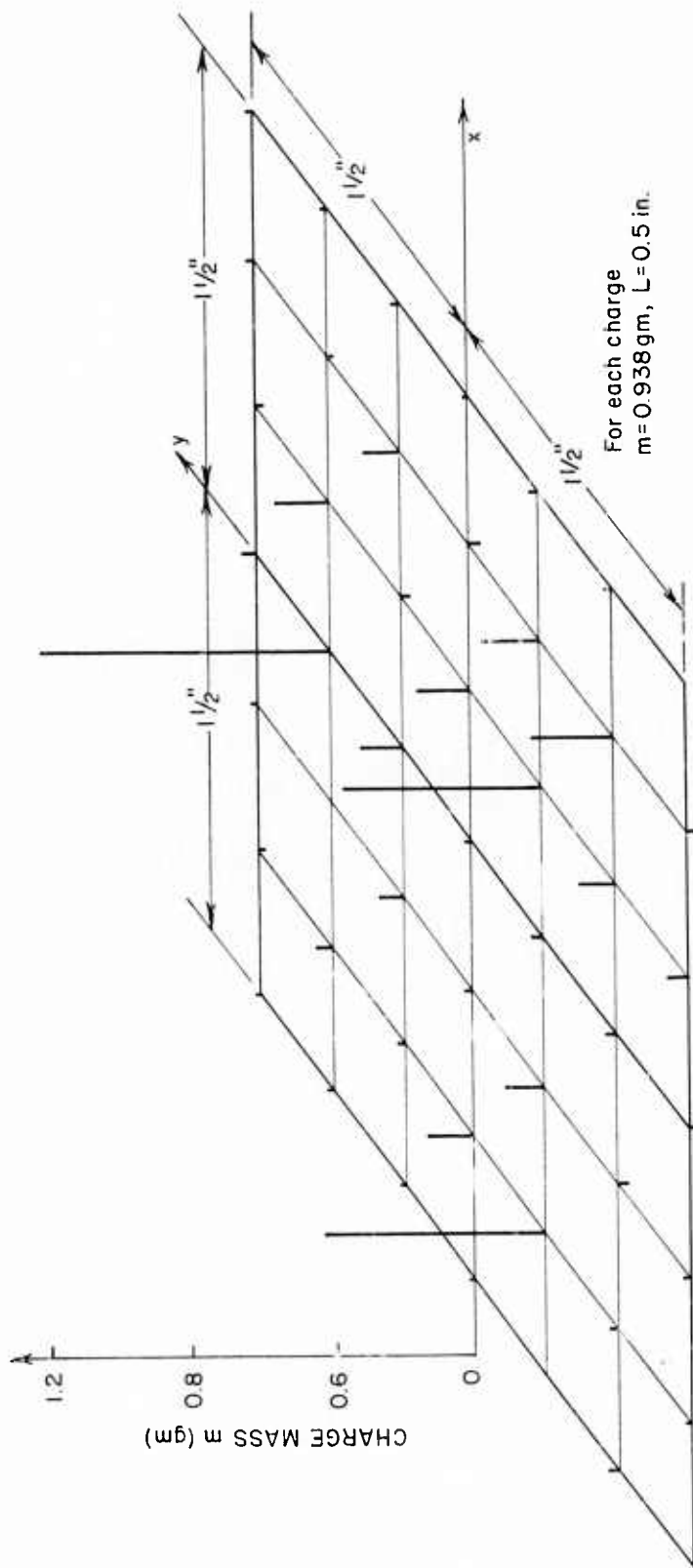
Figure 7. Theoretical charge distribution at 1/2 in. standoff distance necessary to produce the same deflection as in three point charge experiment.